AD-A097 948 SACLANT ASW RESEARCH CENTRE LA SPEZIA (ITALY) F/G 17/1
DETECTION PERFORMANCE OF HORIZONTAL LINEAR HYDROPHONE ARRAYS IN--ETC(U)
DEC 80 R KLEMM
UNCLASSIFIED SACLANTCEN-SR-43 NL

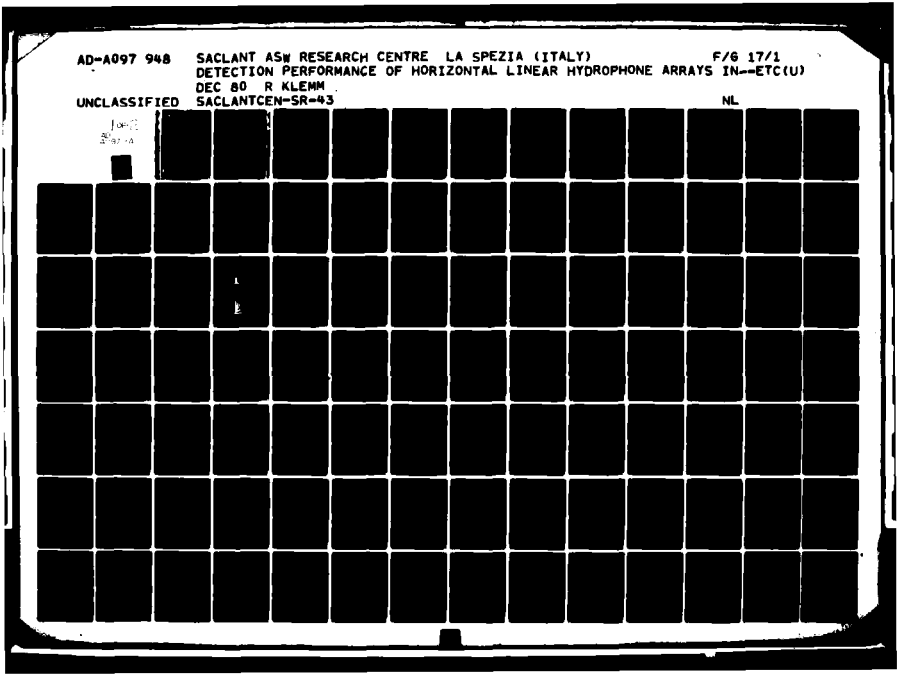

SACLANTCEN Report
SR - 43

SACLANTCEN Report SR - 43

SACLANT ASW
RESEARCH CENTRE
REPORT

DETECTION PERFORMANCE OF HORIZONTAL LINEAR HYDROPHONE ARRAYS IN SHALLOW WATER

by

RICHARD KLEMM

15 DECEMBER 1980

NORTH ATLANTIC TREATY ORGANIZATION

LA SPEZIA, ITALY

Published by

STI

14 SACLANTCEN [redacted]-SR-43

NORTH ATLANTIC TREATY ORGANIZATION

SACLANT ASW Research Centre
Viale San Bartolomeo 400, I-19026 San Bartolomeo (SP), Italy

tel: national 0187 560940
international + 39 187 560940

telex: 271148 SACENT I

DETECTION PERFORMANCE OF HORIZONTAL LINEAR HYDROPHONE ARRAYS IN SHALLOW WATER

by

Richard/Klemm

15 Dec[redacted]80

This report has been prepared as part of Project 02.

APPROVED FOR DISTRIBUTION

B.W. LYTHALL
Director

TABLE OF CONTENTS

Table of Contents (Cont'd)

DETECTION PERFORMANCE OF HORIZONTAL LINEAR HYDROPHONE ARRAYS IN SHALLOW WATER

by

Richard Klemm

ABSTRACT

A comprehensive model study of the use of horizontal hydrophone arrays in shallow water is presented. Existing knowledge of signal-processing techniques is applied to a shallow-water sound-propagation model in order to determine the influence of shallow-water conditions on the design of receiver structures. In particular, the spatial part of the problem of the detection of targets in the presence of directive noise sources is of interest. Most literature on array processing simplifies receiver structures by making simple assumptions about the medium (e.g. coherent plane waves). These approximations may be valid to some extent for sources in deep water and radar; in shallow water, however, one is faced with the problem of target detection in a waveguide. This investigation was therefore made in order to find simple receiver structures when the characteristics of the medium are taken into account. A great variety of array processors (quadratic, linear, adaptive, nonadaptive, optimum, suboptimum) is discussed. In addition, some system limitations (receiver bandwidth, distortion of the array shape, inclusion of the target in the noise estimation in passive systems) are considered.

G L O S S A R Y

Matrix Notations

$\underline{A}$	matrix
$\underline{a}$	vector
a	scalar
$\underline{a}^*$	conjugate complex transpose
$\underline{C} = \underline{A}\,\underline{B}$	matrix product $c_{ik} = \sum_r a_{ir} b_{rk}$
$\underline{B} = \underline{A}^{-1}$	matrix inversion ($\underline{A}$ = square matrix)
$\underline{B} = \underline{H}\,\underline{H}^*$	factorization of positive definite matrices
$\mathrm{tr}(\underline{A})$	trace of the square matrix $\underline{A}$ ($= \sum_i a_{ii}$)
$c = \underline{a}^*\underline{b}$	scalar product $c = \sum_i a_i^* b_i$
$\underline{C} = \underline{a}\,\underline{b}^*$	dyadic product $c_{i,k} = a_i b_k^*$
$\underline{I}$	unity matrix
$\underline{e}_i$	i^{th} column of $\underline{I}$
$\underline{0}$	null matrix
$\underline{o}$	null vector

Abbreviations

AEP	auxiliary element processor
BIN	binomial shading
CBF	conventional beamformer
COS	cosine shading
DIP	dipole processor
E{ }	expectation
I/N	interference-to-noise ratio
MMF	matrix matched filter (generalized beamformer)

MRP	multibeam processor
NFB	narrowband filter bank
NS	noise suppression
OLP	optimum linear processor
OQP	optimum quadratic processor
Re{ }	real part

Symbols

The following symbols are used throughout the report. Symbols that are used only a few times or denote different subjects are explained in the text.

$\underline{A}$	diagonal matrix containing the complex amplitudes of modal arrivals (deterministic part of the model)
β	bearing
$\underline{b}$	beamformer vector
b_i	beamformer coefficients
b	bandwidth
c	sound velocity
$\underline{D}$	dipole- or nullformer matrix
d	spacing between hydrophones
$\underline{e}_i$	i^{th} column of unity matrix
F	number of frequency channels
$\underline{F}$	spatial filter matrix
f	frequency
ϕ_n	random phase
G	gain
$\underline{G}$	angle interval covariance matrix
$\underline{h}$	processor vector
$\underline{H}$	matrix matched filter; generalized beamformer
$\underline{I}$	unity matrix

j	$\sqrt{-1}$
$\underline{k}$	processor vector
k, k_o	wavenumber = $2\pi/\lambda$
k_n	modal wavenumber = $2\pi/\lambda_n$
$\underline{K}$	processor matrix
ℓ	test function
λ	wavelength
L	order of vector space after pre-transform
λ_n	modal wave length
M	number of modes
$\underline{M}$	matrix describing phase relations between modes and sensors
N	number of sensors
$\underline{N}$	noise covariance matrix
$\underline{n}$	noise vector
$\underline{P}$	target-signal covariance matrix
P	pressure
P, P_s, P_N	power
$\underline{Q}$	noise covariance matrix
$\underline{R}$	covariance matrix
ρ, ρ_{ik}	spatial correlation
r, r_i	range
$\underline{S}$	signal covariance matrix
$\underline{s}$	target-signal vector
$\underline{T}$	pre-transform
T	observation time, filter time response duration
t	time
$\underline{U}$	unity matrix
u_o	angle interval

u	directional cosine
$\underline{v}$	vector of random phases
$\underline{V}$	covariance matrix of $\underline{v}$
$\underline{W}$	factorized covariance matrix
$\underline{x}$	vector of received signals
$\underline{X}$	covariance matrix of received signals
$y_n(t)$	modal plane waves
$\underline{y}$	vector of complex modal amplitudes
$\underline{Y}$	covariance matrix of $\underline{y}$

INTRODUCTION

The following investigation has been made to answer the question of which kind of spatial signal processing should be applied to linear horizontal hydrophone arrays in shallow water. The use of horizontal arrays is of special interest for several reasons. On the one hand the detection problem in more or less shallow water is primarily two-dimensional, i.e. horizontal. On the other hand horizontal arrays offer great advantages when installed in mobile system because they can be implemented as flexible array cables. Typical advantages are' no limitation on the aperture, low ship-noise level due to the distance to the towing ship, and directionality of towing ship noise, which makes noise suppression more effective. The obvious disadvantage is the rotational symmetry of the array pattern of line arrays, which makes them sensitive to all kinds of nondirectional noise.

The theory of optimum arrays has been treated repeatedly in the literature *[1,2,3,4]*. Many other papers, *[5,6,7,8,9]* are concerned with suboptimum adaptive approaches to optimum array theory, in particular by replacing the crucial inversion of the noise covariance matrix contained in all adaptive methods for detection and resolution by some adaptive algorithm for minimization of the noise, e.g. the LMS-algorithm. The problem of choosing the right algorithm or even deciding in favour of the most cumbersome way of adaptive noise suppression (estimation and inversion of the noise covariance matrix *[10]*) depends on the temporal behaviour of the noise field and is not the subject of this report.

The major part of the literature on detection theory by linear array discusses processors and their suboptimum implementations. This means, however, that certain assumptions are made about the medium, i.e. that the far fields of point sources are coherent plane waves. Such an assumption may be made in certain applications, for example, with radar, with small arrays, or with sonars in which the beamwidth is broad compared with the spatial distribution of any signal.

In this report, signal-processing techniques are applied to a shallow-water sound propagation model (normal mode). The main objective is to find out the particular influence of the "shallow-water" medium on the design of array processors. Thus a considerable part of the report is concerned with optimum and suboptimum quadratic array processors (e.g. quadratic adaptive sidelobe cancellers). These processors are of special importance for the performance of large arrays in the presence of random wavefronts. The problem of limitation of array length has been discussed for instance in *[11]*; however, this discussion is based on a linear processing scheme (conventional beamformer).

Model studies such as the one presented in this report are usually based on a number of assumptions (see Ch. 1) that tend to simplify the problem so that it becomes feasible for numerical calculations. Therefore the results achieved have to be considered as quite optimistic. It turns out, nevertheless, that even under these optimistic assumptions it is possible to draw conclusions on which kind of processing should be taken into consideration and on which method should be rejected. In that sense the results presented here can be used to compare different array processors rather than being considered as absolute measures of the array performance. The actual array gain depends on many unreliable parameters, such as the sound-speed profile (which may change with time), the weather conditions, the particular area, the noise configuration, and others. Consequently, experimental results will give more realistic figures of performance, but only for the special conditions of the experiment. The model study may suffer from too many idealizations, but is more general in that it does not depend on any special area or on temporary environmental conditions; it seems, therefore, to be the right way for systems design. The experimental validation of the results achieved has to be done anyway, but it will be confined to those processor schemes that have proved to be useful.

As is well known, array processing can be carried out in the time/space domain or in the frequency/space domain. For very large arrays (spatial correlation length small compared with the aperture of array) a frequency/wavenumber representation, i.e. Fourier-transform in time and space, offers some advantages. In the following only the frequency/space representation

of signals is considered. That means that all sensor output signals are first subjected to spectral analysis and that spatial processing is carried out for each frequency separately. There are several good reasons for the frequency domain approach. First of all, the normal-mode solution of the wave equation is, by definition, valid for only one single frequency. Therefore, modelling of broadband signals by running the mode program several times for different frequency is a quite cumbersome process, but is still a rough approximation. Furthermore, the consideration of broadband signals introduces another dimension of degrees of freedom in that the array gain depends now on the spatial and the spectral energy distribution. Thirdly, from the viewpoint of implementation of adaptive broadband systems, the frequency domain approach yields significant saving in arithmetic operations.

The main subject of this report is the detection performance of horizontal arrays in the presence of more or less directive noise sources. In addition, some spatially white noise is always assumed. In order to distinguish between them, directive noise sources are referred to as interference, and the white component is called noise. This distinction is important, particularly because the interference-to-noise ratio is the key parameter in all array gain calculations, whereas the signal-to-noise ratio does not have any influence on the gain.

1 ASSUMPTIONS

The following assumptions have to be made to simplify the problem so that it can be handled numerically with reasonable effort. Therefore the results achieved have to be considered to be somewhat optimistic and not generally valid for all scopes of application. Nevertheless, for the purpose of a comparative study on array-processing schemes it turns out that even under the optimistic assumptions listed below it is possible to decide quite well which kind of processing should or should not be chosen under certain conditions.

1.1 Signal Source

The signal source is either the sound radiated by a target or the echo of a target due to a transmitted pulse. The target is point shaped.

1.2 Sound Propagation Model

The propagation of sound due to point sources is modelled by the normal-mode SNAP program *[12]*. This program calculates the far field of a point source for a three-layer medium (water, sediment, sub-bottom). Input parameters are

- sound parameter
- water depth
- sediment depth
- frequency
- densities of sediment and sub-bottom
- compressional attenuations in sediment and sub-bottom
- compressional speed in sediment and sub-bottom
- shear attenuation in sub-bottom

Thus a considerable number of parameters can be varied. For our investigation only two different sets of channel parameters (summer and winter profile) are considered for three frequencies (200, 800, 3200 Hz).

The pressure at a point (r,z) of the sound field due to a point source in the origin $(0, z_o)$ can be expressed as:

$$p(r,z) = a \cdot \frac{\omega \rho_1^2}{H} \sqrt{\frac{1}{8\pi r}} \sum_{n=1}^{M} \frac{u_n(z_o)u_n(z)}{k_n} \cdot e^{-\alpha_n r} \qquad \text{[Eq. 1]}$$

$$\cdot e^{j(k_n r - \omega t - \frac{\pi}{4})} ,$$

where a = sound pressure 1 m apart from the source
H = water depth
$u_n(z)$ = normal mode functions
k_n = modal wavenumbers
α_n = modal attenuation coefficient
ρ = water density
ω = source frequency.

By means of the following abbreviations

$$C = a \frac{\omega \rho_1^2}{H} \frac{1}{8\pi r}$$

$$A_n = \frac{u_n(z_o)u_n(z)}{k_n} e^{-\alpha_n r}$$

equation 1 becomes

$$p(r,z) = C \sum_{n=1}^{M} A_n e^{j(k_n r - \omega t - \frac{\pi}{4})} \qquad \text{[Eq. 2]}$$

The values A_n and the wavenumbers k_n are calculated by the SNAP program.

1.3 Homogeneity

The sound field is supposed to be homogeneous within the dimensions of the horizontal array. Thus spatial correlation between hydrophones is independent of the position within the aperture, i.e. the correlation of an equally-spaced array between the i-th and k-th hydrophone is

$$\rho_{ik} = \rho_{i+\ell,k+\ell} = \rho_{i-k} = \rho^*_{k-1} . \qquad \text{[Eq. 3]}$$

This yields some advantage for calculating the gain of large arrays, rather than having significant influence on the results. On the one hand the modelling program has to be run only once for the array instead of once for each hydrophone (saving of computer time). On the other hand this property [Eq. 3] causes the covariance matrices to be Toeplitz matrices, which are completely described by their first column (saving of computer memory).

1.4 Stationarity

The sound field is supposed to be short-time stationary. That means that any changes in the statistics of the sound field are slow compared with the time needed for signal processing, so that sufficiently stable estimates of the covariance matrices for signals and noise can be obtained, or, equivalently, that adaptive algorithms for noise suppression (e.g. LMS-algorithm) get enough data for convergence.

1.5 The Noise Field

The noise field may contain

- Point sources (interference), e.g. ships or jammers
- Uncorrelated (spatially white) noise, e.g. receiver noise, flow noise, ambient noise.
- Wide-angle noise, i.e. noise uniformly distributed over a certain wide angle interval, which is for the rough modelling of noise radiated by sources that cannot be considered to be point-shaped (e.g. dense shipping areas). In the limit (i.e. for 180°) the noise becomes isotropic, which may be a rough approach to reverberations, surface noise, and other kind of ambient noise *[13,14,15]*.

1.6 Correlation between Modes

Information about correlation between modes is not generally available. For horizontal arrays the modal amplitudes $CA_n \exp(-\alpha_n r)$ are constant for all sensors. Therefore, Eq. 2 describes a sum of plane waves travelling at

different angles $\cos \gamma_n = k_n/k_0 (k_0 = \frac{\omega}{c(z)}$, where $c(z)$ is the sound speed at receiver depth. Therefore the path length is different for every wavenumber. It is supposed that the time-varying surface causes a phase modulation for each plane wave, so that the pressure becomes

$$p(r,z) = C \cdot \sum_{n=1}^{M} A_n \, e^{j(k_n r - \omega t + \frac{\omega}{4} + \phi_n)} \qquad \text{[Eq. 4]}$$

If the modal phase ϕ_n is random between observations and uniformly distributed, different arrivals are uncorrelated with one another.

Assuming different modes to be uncorrelated with one another also causes random wave fronts for noise and signal, which will have some significant influence on the spatial signal processing. In this sense uncorrelated modes are a worst-case assumption.

On the other hand any range dependence of the sound field due to mode interference is omitted by assuming uncorrelated modes. That means that no mode interference appears along the array aperture. For low frequencies, therefore, omitting the phase relations among modes might be an optimistic approach, because the sound field consists only of a few modes. Furthermore, at low sea state, the amplitudes of the time-varying surface are small compared with the wavelength of the sound wave. Therefore, relatively high coherence and hence some interference among modes can be expected.

At higher frequencies even small variations of the surface will have considerable influence on the modal phase ϕ_n. Furthermore, the distribution of the signal (or noise) energy over a high number of modes will cause some equalization in range rather than a distinct interference pattern.

1.7 Far-Field Conditions

The receiving array is supposed to be in any case in the far field of signal and noise sources. For the vertical dimension this has been done

already by assuming the sound field to be described in terms of discrete modes. Replacing the range-dependent Hankel-function by an exponential term in Eq. 2 is another far-field approximation. Furthermore, the near field of the receiver, due to scattering of the sound energy coming from long distance at the random surface, is neglected. This part of the sound field, and surface noise as well, are supposed not to be highly directive and therefore may be considered to be a part of the isotropic or even white noise [16]. It is assumed, furthermore, that the different arrivals due to different modes are plane waves (i.e. $R > D^2/\lambda$), which is not strictly true in all numerical examples. This has no significant influence on the signal because any beamforming network can be matched to either plane or non-plane waves if the range is known. Slight differences might occur for the interference (noise sources); however, the results show that there is no significant influence on the performance of noise suppression systems due to the assumption of plane modal waves.

1.8 Statistics

Signal and noise are assumed to be stationary, zero mean, gaussian processes. The gaussian assumption is justified by the fact that each signal is a sum of independent stochastic variables (central limit theorem). It is true especially for high frequencies, since there is usually a large number of modes. The zero-mean assumption can in practice be verified by subtraction of the mean value. Sampling the sound field in time (A/D) and space (array) leads to multivariable, complex, gaussian distributions.

1.9 Zero Bandwidth

It is assumed throughout the report that the bandwidth of the sensor channels is zero, i.e. received signals are sinusoid. This seems to be a contradiction to the assumption of Sect. 1.6 (uncorrelated modes). It means, however, in practice that the channel bandwidth of the sensor is small compared with the inverse sound-travel time over the aperture of the array. If the sampling rate is less than the relative bandwidth the phases among modes may still be random.

2 SIGNAL AND NOISE MODELS

2.1 Point Sources (see assumptions of Sects. 1.1 and 1.5)

The far field of a point source in free space is a plane wave described by

$$y(t) = a \cdot e^{j(kr-\omega t)}, \qquad \text{[Eq. 5]}$$

where $k = 2\pi/\lambda$, a the source amplitude and r the distance between source and receiver.

In the shallow-water sound-propagation channel the horizontal part of the wave equation gives a superposition of plane waves (see Eq. 2) of the form

$$y_n(t) = a_n e^{j(k_n r-\omega t)}, \qquad \text{[Eq. 6]}$$

where a_n = amplitude of n-th mode
k_n = the horizontal wavenumber = $2\pi/\lambda_n$.

Now let us introduce the concept of a random phase among modes (see assumption of Sect. 1.6):

$$y_n(t) = a_n e^{j(k_n r-\omega t)} e^{j\phi_n} \qquad \text{[Eq. 7]}$$

This system of equations may be written in matrix form

$$\underline{y}(t) = e^{-j\omega t} \underline{A}\, \underline{v}, \qquad \text{[Eq. 8]}$$

where

$$A \equiv \begin{pmatrix} a_1 e^{jk_1 r} & & 0 \\ & \ddots & \\ & & a_n e^{jk_n r} \\ & \ddots & \\ 0 & & a_M e^{jk_M r} \end{pmatrix}$$

and

$$\underline{v} \equiv \begin{pmatrix} e^{j\phi_1} \\ \vdots \\ e^{j\phi_n} \\ \vdots \\ e^{j\phi_M} \end{pmatrix}$$

The vector $\underline{y}$ contains all the modal plane waves arriving at distance r. The covariance matrix among modes is

$$\underline{Y} = E\{yy^*\} = E\{\underline{A}\ \underline{v}\ \underline{v}^*\ \underline{A}^*\} = \underline{A}\ \underline{V}\ \underline{A}^* \qquad \text{[Eq. 9]}$$

where $\underline{V}$ is the covariance matrix of the random part of the model: $\underline{V} = E\{\underline{v}\ \underline{v}^*\}$.

2.2 Linear Array

At the i-th sensor of a linear array one gets a sum over modal plane waves

$$x_i = \sum_{n=1}^{M} a_n\, e^{-j\omega t}\, e^{j\phi_n}\, e^{jk_n r}\, e^{jk_n r_i}\ , \qquad \text{[Eq. 10]}$$

where $e^{jk_n r_i}$ is an additional phase term due to the distance r_i between the i-th sensor and the point r. Let us define a set of vectors

$$\underline{m}_i = \begin{pmatrix} e^{-jk_1 r_i} \\ \vdots \\ e^{-jk_n r_i} \\ \vdots \\ e^{-jk_M r_i} \end{pmatrix} \qquad \text{[Eq. 11]}$$

i.e. vectors describing the array geometry, [Eq. 10] can be written

$$x_i = \underline{m}_i^*\ \underline{A}\ \underline{v}\ e^{-j\omega t}\ . \qquad \text{[Eq. 12]}$$

Defining a matrix

$$\underline{M}^* \equiv \begin{pmatrix} \underline{m}_1^* \\ \vdots \\ \underline{m}_i^* \\ \vdots \\ \underline{m}_N \end{pmatrix} \qquad \text{[Eq. 13]}$$

we get the vector equation

$$\underline{x} = \underline{M}^* \, \underline{y}(t) = \underline{M}^* \, \underline{A} \, \underline{v} \cdot e^{-j\omega t} \, . \qquad \text{[Eq. 14]}$$

$\underline{x}$ is now the vector of received signals at the outputs of a horizontal array. For the particular case of an equally-spaced array one gets

$$r_i = d \cdot i \cdot \cos\beta, \qquad \text{[Eq. 15]}$$

where β is the bearing between source and array axis. In particular, $\beta = 90°$ means broadside. Equation 14 now represents the model for point sources used throughout this report. It is a product of a random part due to randomness of the medium ($\underline{v}$), a deterministic part of the sound field $\underline{A}$, which will be determined by the normal mode program, and a geometric part $\underline{M}^*$ describing the particular array.

The covariance matrix of received signals now becomes

$$\underline{R} = E\{\underline{x} \, \underline{x}^*\} = E\{\underline{M}^* \, \underline{A} \, \underline{v} \, \underline{v}^* \, \underline{A}^* \, \underline{M}\} = \underline{M}^* \, \underline{A} \, \underline{V} \, \underline{A}^* \, \underline{M}. \qquad \text{[Eq. 16]}$$

The matrix $\underline{R}$ is positive definite if

1) $\underline{V}$ is positive definite,
2) the rank of $\underline{A}$ is not less than N,
3) the rows of $\underline{M}^*$ are linearly independent,
4) M>N, i.e. there are more arrivals than sensors, otherwise it is positive semi-definite.

The rank of $\underline{A}$ is equal to M if none of the modal amplitudes ϕ_n is zero. Condition 3 is satisfied if all arrivals come from different directions, which is verified if the modal wavenumbers k_n are different. Condition 1

is satisfied if $\underline{v}$ is a random vector. In particular, if ϕ_n is uniformly distributed, the products $e^{j\phi_n}\ e^{-j\phi_m}$ become uncorrelated, i.e.

$$\underline{V} = \underline{I} \quad , \qquad \text{[Eq. 17]}$$

$\underline{I}$ being the unity matrix. In this case $\underline{V}$ is of course positive definite. If, however, $\phi_n = \phi_m$ for all n,m, one achieves

$$\underline{V} = \underline{U} \ , \qquad \text{[Eq. 18]}$$

which is a matrix containing only the value one

$$\underline{U} \equiv \begin{pmatrix} 1 & 1 & 1 & . & . & . \\ 1 & 1 & 1 & . & . & . \\ 1 & 1 & 1 & . & . & . \\ . & . & . & & & \\ . & . & . & . & & \end{pmatrix} \ . \qquad \text{[Eq. 19]}$$

This is the case of complete coherence among modes, and $\underline{V}$, and hence $\underline{R}$, becomes positive-semi-definite, i.e. the received signals are deterministic.

The matrix $\underline{R}$ may become positive semidefinite even by another reason. At broadside direction, i.e. $\beta = 90°$ [Eq. 12] becomes

$$r_{i,\ell} = d\cdot(i-\ell)\cdot\cos\beta = 0,$$

so that the vectors $\underline{m}_i$ as defined in Eq. 10 become

$$\underline{m}_i = e^{j\omega t} \begin{pmatrix} e^{-jk_1 r_o} \\ \vdots \\ e^{-jk_n r_o} \\ \vdots \\ e^{-jk_M r_o} \end{pmatrix} \qquad \text{[Eq. 20]}$$

for all i. Assume, for simplicity, equal modal amplitudes, i.e. $\underline{A} = \underline{I}$, and uncorrelated modes, i.e. $\underline{V} = \underline{I}$. Hence one gets

$$\underline{K} = \underline{M}^* \ \underline{I} \ \underline{I} \ \underline{I} \ \underline{M} \ = \ \underline{M}^*\underline{M}.$$

Since by Eq. 20

$\underline{m}_i^* \ \underline{m}_k = N$, for all i,k, one gets

$$\underline{K} = \begin{pmatrix} N & N & N & . & . & . \\ N & N & . & . & . & . \\ . & . & . & . & . & . \\ . & . & . & . & . & . \end{pmatrix} = N \ \underline{U} \ , \qquad \text{[Eq. 21]}$$

which is again a dyadic like Eq. 20. Consequently, any point source appears to the array as a coherent plane wave at broadside.

2.3 Numerical Examples

The modal amplitudes $a_1 \ldots a_M$ and the modal wavenumbers $k_1 \ldots k_M$, which are needed for calculation of the elements of $\underline{M}$ and $\underline{A}$ in Eq. 16, are computed by the SNAP-program *[12]*. As the normal-mode program is entirely deterministic, some additional assumptions have to be made on the random part of the covariance matrix $\underline{K}$, i.e. the matrix $\underline{V}$ that contains the normalized correlation values between modes. It is assumed throughout this report that different modes are uncorrelated among each other, i.e. $\underline{V} = \underline{I}$ [assumption of Sect. 1.6]. Nevertheless, comparison between the cases of total coherence and of no coherence between different arrivals can easily be made by comparing results achieved for broadside direction with other directions. At broadside (as pointed out in the previous chapter) any point source appears to be a plane wave, independently of the coherence among modes.

It is the major purpose of this report to find appropriate receiver structures, i.e. to consider different kinds of array processors and vary the system parameters (such as the number of hydrophones, spacing, bandwidth etc.) rather than to discuss special characteristics of the medium. Therefore, only a few typical examples are chosen in order to keep the investigation within reasonable limits.

Two sound-speed profiles are considered. One of them (Fig. 1a) is almost an isovelocity profile, as may happen under winter conditions. The other is a typical summer profile (Fig. 1b).

In addition, three frequencies are considered (200, 800, and 3200 Hz). So six different outputs of the SNAP program are used as input for the signal processing. Different assumptions are made for target and noise source: noise sources are supposed to be located at 1 km from the array (which is just enough to satisfy the far-field condition) and at 2 m depth, thus modelling surface ships, in particular the towing ship of a towed-array

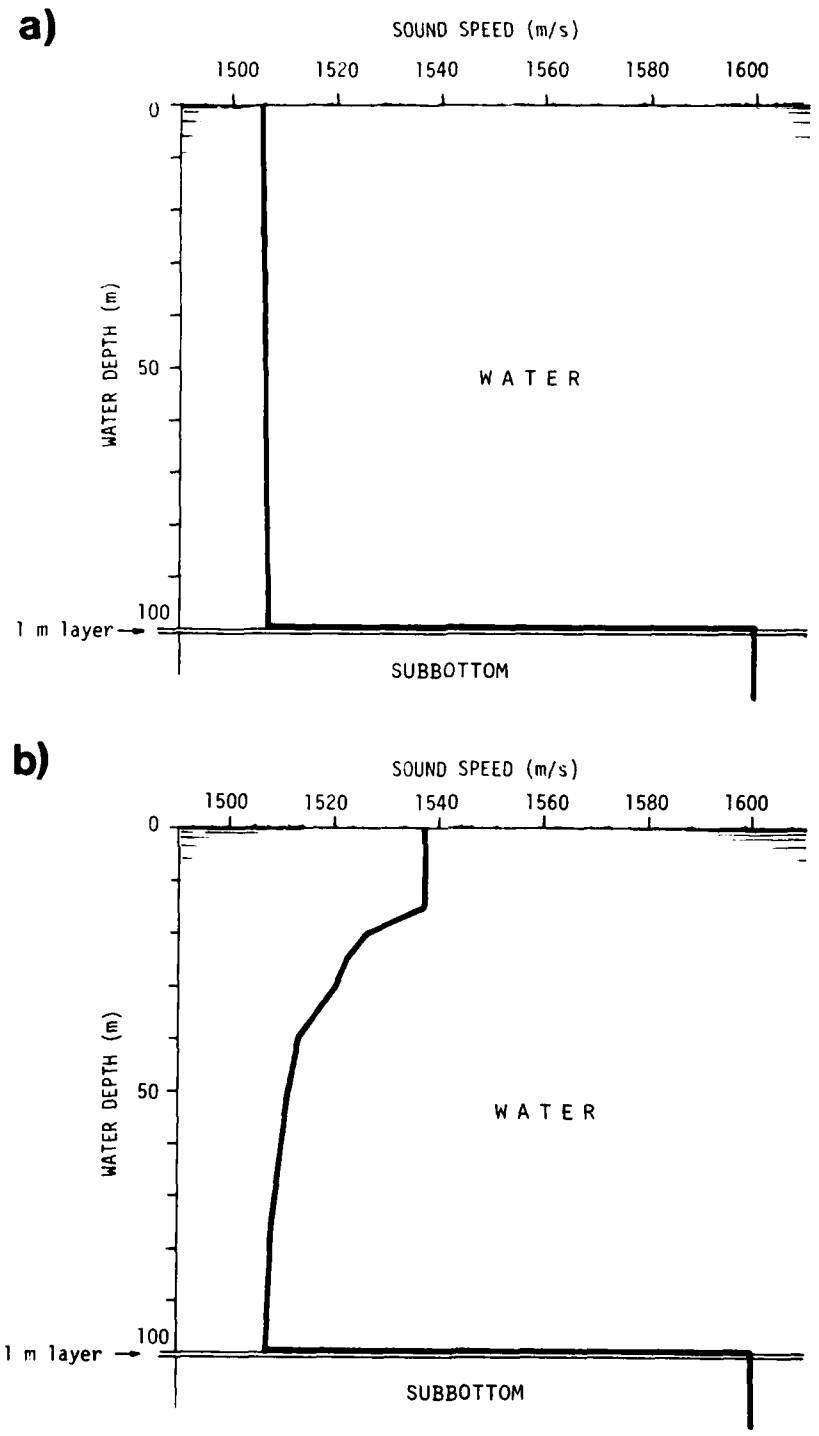

FIG. 1 SOUND-SPEED PROFILES

a) Winter (SVP1)
b) Summer (SVP2)

sonar. The target is supposed to be a submarine at 50 m depth and 10 km range. Therefore, 12 outputs of the SNAP program are required, which are presented in Figs. 2 to 13. The plots show the modal amplitudes (in logarithmic scale) versus the vertical angle of arrival at the array. The vertical angle is defined by $\cos\gamma = k_n/k_o$, where $k_o = \omega/c(z)$, where $c(z)$ is the sound speed at the array depth.

A few details are worth special note. The summer profile causes the noise energy to arrive only from a vertical angle interval between roughly 10° and 20°. It can therefore be expected that at endfire direction some detections may be made even though there is a noise source (e.g. towing ship), provided that the energy distribution of the target covers the vertical angle interval from 0° to 10°. This may happen when the target is at a range or depth different from that of the noise source, which is the case in the examples chosen (compare Figs. 6 and 7).

Another point is that, at high frequencies, modes tend to form bunches, see Fig. 13, for example. That means that the ratio between water depth and wavelength is such that we are already at the border between mode and ray theory.

2.4 Wide-Angle Noise

For wide-angle noise a simple, well-known model is used. Suppose a certain bearing interval is given by the directional cosines $u_m - u_o \ldots u_m + u_o$, such that the interval is $2u_o$. Let us assume that plane waves are continuously and uniformly distributed over the interval. Hence a single sensor receives the signal

$$x(t) = \int_{u_m-u_o}^{u_m+u_o} a(u)\exp(j(kr-\omega t))du.$$

The spatial correlation coefficient between the locations r and r + d becomes

$$\rho(d) = E\{x_r(t) \cdot x^*_{r+d}(t)\}$$

$$= E\{ \int_{u_m-u_o}^{u_m+u_o} a(u) \cdot \exp(j(k_r-\omega t)du\} \cdot \int a^*(v) \exp(j(k(r+d)-\omega t)dv\}$$

$$= E\{\int a(u)du \int a^*(v)\exp(-jkdv)dv\}.$$

Assuming uncorrelated arrivals within the interval, i.e.

$$E\{a(u)a^*(v)\} = \frac{1}{u_o} \quad u = v$$

$$= 0 \quad u \neq v$$

one gets

$$\rho(d) = \frac{1}{u_o} \int_{u_m-u_o}^{u_m+u_o} \exp(-jkdv)dv$$

$$\rho(d) = 2 \frac{\sin(kdu_o)}{kdu_o} \cdot \exp(jkdu_m) \qquad \text{[Eq. 22]}$$

For an equally spaced array the elements of the covariance matrix become

$$\rho(i-\ell) = \frac{\sin(k \cdot d \cdot (i-\ell) \cdot u_o)}{kd(i-\ell)u_o} \cdot \exp(-jkd(i-\ell)u_m) \qquad \text{[Eq. 23]}$$

For $u_m = 0$ and $u_o = 1$ one gets the particular case of isotropic noise.

2.5 White Noise

Spatially white noise is simply given by

$$\underline{R}_w = P_w \underline{I} \ , \qquad \text{[Eq. 24]}$$

P_w being the white-noise power.

2.6 Conclusions on Signal and Noise Models

a. The vertical spread of the signal energy of a point source in shallow water appears as a horizontal spread projected on the horizontal array. The horizontal spread is proportional to the cosine of the bearing, e.g. it is equal to zero for broadside direction. The spread is asymmetrical. The true position of the source is at the left edge of the signal spread area for $\beta < 90°$ and at the right edge for $\beta > 90°$. Therefore, position finding by looking for the energy maximum (beamformer) or energy minimum by split-beam technique is misleading for directions other than broadside.

b. The unsymmetrical spread is a property of the linear horizontal array. A horizontal circular array will have a symmetric horizontal energy spread.

c. Any broadside signal (random in time and space) appears to the linear array as a coherent plane wave. At other directions the wavefront appears to be random if the phases between modes are random. The wavefront is non-plane in the mean. If modes are correlated among each other (constant phase) the wavefront is non-plane and coherent.

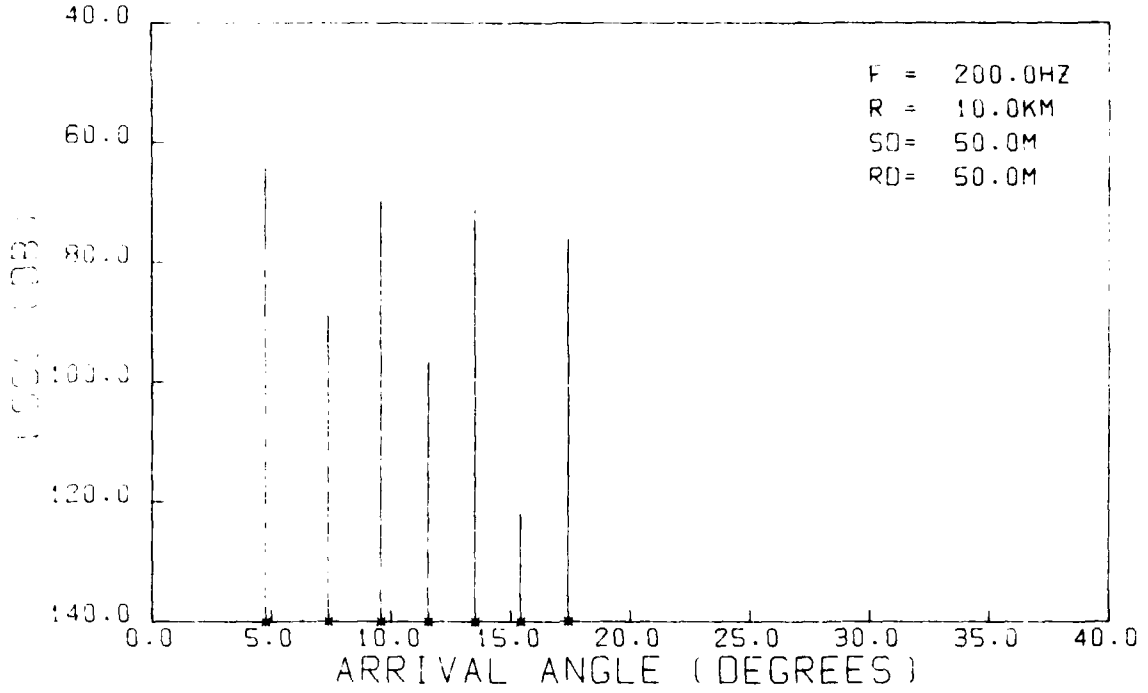

FIG. 2 VERTICAL ENERGY DISTRIBUTION OF TARGET (SUMMER PROFILE)

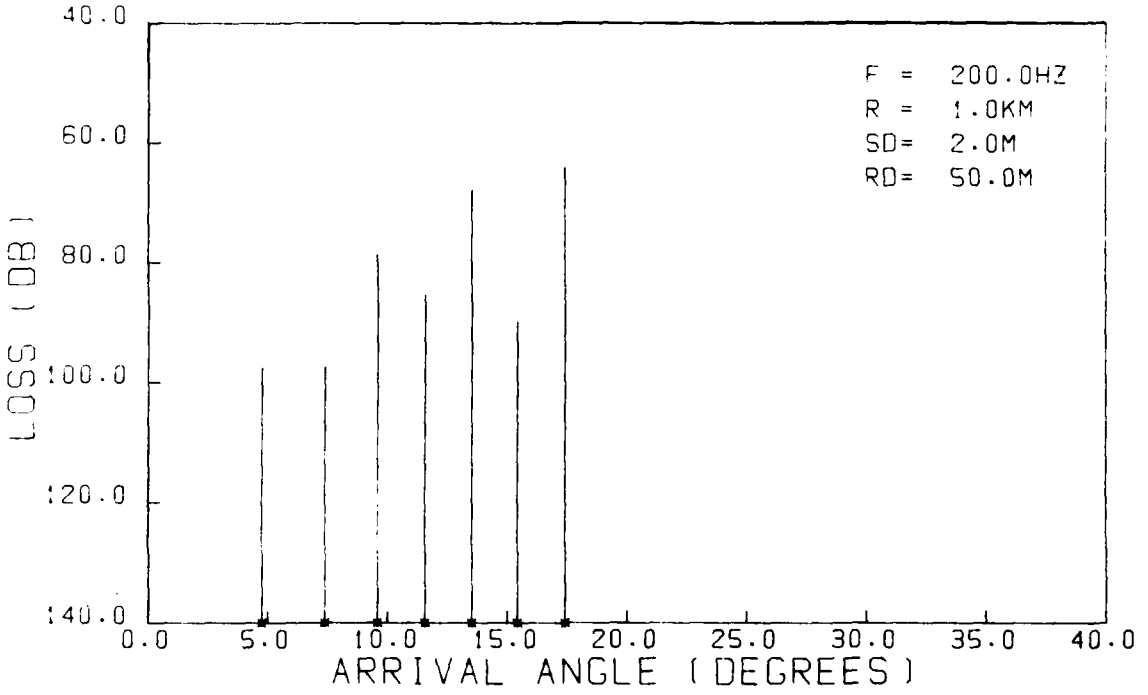

FIG. 3 VERTICAL ENERGY DISTRIBUTION OF INTERFERENCE (SUMMER PROFILE)

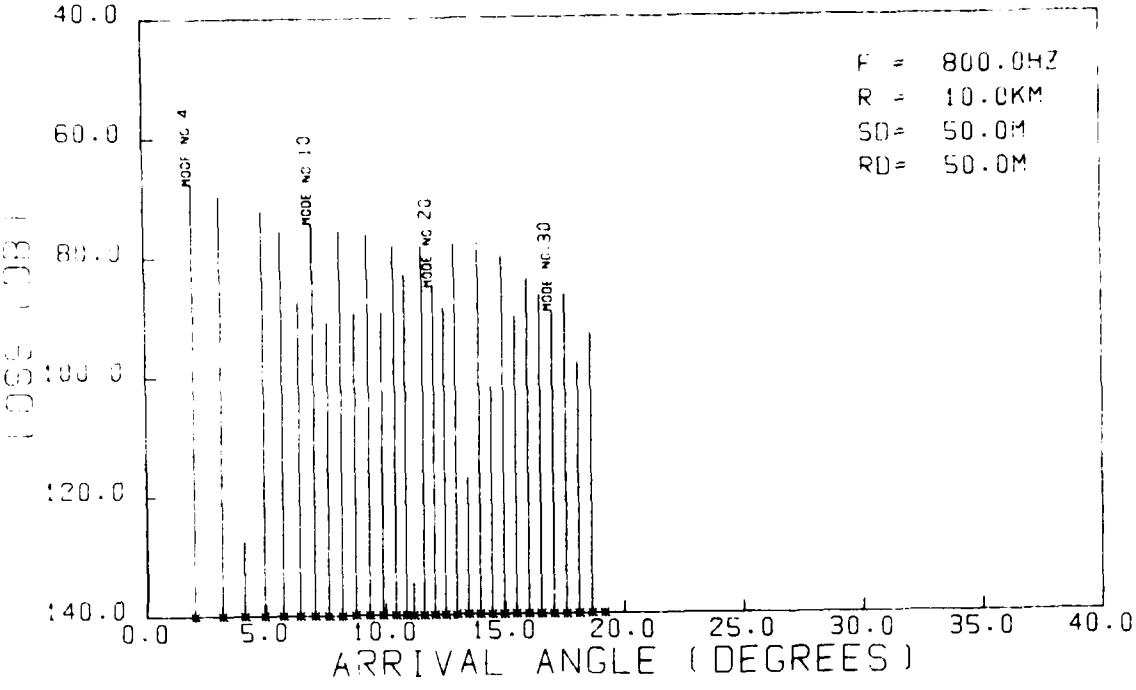

FIG. 4 VERTICAL ENERGY DISTRIBUTION OF TARGET (SUMMER PROFILE)

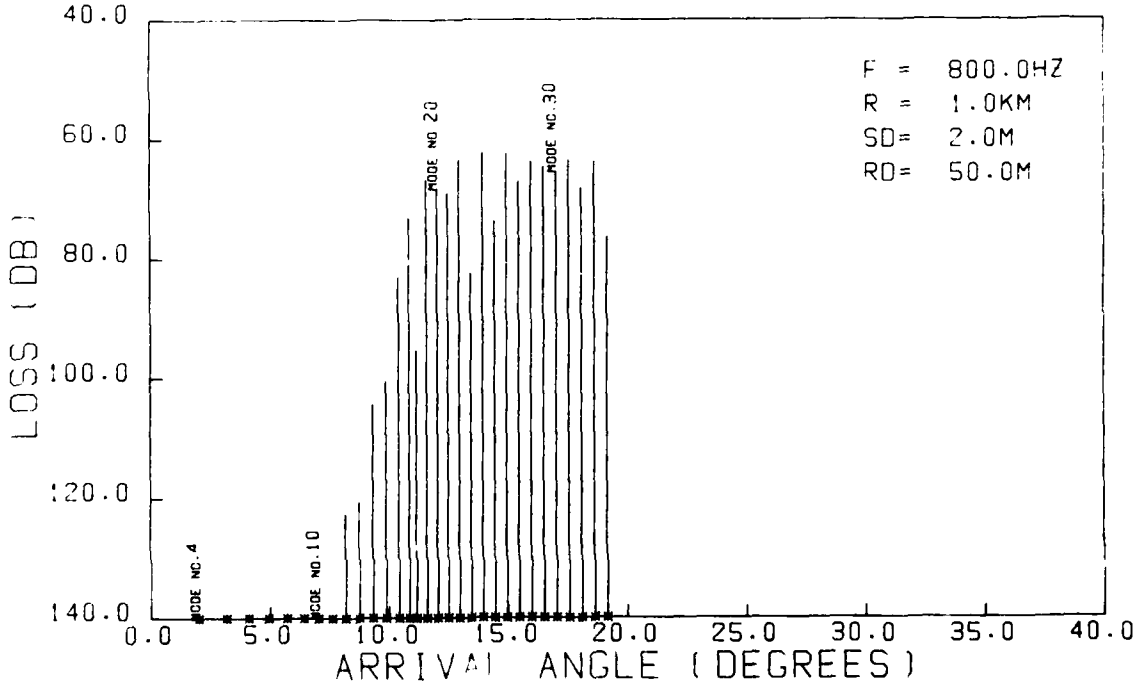

FIG. 5 VERTICAL ENERGY DISTRIBUTION OF INTERFERENCE (SUMMER PROFILE)

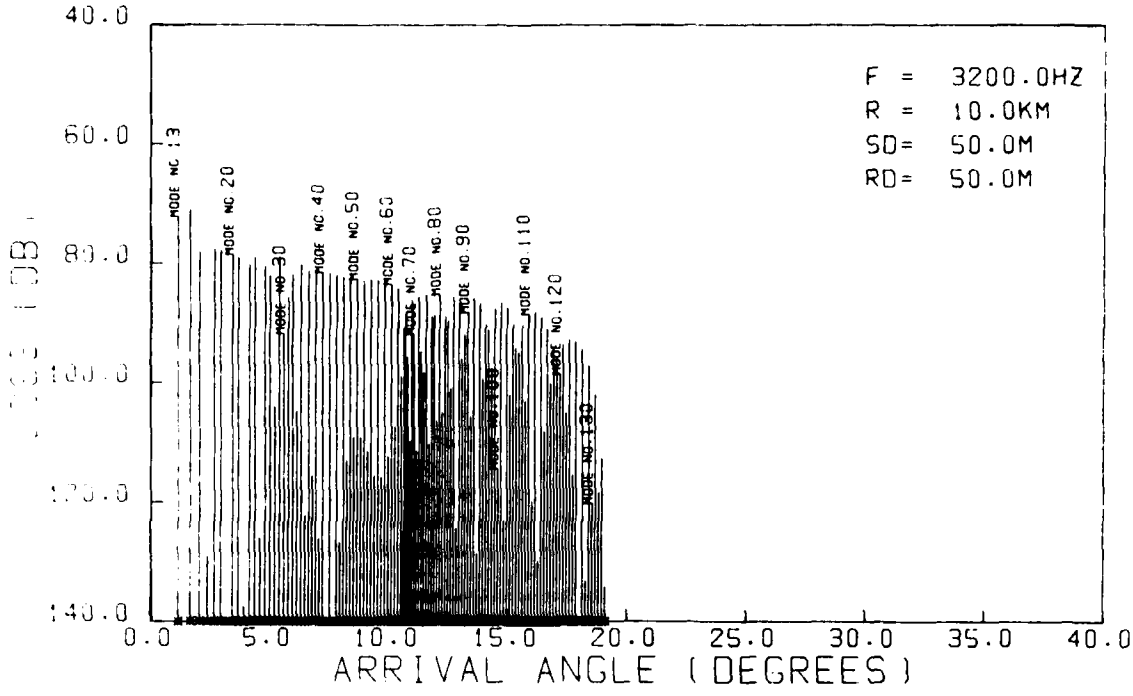

FIG. 6 VERTICAL ENERGY DISTRIBUTION OF TARGET (SUMMER PROFILE)

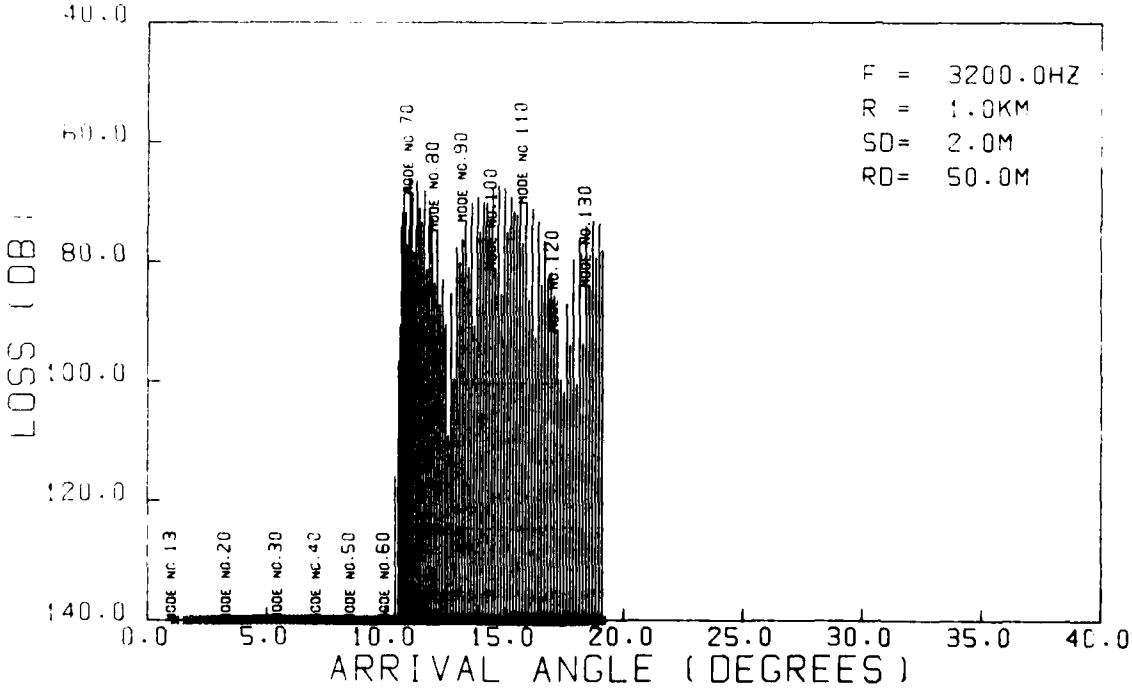

FIG. 7 VERTICAL ENERGY DISTRIBUTION OF INTERFERENCE (SUMMER PROFILE)

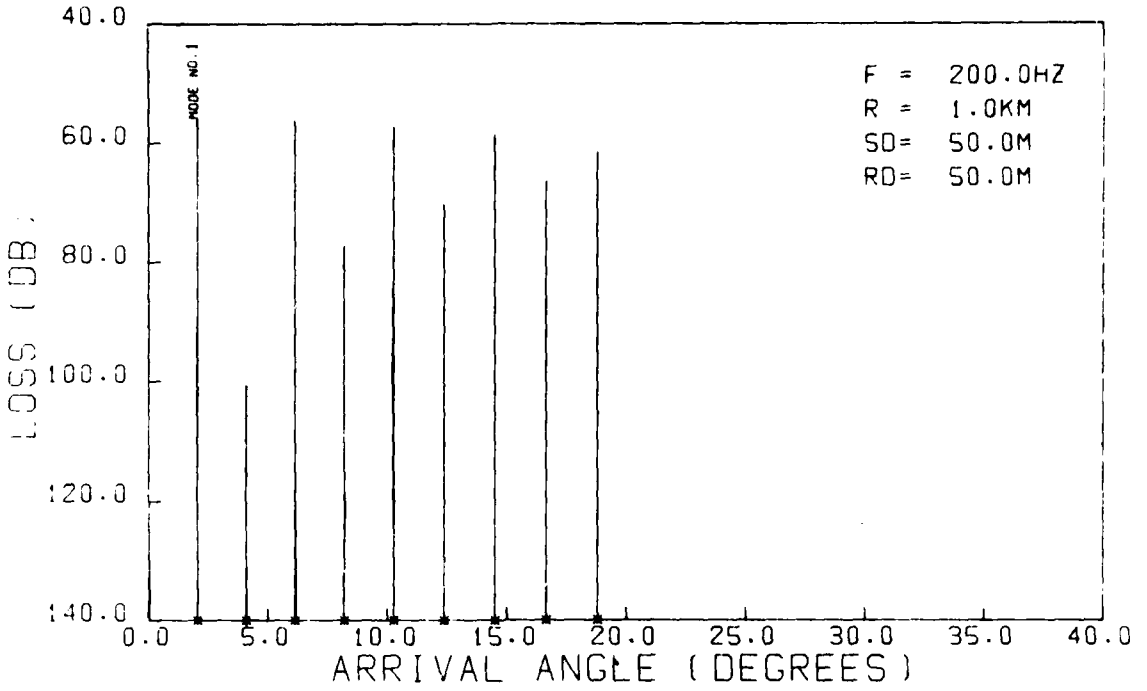

FIG. 8 VERTICAL ENERGY DISTRIBUTION OF TARGET (WINTER PROFILE)

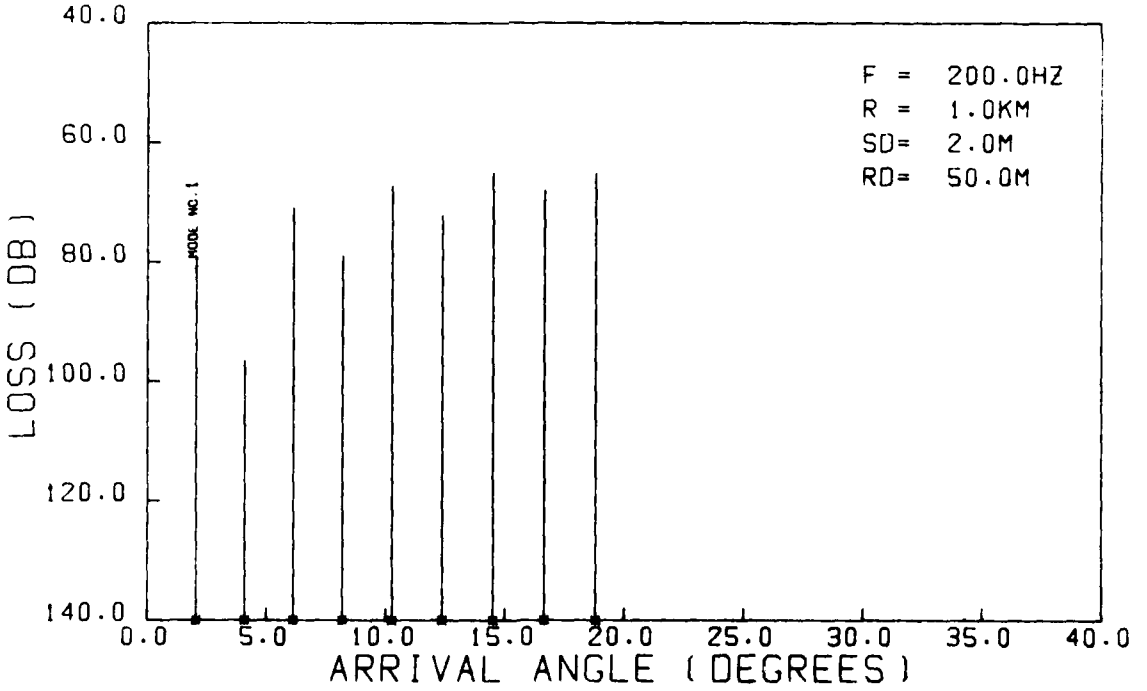

FIG. 9 VERTICAL ENERGY DISTRIBUTION OF INTERFERENCE (WINTER PROFILE)

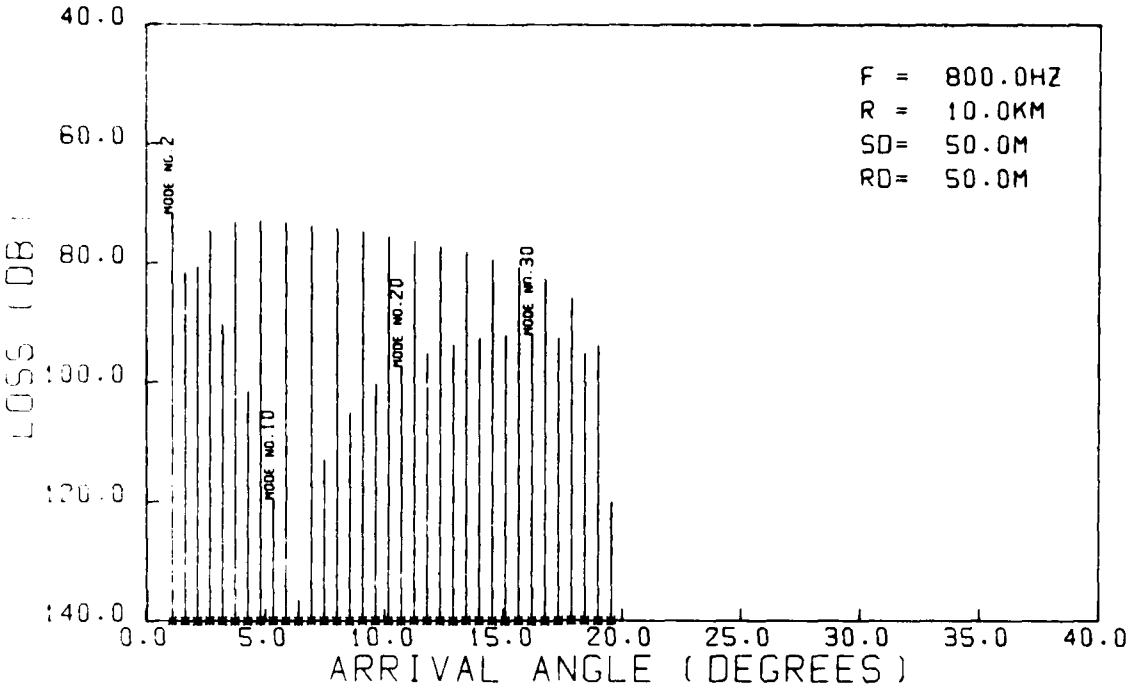

FIG. 10 VERTICAL ENERGY DISTRIBUTION OF TARGET (WINTER PROFILE)

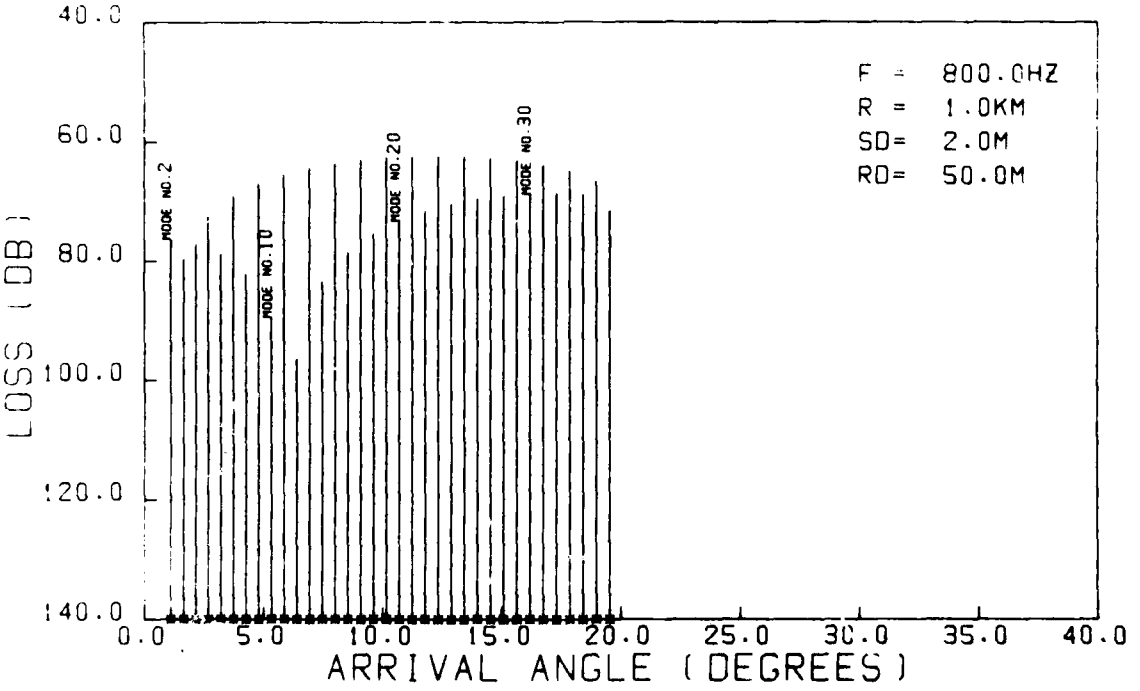

FIG. 11 VERTICAL ENERGY DISTRIBUTION OF INTERFERENCE (WINTER PROFILE)

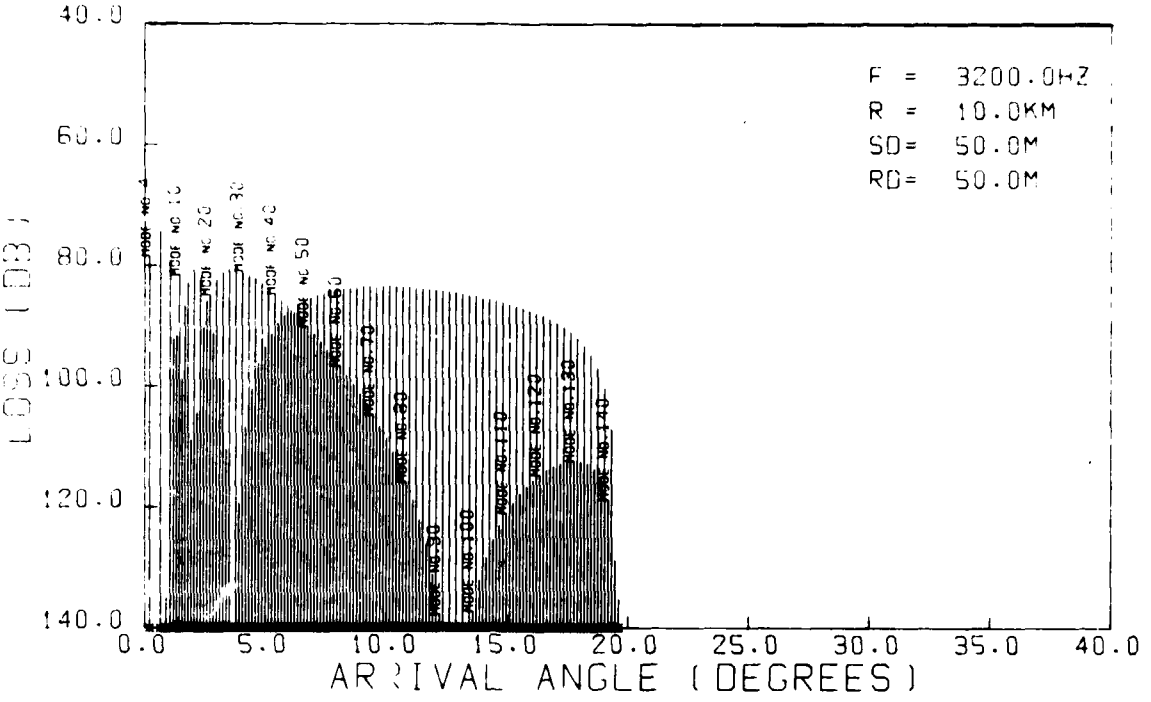

FIG. 12 VERTICAL ENERGY DISTRIBUTION OF TARGET (WINTER PROFILE)

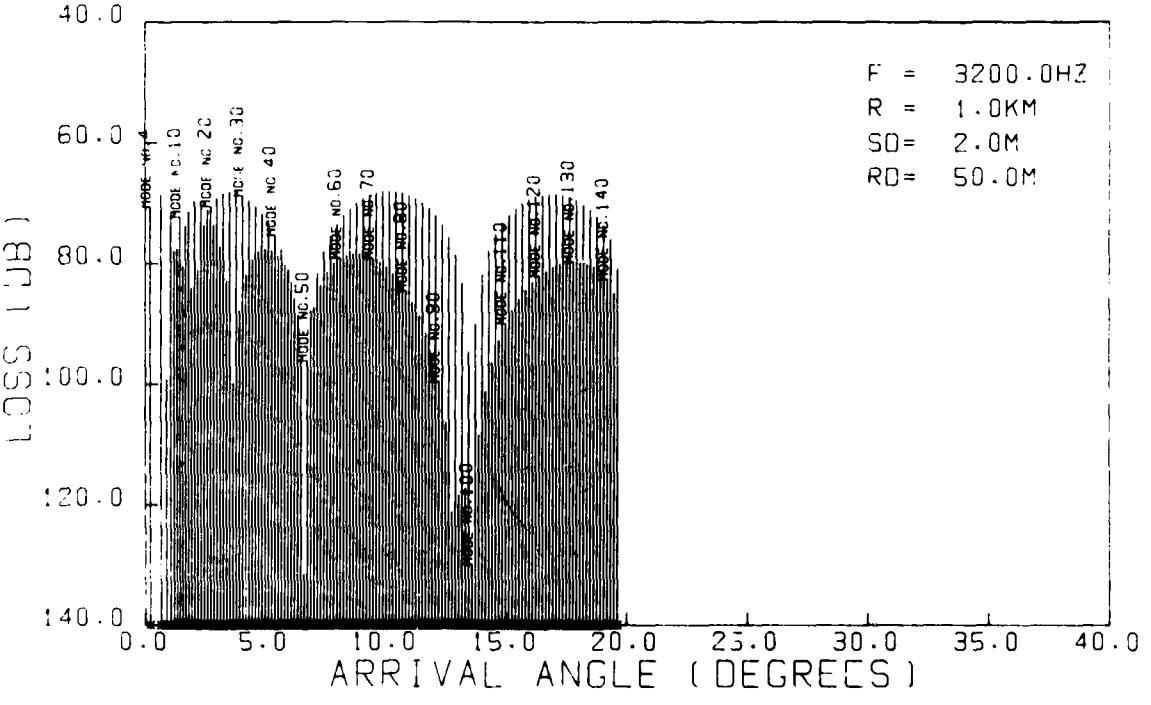

FIG. 13 VERTICAL ENERGY DISTRIBUTION OF INTERFERENCE (WINTER PROFILE)

3 THE OPTIMUM QUADRATIC PROCESSOR (OQP)

3.1 General Description

The quadratic processor discussed in this chapter is given by the quadratic (or hermitian) form

$$\ell \equiv \underline{x}^* \, \underline{K} \, \underline{x} \;\underset{>}{\overset{<}{}}\; n \,, \qquad \text{[Eq. 25]}$$

where $\underline{x}$ is the vector of input signals:

$$\underline{x} = \underline{s} + \underline{n} \quad \text{or}$$
$$= \underline{n}.$$

If ℓ exceeds a given threshold n, the hypothesis of "target plus noise" is accepted, "noise alone" otherwise. For gaussian signal and noise the quadratic form [Eq. 25] can be optimized in the likelihood ratio sense (Bayes or Neyman-Pearson) by setting

$$\underline{K} = \underline{Q}^{-1} - (\underline{P} + \underline{Q})^{-1}, \qquad \text{[Eq. 26]}$$

where $\underline{Q} = E\{\underline{n}\,\underline{n}^*\}$ and $\underline{P} = E\{\underline{s}\,\underline{s}^*\}$ are the covariance matrices of noise and signal respectively. This processor, however, is not very useful for practical applications because, due to the sum $\underline{Q} + \underline{P}$ in Eq. 26, the absolute power levels of noise and signal have to be known *a priori*. The signal power is usually unknown because it depends on various unknown parameters, such as target strength, range, aspect angle, and transmission loss of the channel. Replacing Eq. 26 in Eq. 25 by

$$\underline{K} = \underline{Q}^{-1} \, \underline{P} \, \underline{Q}^{-1} \qquad \text{[Eq. 27]}$$

we get a processor that is insensitive to the signal power, provided that $\underline{Q}$ and $\underline{P}$ are Toeplitz and hence the diagonal terms of $\underline{Q}$ and $\underline{P}$ are constant (which is done for the horizontal detection problem, see the assumption of Sect. 1.4). Any choice of the signal power (diagonal elements of $\underline{P}$) is equivalent to a constant factor on the detection threshold n in Eq. 25. The processor (Eqs. 25 & 27) maximizes the signal-to-noise ratio for

gaussian noise and arbitrary signal. It can, furthermore, be interpreted as a small signal approximation of the likelihood-ratio processors (Eqs. 25 & 26).

For an array with N hydrophones and T time samples taken from each channel the input signal vector will become

$$\underline{x} \equiv \begin{pmatrix} \underline{x}(t_1) \\ \underline{x}(t_2) \\ \cdot \\ \cdot \\ \underline{x}(t_T) \end{pmatrix} = \begin{pmatrix} \underline{S}(t_1) \\ \underline{S}(t_2) \\ \cdot \\ \cdot \\ \underline{S}(t_T) \end{pmatrix} + \begin{pmatrix} \underline{n}(t_1) \\ \underline{n}(t_2) \\ \cdot \\ \cdot \\ \underline{n}(t_T) \end{pmatrix} \qquad \text{[Eq. 28]}$$

where $\underline{x}(t_i)$ contains the output signals of all sensors at time t_i. Some simplification can be achieved by subjecting the time sequences of all sensors to spectral analysis and perform filtering and detection in the frequency domain (space/frequency representation) instead of applying the processor [Eq. 25] to the time-space signal vector [Eq. 28]. The crucial step in Eq. 27 is the matrix inversion even when using a special algorithm for Toeplitz matrix inversion, e.g. *[17]*, or replacing the inversion by some adaptive algorithm, e.g. *[6,7,8,18]*. After multichannel spectral analysis Eq. 28 becomes

$$\underline{x} \equiv \begin{pmatrix} \underline{x}(f_1) \\ \underline{x}(f_2) \\ \cdot \\ \cdot \\ \underline{x}(f_F) \end{pmatrix} = \begin{pmatrix} \underline{s}(f_1) \\ \underline{S}(f_2) \\ \cdot \\ \cdot \\ \underline{S}(f_F) \end{pmatrix} + \begin{pmatrix} \underline{n}(f_1) \\ \underline{n}(f_2) \\ \cdot \\ \cdot \\ \underline{n}(f_F) \end{pmatrix} \qquad \text{[Eq. 29]}$$

which is the space/frequency representation of the received signals. Due to the assumption of Sect. 1.4, signals of different frequencies are uncorrelated, i.e.

$$E\{x(f_i)\, x^*(f_k)\} = 0$$

$$E\{\underline{x}(f_i)\, \underline{x}^*(f_k)\} = \underline{0}, \quad i \neq k \ .$$

Therefore, covariance matrices of signal and noise become block-diagonal:

$$\underline{P} = \begin{pmatrix} \underline{P}(f_1) & & & \\ & \underline{P}(f_2) & & 0 \\ & & \ddots & \\ 0 & & & \underline{P}(f_F) \end{pmatrix}$$

and [Eq. 30]

$$\underline{Q} = \begin{pmatrix} \underline{Q}(f_1) & & & \\ & \underline{Q}(f_2) & & 0 \\ & & \ddots & \\ 0 & & & \underline{Q}(f_F) \end{pmatrix}$$

where

$$\underline{P}(f_i) = E\{\underline{s}(f_i)\underline{s}^*(f_i)\}$$

$$\underline{Q}(f_i) = E\{\underline{n}(f_i)\underline{n}^*(f_i)\} .$$

Normalization of the submatrices gives

$$\underline{Q} = \begin{pmatrix} \underline{Q}_s(f_1) & & & \\ & \underline{Q}_s(f_2) & & 0 \\ & & \ddots & \\ 0 & & & \underline{Q}_s(f_F) \end{pmatrix} \begin{pmatrix} \underline{Q}_f(f_1) & & & \\ & \underline{Q}_f(f_2) & & 0 \\ & & \ddots & \\ 0 & & & \underline{Q}_f(f_F) \end{pmatrix} \qquad \text{[Eq. 31]}$$

$$= \underline{Q}_s \cdot \underline{Q}_f ,$$

thus factorizing $\underline{Q}$ in a spatial and a frequency dependent part. The $\underline{Q}_f(f_i)$ are simply

$$\underline{Q}_f(f_i) = q(f_i) \cdot \underline{I}, \qquad \text{[Eq. 32]}$$

$q(f_i)$ being the discrete power spectrum and $\underline{I}$ the unity matrix. The same is valid of course for the signal:

$$\underline{P} = \underline{P}_s \ \underline{P}_f \quad \text{and} \quad \underline{P}_f(f_i) = p(f_i) \ \underline{I}.$$

Furthermore, $\underline{P}$ can be factorized in the following way:

$$\underline{P} = \underline{H}_s\underline{H}_f\underline{H}_f^*\underline{H}_s^* , \qquad \text{[Eq. 33]}$$

where

$$\underline{P}_s = \underline{H}_s \underline{H}_s^* \quad \text{and} \quad \underline{P}_f = \underline{H}_f \underline{H}_f^*$$

$$P_s(f_i) = H_s(f_i) H_s^*(f_i) \quad \text{and} \quad \underline{P}_f(f_i) = \underline{H}_f(f_i) \underline{H}_f^*(f_i).$$

Now the detection rule [Eq. 25] can be written:

$$\ell \equiv \underline{x}^* \, \underline{Q}_s^{-1} \underline{Q}_f^{-1} \, \underline{H}_s \underline{H}_f \underline{H}_f^* \underline{H}_s^* \, \underline{Q}_f^{-1} \underline{Q}_s^{-1} \, \underline{x}$$

or, equivalently,

$$\ell \equiv \left| \underline{x}^* \, \underline{Q}^{-1} \, \underline{Q}^{-1} \, \underline{H}_s \underline{H}_f \right|^2 . \qquad \text{[Eq. 34]}$$

Equation 33 can be interpreted as follows: the received signal vector $\underline{x}^*$ is multiplied by the spatial part of the inverse covariance matrix $\underline{Q}_s^{-1}$. As $\underline{Q}$ and $\underline{Q}^{-1}$ are hermitian and positive definite, they can be factorized

$$\underline{Q}_s^{-1} = \underline{K} \, \underline{K}^* . \qquad \text{[Eq. 35]}$$

$\underline{K}$ is a spatial whitening filter. $\underline{K}^*$ matches the subsequent processing to the target signal $\underline{s}^*$ contained in $\underline{x}^*$, which is now distorted by multiplication with $\underline{K}$. $\underline{Q}_f^{-1}$ contains just the inverse power spectrum of the noise $1/q(f_i)$:

$$\underline{Q}_f^{-1} = \begin{pmatrix} 1/q_1 & & & & & & \\ & \ddots & & & & & \\ & & 1/q_1, & & & & \\ & & & 1/q_2 & & & \\ & & & & \ddots & & \\ & & & & & 1/q_F & \\ & & & & & & \ddots \\ & & & & & & & 1/q_F \end{pmatrix}$$

Factorizing $\underline{Q}_f^{-1}$ similarly to Eq. 35 gives a product of two diagonal matrices where the elements are given by

$$\frac{1}{q_i} = \frac{1}{a_i} \, \frac{1}{a_i^*} . \qquad \text{[Eq. 36]}$$

The factors $1/a_i$ represent the transmission characteristic of a spectral whitening filter, the $1/a_i^*$ again match the subsequent processing to the distortion of the signal $\underline{s}^*$ achieved by the spectral whitening filter $1/a_i$.

The matrix $\underline{H}_s$ represents a generalized spatial matched filter (generalized beamformer) matched to a random wavefront $\underline{s}^*$. The coefficient h_i contained in the diagonal matrix

$$\underline{H}_f \equiv \begin{pmatrix} h_1 & & & & & & 0 \\ & \ddots & & & & & \\ & & h_1, h_2 & & & & \\ & & & \ddots & & & \\ & & & & h_2, & & \\ & & & & & \ddots & \\ 0 & & & & & & h_F \end{pmatrix}$$

represent the transmission characteristic of a filter matched to the power spectrum of the signal. A block diagram of the processor [Eq. 34] is shown in Fig. 14. The input signals are subjected first to spectral analysis by means of a narrowband filter bank (NFB). After the NFB, spatial processing is performed separately for each frequency. After whitening and matching in space and time, all signal components are integrated incoherently.

As this report discusses only the spatial part of the detection problem, just one branch of the processing scheme is considered (see narrowband array processor box) in the following. The results, therefore, are applicable directly to narrowband (i.e. active) systems, observing the bandwidth constraints discussed in Ch. 8.

An appropriate measure for judging the performance of an array and the subsequent array processor is the gain in signal-to-noise ratio at the processor output compared with that at a single sensor. For the quadratic processor the gain has been derived in *1* :

$$G = \frac{\mathrm{tr}(\underline{F}^* \underline{P} \underline{F})}{\sqrt{\mathrm{tr}(\underline{F}^* \underline{Q} \underline{F})}} \cdot \frac{P_n}{P_s}, \qquad \text{[Eq. 37]}$$

P_n and P_s being the powers of noise and signal respectively.

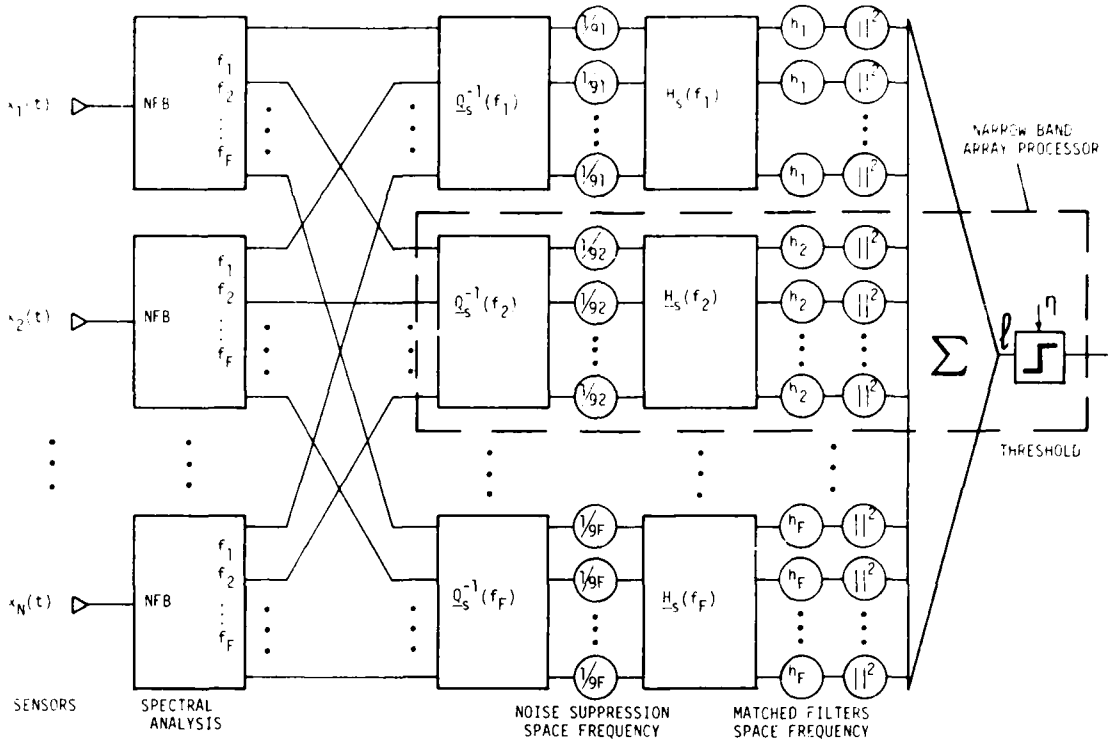

FIG. 14 QUADRATIC BROADBAND ARRAY PROCESSOR

The matrix $\underline{F}$ describes the array processor and is defined by

$$\underline{K} = \underline{F}\,\underline{F}^{*}.$$

In particular, one gets for the optimum quadratic processor

$$\underline{K} = \underline{Q}^{-1}\,\underline{H}\,\underline{H}^{*}\,\underline{Q}^{-1},$$

so that $\underline{F} = \underline{Q}^{-1}\,\underline{H}$, which is the spatial optimum filter. The gain for the optimum processor becomes

$$G_{OPT} = \sqrt{\mathrm{tr}(\underline{Q}^{-1}\,\underline{P})}.$$

3.2 Detection in the presence of Point-Shaped Interference

Figures 15 to 20 show the gain of the OQP in the presence of two interfering sources (0° and 90°). Different curves of each plot are due to different numbers of hydrophones N. Different plots refer to different (summer and winter) sound-speed profiles and to different frequencies (200, 800 and 3200 Hz). Additional white noise is assumed to be 20 dB below the power level of the interfering sources. The spacing between sensors is 0.5λ. Two interfering sources were chosen in order to demonstrate how the vertical spread of signals and noise depends on bearing. The broadside source appears in its real shape (i.e. point shaped) whereas at endfire the total spread of the interfering source is perceived by the array. Suppression of point sources has been treated repeatedly in literature. The more interesting problem seems to be the suppression of interference radiating from endfire direction. In practice this problem arises particularly in towed arrays, where the towing ship is an endfire noise source.

Comparing these six plots with one another, the general impression is that there are no significant differences. The curves differ only in the area of the endfire noise source according to the particular spatial energy distribution due to the sound-speed profile and the frequency. For instance, in Fig. 20 the noise source appears to be shifted by about 10° to 20° from above and below the array.

Therefore, under certain conditions, relatively high array gain can be achieved in the direction of an interfering source, provided that the

vertical energy distributions of target and interference are different. This can happen if target and interference are at different depth. This happens for instance in Fig. 20 (compare the vertical energy distribution of target and interference Figs. 6 and 7). If, however, the energy of both interference and signal are almost uniformly distributed between 0° and ±20° a broad gain minimum appears at endfire.

The plane horizontal parts denote the white-noise limitation. The maximum achievable gain is G_{max} = I/N + N (interference-to-noise ratio + white-noise gain of the array). It is achieved in all examples and depends more or less on the number of sensors, i.e. on the resolution of the array. The minimum at 180° is a "grating null", i.e. a periodic repetition of the minimum at 0° entering the visible domain. This is a consequence of the $\lambda/2$-spacing assumed. For slightly smaller spacing the grating null will vanish. As can be seen, the width and the depth of the grating null depends on spacing and array length as well.

At broadside (90°) a remaining gain of 3 dB is observed. This is the gain achieved in the direction of one interfering source over the second one at 0°. It can be shown in general that in the presence of M interfering sources with equal strength the gain in the direction of one of them approaches M if the white-noise component goes to zero.

This idea applies also to an interfering source distributed over a certain area. At any point inside the noisy area some gain is achieved over the rest of it. Therefore the gain in the direction of a distributed noise source will be higher than that in the direction of a point source.

However, there is still another effect that supports the detection performance in the noisy area. The matrix $\underline{H}_S$ (generalized spatial beamformer) provides spatial coherent integration of the signal, which is spread by the channel as well. If the spatial signal structure is different from that of the interference (as in Figs. 6 and 7) the gain in the interference direction may increase with increasing array length, because the resolution of the signal structure (i.e. approximation of the spatial covariance of the signal by a finite number of sensors) from the noisy background improves with increasing array length. Notice that at broadside the gain is independent of the array length.

Figure 21 shows a gain curve for N = 160 (One interfering source, 800 Hz, winter sound-speed profile). Approaching broadside, a slight increase in gain can be observed; the reason is simply that a point source at broadside appears to the horizontal array always as a coherent plane wave. Therefore the slight difference in gain between broadside and any other point in the white-noise-limited area can be considered to be the loss due to uncorrelated modes (Assumption of Sect. 1.7).

3.3 Wide-Angle Interference

Figures 22 to 26 show some examples for wide-angle interference as described by Eq. 23. The example in Fig. 22 shows the array gain for different numbers of sensors, N, and the interference uniformly distributed over about 35°. Additional white noise is supposed to be 20 dB below the interference level. Far away from the interference, the gain is limited by the white noise, e.g. the curve for N = 10 approaches 30 dB (20 dB I/N + 10 dB white-noise array gain). Very close to the interference the gain depends much more on the array length, i.e. the rectangular noise interval can be better approximated by the array as the number of degrees of freedom increases. However, for practice, even small arrays (e.g. N = 10) yield satisfying discrimination between target and interference.

Figure 23 shows gain curves for a 20-hydrophone array for interference areas of different widths. If the angle interval becomes 180° the noise is isotropic. For a $\lambda/2$-spaced array, isotropic noise is uncorrelated because the sinc-shaped spatial correlation function is sampled right at the zeros. Therefore, for 180°, just the white-noise gain is achieved (e.g. 13 dB for N = 20). For the other examples (11°, 23°, 60°) the maximum achievable gain (33 dB) is reached quite well outside the interference area.

Figures 24 and 25 show the gain for an array with 20 hydrophones spaced at 0.1λ. By choosing the spacing smaller than 0.5λ, isotropic noise is no longer uncorrelated between sensors.

This promises some more gain over isotropic noise than just the white-noise gain. In particular, the high correlation values of the main lobe of the sin x/x function have to be taken into account. Clearly, the resolution of

the array is much poorer (if N is kept constant); therefore the performance in the vicinity of the interference is worse than before (see Fig. 23). For the isotropic case (180°) little improvement over the white-noise gain can be observed, particularly at endfire and backfire (0° and 180°). This is due to the fact that, for the geometry of a line array, isotropic noise appears to be broadside rather than endfire (in particular, the spatial correlation function is real, like that of a source at broadside). Figure 26 shows curves for different power ratios of directional to omni noise.

3.4 Suboptimum Generalized Beamformers

The application of the OQP requires the *a priori* knowledge of the spatial covariance matrix of the signal for designing the generalized beamformer (or matrix matched filter) $\underline{H}_S$. This knowledge is usually not available and must be achieved somehow. One way is to run a modelling program with the actual channel parameters. Alternatively, an auxiliary source may be used for transmission of test signals. Signal covariance matrices have to be estimated and stored for all ranges and bearings. This is a cumbersome procedure and not feasible in practice, particularly not under changing environmental conditions.

Another, simpler approach is to estimate the signal covariance matrix for just one point of the sound field in order to get an idea of what kind of signal spread has to be taken into account. For instance, in a towed array sonar the towing ship noise is well suited as test signal.

The next step is to use the function

$$\rho_{i\ell} = \frac{\sin[a_0(i-\ell)]}{a_0(i-\ell)} \; e^{jb_0(i-\ell)} \qquad \text{[Eq. 38]}$$

to approximate the measured signal correlation by varying the factors a_0 and b_0, thus replacing the actual signal spread by an equivalent angle interval with uniform energy distribution. The values a_0 and b_0 depend on the following quantitites

$$a_0 = d \cdot k \; \frac{u_0}{2} \cdot |\cos\beta_0| \qquad \text{[Eq. 39]}$$

$$b_0 = d \cdot k \cdot \cos\beta_0,$$

where β_o is the bearing of the test source and u_o the angle interval. If the position of the test source is unknown or not well known it will be achieved by varying b_o such that the spatial frequency term in Eq. 38 gives a best fit to the measured correlation function. Varying a_o so that the equivalent interval is a best fit to the signal spread gives an estimate for the angle interval u_o if $\cos\beta_o$ is known. Now the equivalent angle intervals can be calculated for other directions

$$a_n = d \cdot k(i-\ell) \frac{u_o}{2} \cdot |\cos\beta_n| . \qquad \text{[Eq. 40]}$$

Replacing a_o and b_o in Eq. 38 by a_i and $b_n = k(i-\ell) \cdot d \cdot \cos\beta_n$ gives the approximate signal covariance matrices for other directions, β_i.

This adaptive procedure may even be spared if some rough information about the signal spread is available (e.g. by averaging over a large number of different channels). In this case Eq. 38 can be directly applied for computing the beamformer matrix $\underline{H}_s$. Of course it may sometimes happen that there is some mismatch between $\underline{H}_s$ derived from Eq. 38 and the actual signal spread; which means that the angle interval, u_o, in Eq. 39 is chosen too small or too large. The effect of the mismatch of a generalized beamformer $\underline{H}_s$ to the width of a distributed signal is discussed in the following in some detail.

Suppose that the signal energy is uniformly distributed over an interval u that is the difference of two directional cosines

$$u = u_1 - u_2 .$$

The elements of the corresponding covariance matrix $\underline{P}$ have then the form

$$\rho_{i\ell} = \frac{\sin(k \cdot d \cdot (i-\ell) \cdot \frac{u}{2}}{k \cdot d(i-\ell) \frac{u}{2}} ,$$

if u is centred around broadside, which we assume here for simplicity. Consider a second matrix $\underline{R}$ with the elements

$$r_{i\ell} = \frac{\sin(d.k(i-\ell) \frac{v}{2}}{d \cdot k \cdot (i-\ell) \frac{v}{2}}$$

so that $v < u$. Suppose that $\underline{P}$ describes the signal and $\underline{R} = \underline{H}\,\underline{H}^*$ the generalized beamformer. The signal power response is simply

$$\begin{aligned} P_s &= E\{tr(\underline{H}^*\,\underline{s}\underline{s}^*\,\underline{H})\} \\ &= E\{tr(\underline{H}^*\,\underline{P}\,\underline{H})\} \\ &= tr(\underline{P}\,\underline{R}), \end{aligned} \qquad \text{[Eq. 41]}$$

which is obviously the same if $\underline{P}$ and $\underline{R}$ change their roles, i.e. $\underline{P} = \underline{H}\,\underline{H}^*$ describes the beamformer and $\underline{R}$ the signal. The power response to white noise is

$$P_{WN}^R = \sqrt{tr(\underline{H}^*\,\underline{I}\,\underline{H})^2} = \sqrt{tr(\underline{R})^2} \quad \text{or}$$

$$P_{WN}^P = \sqrt{tr\,\underline{P}^2}.$$

If $v < u$ one achieves $tr\,\underline{P}^2 < tr\,\underline{R}^2$ and

$$P_{WN}^P < P_{WN}^R \quad .$$

The white-noise gain becomes

$$G_W^R = \frac{P_s}{P_{WN}^R}$$

$$G_W^P = \frac{P_s}{P_{WN}^P} \quad .$$

Hence, we can conclude that

$$G_W^R < G_W^P \; .$$

In other words, if there is a mismatch between the width of a generalized beamformer (MMF) and a signal distributed over a certain angle interval the signal power is independent of whether the beam is too narrow or to broad by a certain amount. The narrower beam however becomes more sensitive to white noise; therefore the white noise gain is greater for the broader beam than for the narrower one.

3.5 Conclusions on the Optimum Quadratic Processor

a. The results achieved by application of the optimum quadratic processor (OQP) to horizontal line arrays in shallow water have shown that, under the optimistic assumptions listed in Ch. 1, there is basically no significant limitation on detection performance due to the medium if additional white noise is taken into consideration. The white noise is the major limiting component outside the interference area. The array gain is almost independent of the channel parameters (sound-speed profile, depth of water, source, receiver, frequency).

b. As the matrix matched filter $\underline{H}_s$ (generalized beamformer) integrates all different arrivals due to one signal source out of the noisy background, the gain in the direction of an endfire noise source becomes greater than the gain in the direction of a noise source at broadside, which in particular is completely independent of the array length.

c. The OQP may be used for small arrays (N not greater than 10 to 20) and mainly in active systems where pauses between pings can be used for signal-free updating of the inverse noise covariance matrix. As the matrix is Toeplitz (assumption of Sect. 1.3) the Levinson-algorithm may be used for efficient matrix inversion. The implementation of any matrix inversion process on a special-purpose, low-precision computer will involve accuracy problems if $\underline{Q}$ becomes ill-conditioned. This happens particularly where strong sources are radiating from broadside. With increasing order of $\underline{Q}$ (i.e. N) the accuracy problems become more and more serious. The implementation of the optimum generalized beamformer requires the exact knowledge of the vertical signal distribution. This knowledge is not available and has to be replaced by some prediction (e.g. running a modelling program, assuming an equivalent angle interval with uniform energy distribution). Both the matrix inversion and the generalized beamformer involve a considerable number of arithmetic operations. Therefore, in the subsequent discussions on suboptimum systems, the OQP will be used for comparison rather than being considered for application.

d. The generalized beamformer (MMF) may be approximated by assuming the signal to be uniformly distributed over a certain angle interval, thus finding a suboptimum quadratic beamformer that is independent of actual

channel parameters (e.g. sound-speed profile). If there are doubts about the actual width of the spread signal the width of the generalized beamformer should be made a bit too large rather than too narrow. This kind of approximation is just some kind of defocussing to broaden the beam without degrading the signal-to-noise ratio (which happens if defocussing is done by shading). The suboptimum quadratic beamformer looks for the energy maximum rather than making use of any knowledge about the spatial distribution of the signal, thus leading to an offset in bearing for all directions other than broadside.

e. Degradation of the array gain due to incoherence among modes becomes significant only for array lengths greater than roughly 100λ.

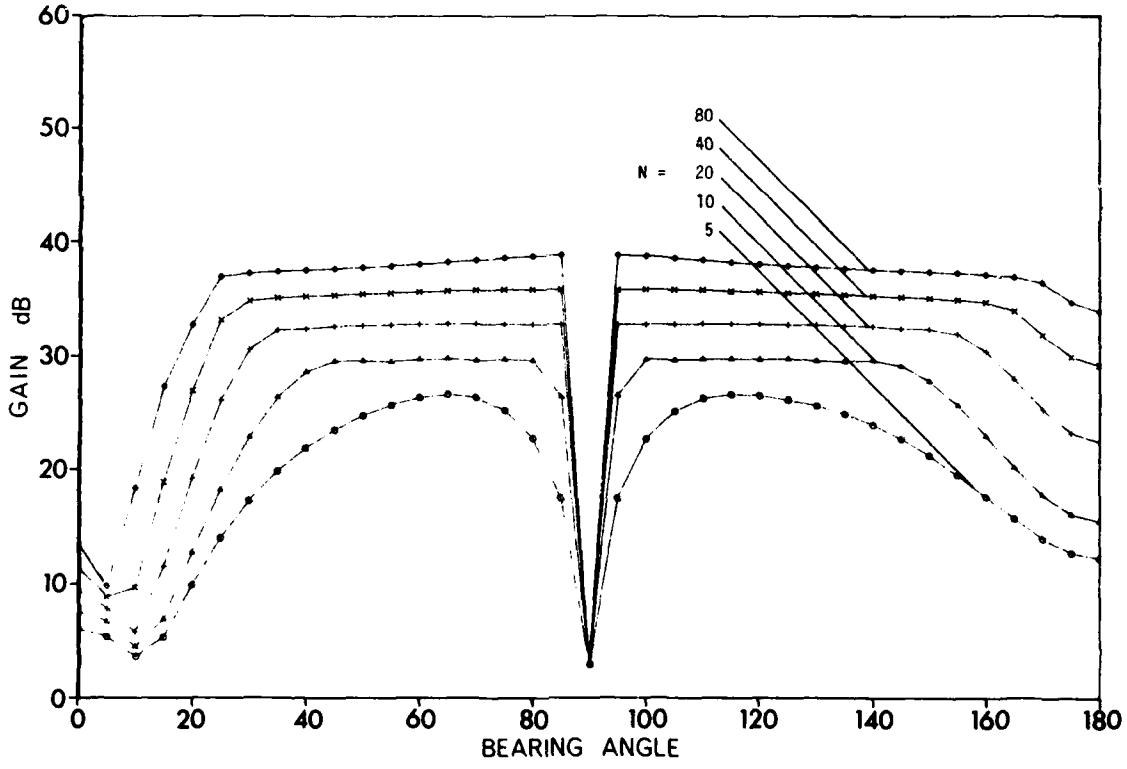

FIG. 15 OQP PERFORMANCE (WINTER PROFILE, 200 Hz)

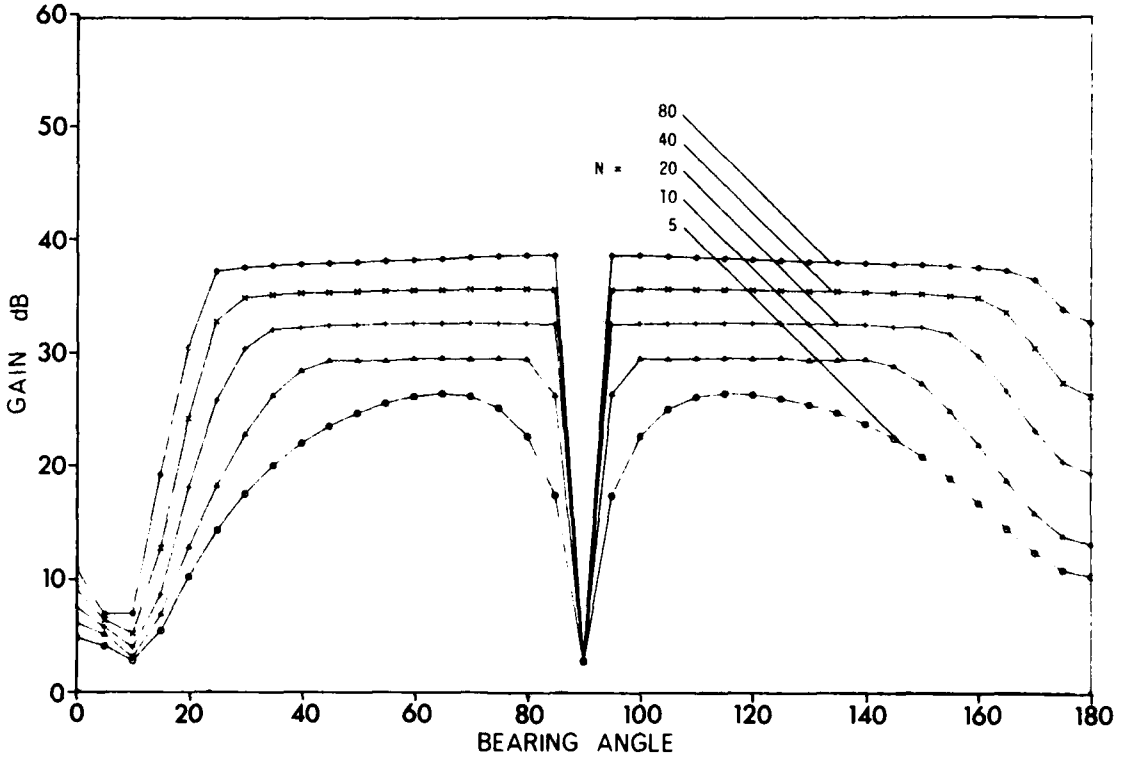

FIG. 16 OQP PERFORMANCE (WINTER PROFILE, 800 Hz)

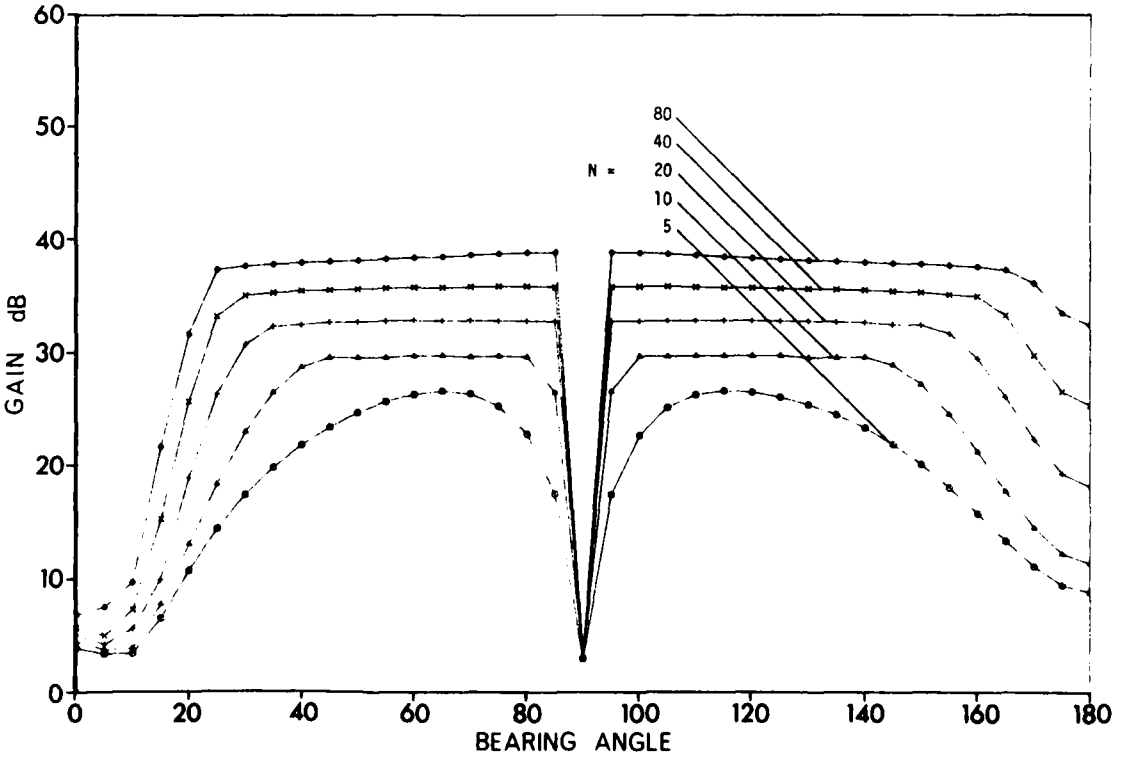

FIG. 17 OQP PERFORMANCE (WINTER PROFILE, 3200 Hz)

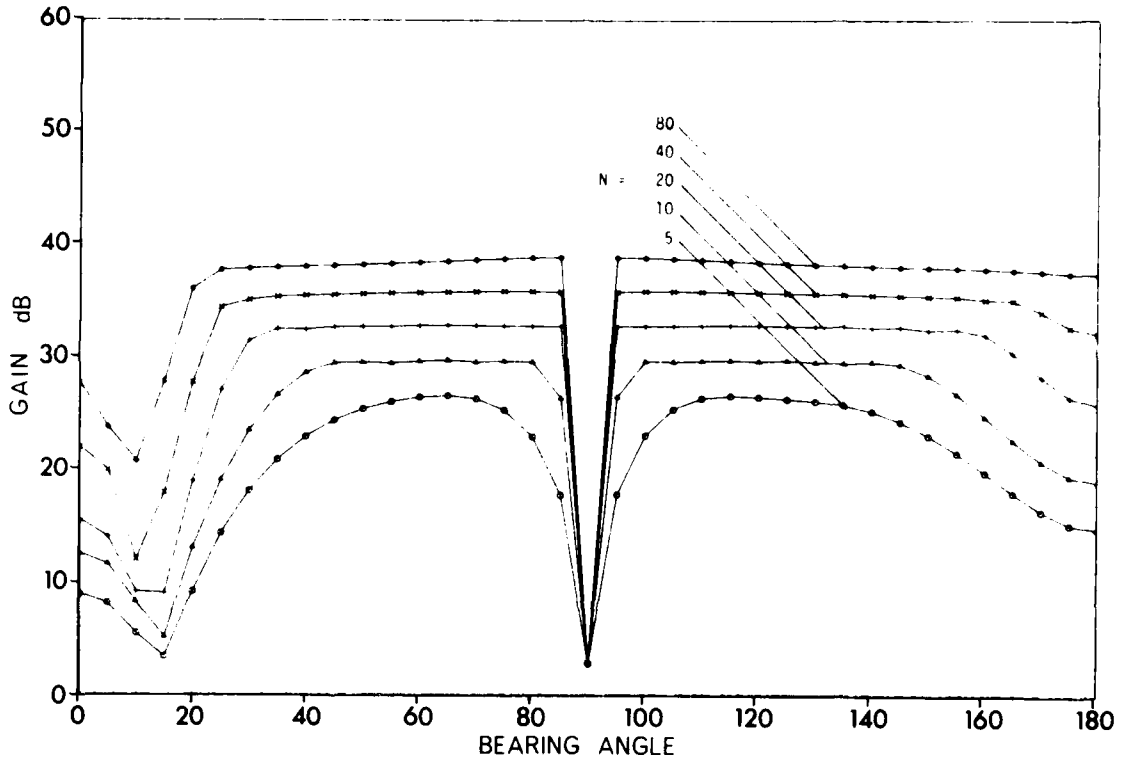

FIG. 18 OQP PERFORMANCE (SUMMER PROFILE, 200 Hz)

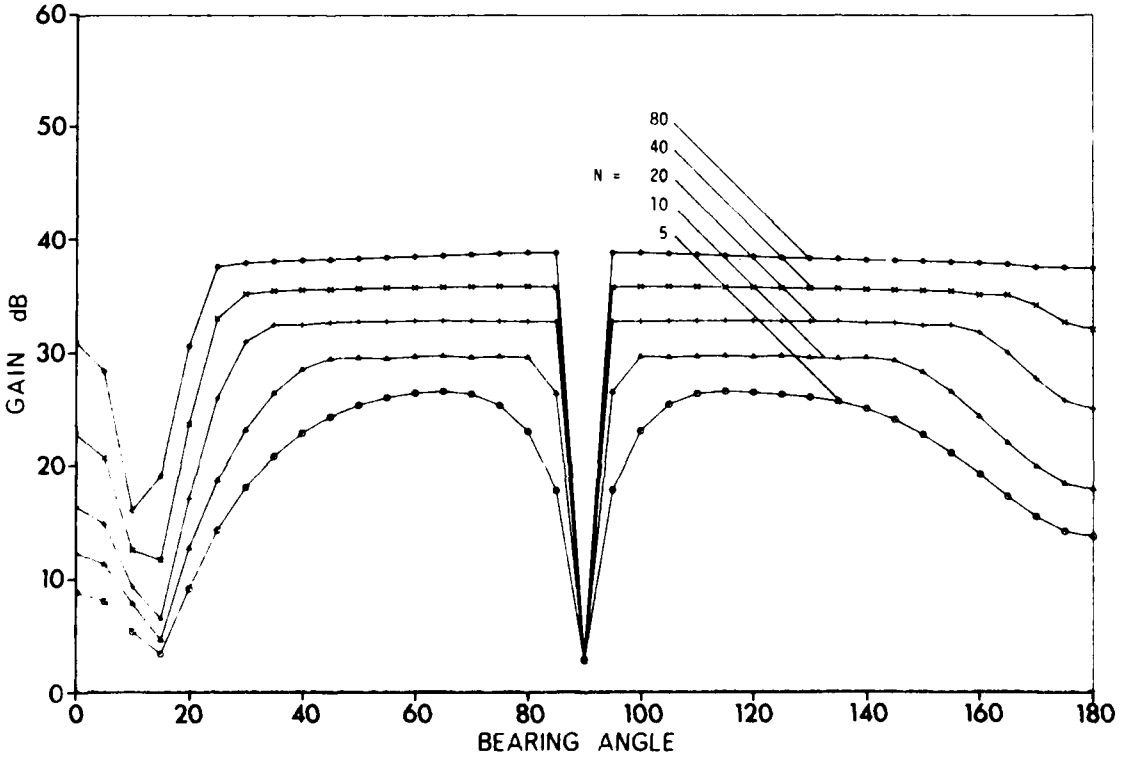

FIG. 19 OQP PERFORMANCE (SUMMER PROFILE, 800 Hz)

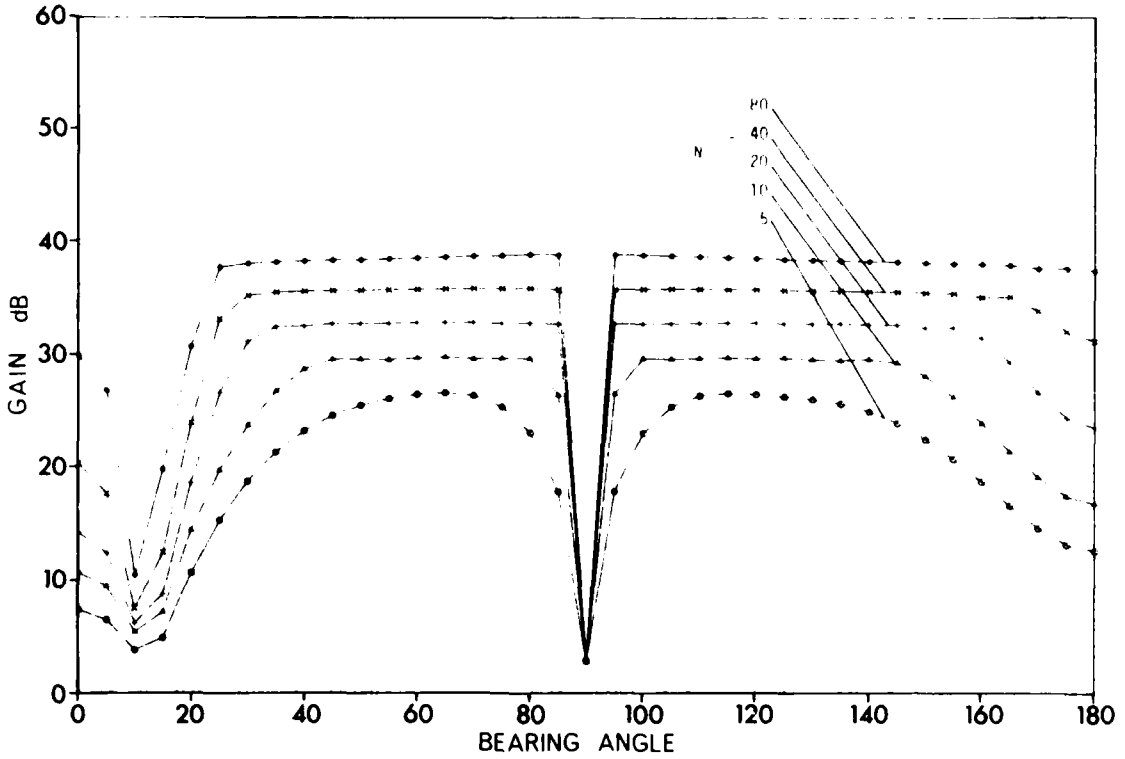

FIG. 20 OQP PERFORMANCE (SUMMER PROFILE, 3200 Hz)

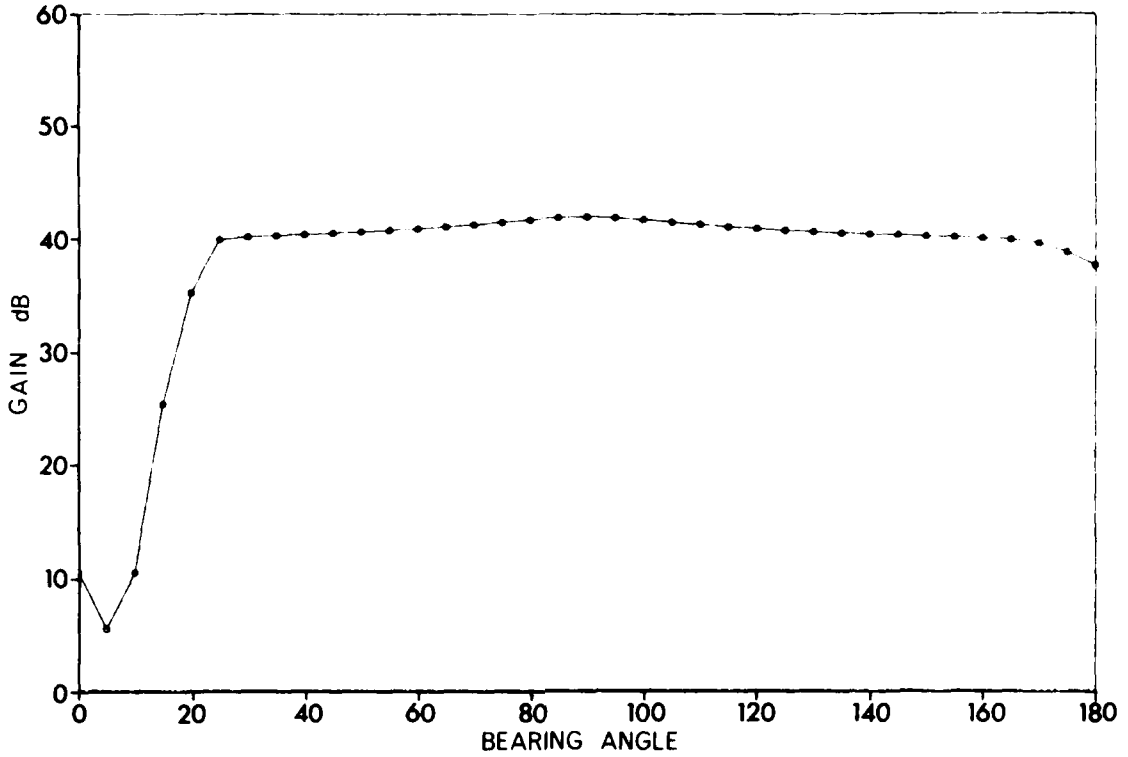

FIG. 21 OQP PERFORMANCE (WINTER PROFILE, 800 Hz, N = 160, 0.5λ SPACING)

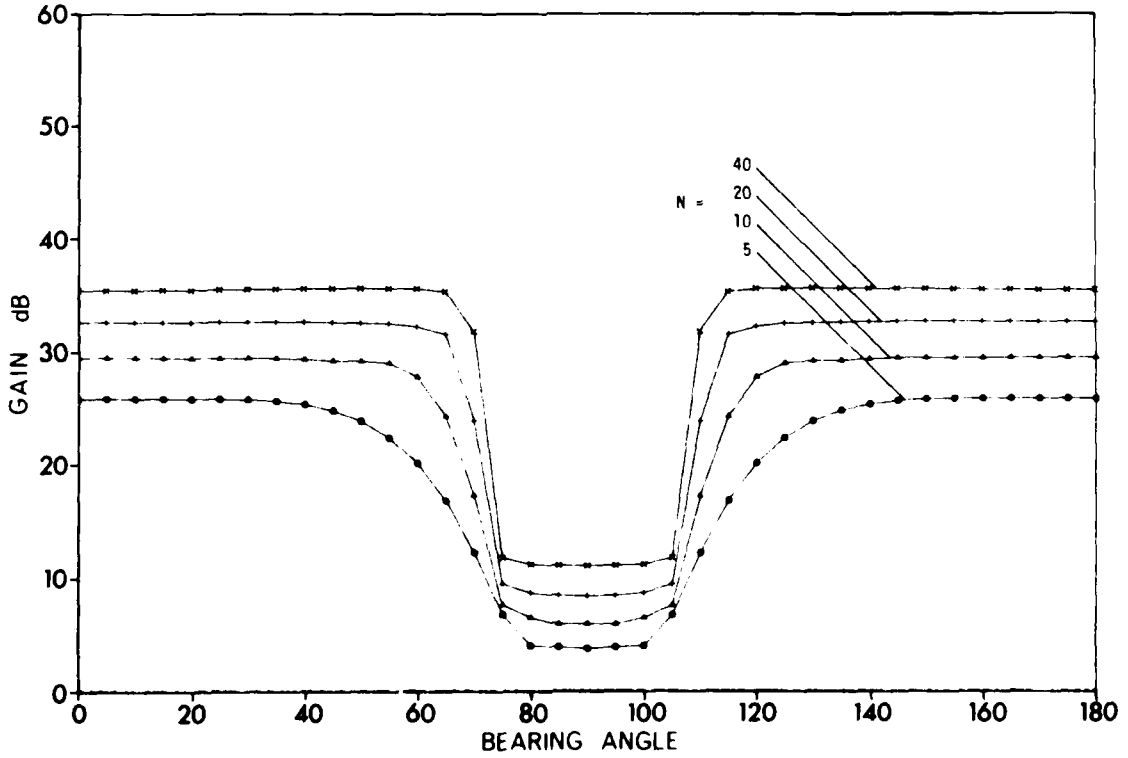

FIG. 22 OQP: WIDE-ANGLE NOISE (0.5λ SPACING, 5, 10, 20 and 40 HYDROPHONES)

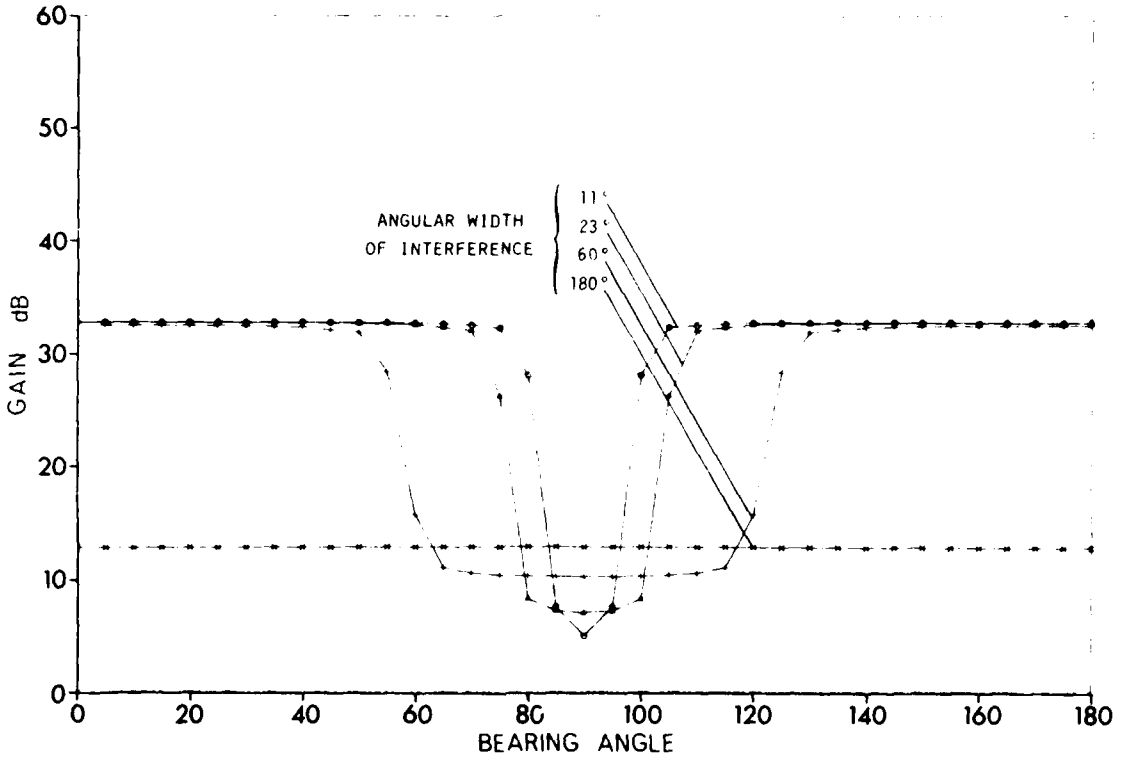

FIG. 23 OQP: WIDE-ANGLE NOISE (0.5λ SPACING, 20 dB I/N)

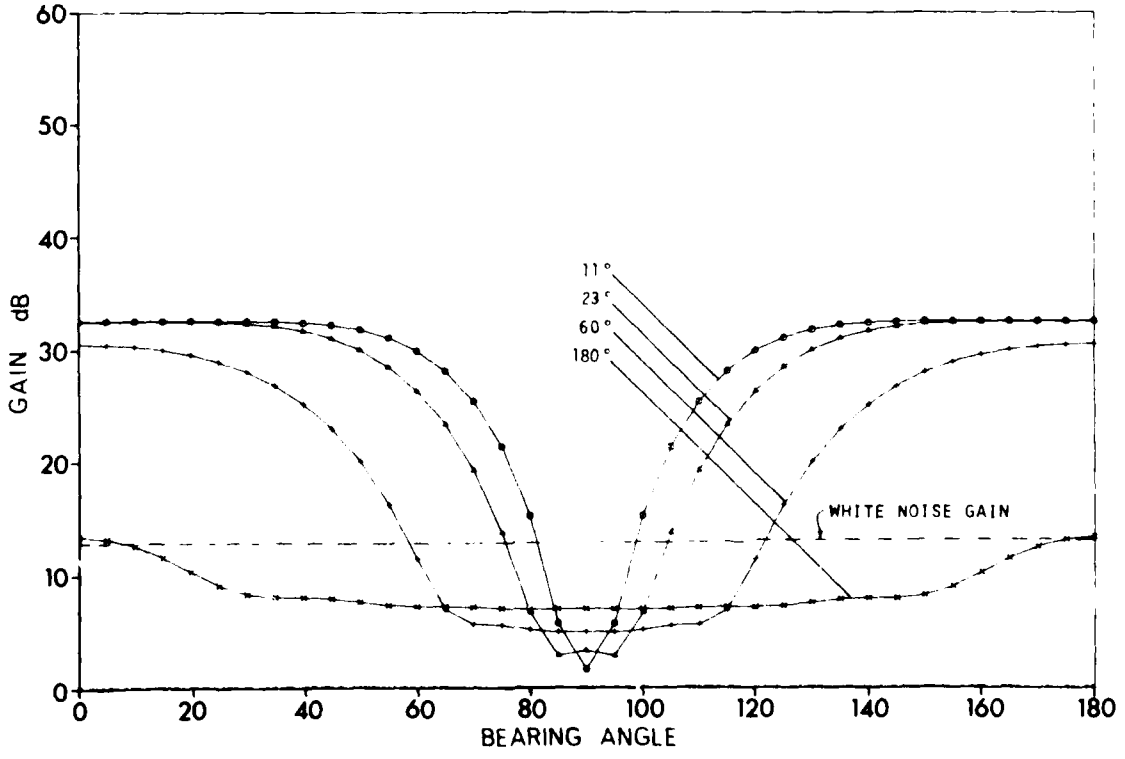

FIG. 24 OQP: WIDE-ANGLE NOISE (0.1λ SPACING, 20 dB I/N)

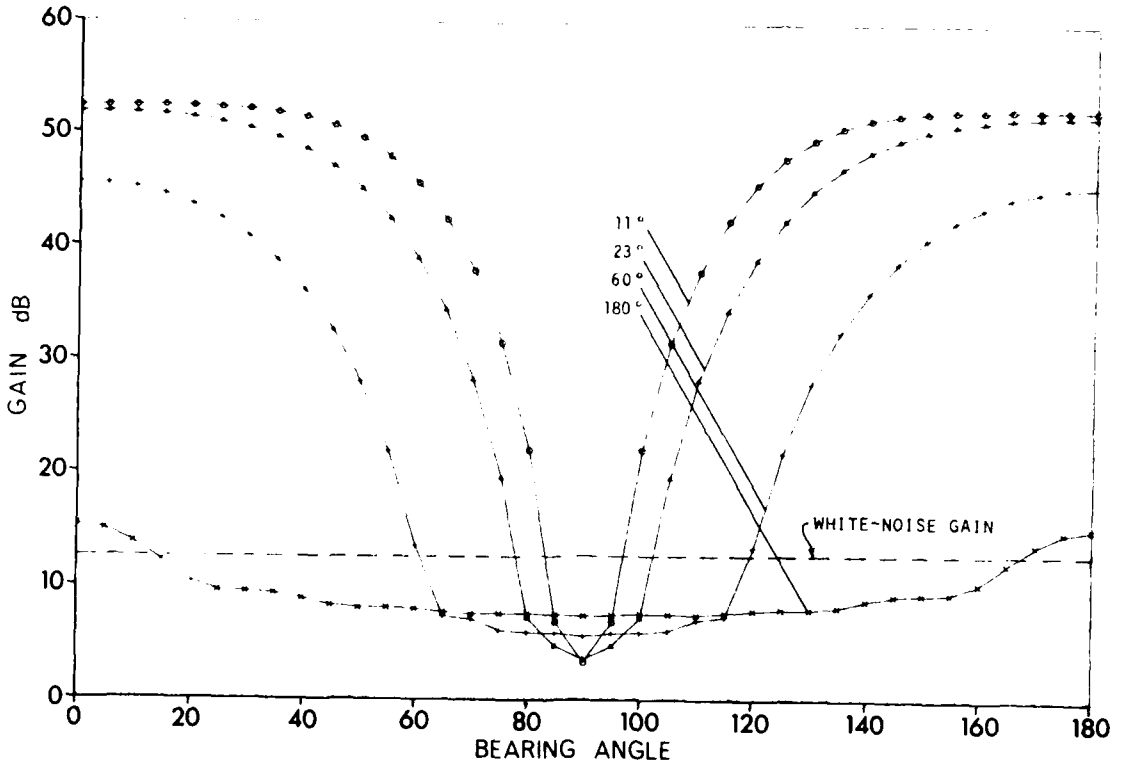

FIG. 25 OQP: WIDE-ANGLE NOISE (0.1λ SPACING, 40 dB I/N)

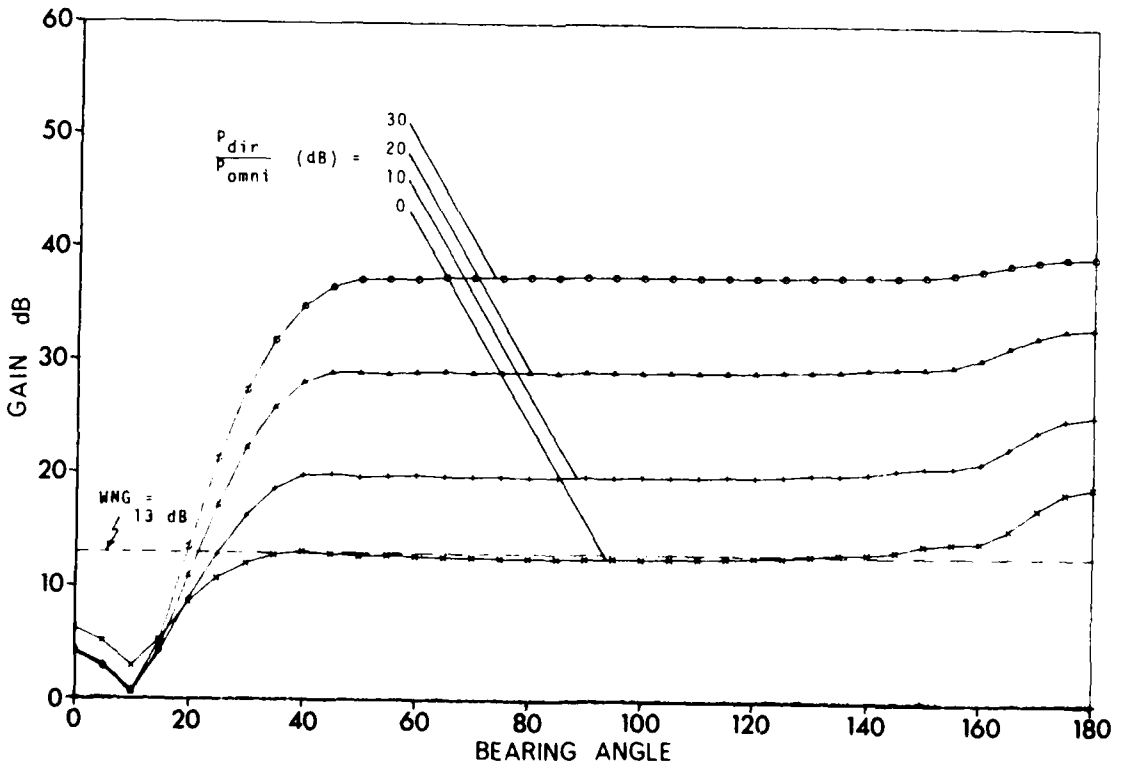

FIG. 26 OQP FOR DIRECTIONAL AND OMNIDIRECTIONAL NOISE (0.2λ SPACING)

4 THE OPTIMUM LINEAR PROCESSOR (OLP)

4.1 Introductory

Any linear processor is defined by the scalar product

$$\ell \equiv \mathrm{Re}\{\underline{x}^*\underline{h}\} \lessgtr \eta \quad \text{decision} < \begin{matrix}\text{target + noise}\\ \text{noise}\end{matrix} \qquad \text{[Eq. 42]}$$

If both the noise and the signal are random, $\underline{h}$ can be optimized such that the signal-to-noise ratio at the output is maximum, i.e.

$$\max_{\underline{h}} \frac{\underline{h}^*\underline{P}\,\underline{h}}{\underline{h}^*\underline{Q}\,\underline{h}}\ , \qquad \text{[Eq. 43]}$$

which is satisfied by $\underline{h}$ being the eigenvector belonging to the maximum eigenvalue of the generalized eigenvalue problem

$$(\underline{P} - \lambda\,\underline{Q})\underline{h} = \underline{0}. \qquad \text{[Eq. 44]}$$

Equation 42 is the Rayleigh-quotient of the generalized eigenvalue problem (Eq. 44). If $\underline{Q}$ is regular (which occurs for spatially random noise) Eq. 44 can be written

$$(\underline{Q}^{-1}\,\underline{P} - \lambda\,\underline{I})\underline{h} = \underline{0}, \qquad \text{[Eq. 45]}$$

thus reducing it to the ordinary eigenvalue problem. As can be seen, the solution for the first eigenvalue and the corresponding eigenvector requires a matrix inversion, a matrix product, and the solution of the eigenvalue problem, i.e. many more arithmetic operations than are needed for the calculation of the OQP. As the OQP is, however, optimum in the sense of the same criterion used here for optimization, its performance will always be equal or superior to any linear processor. Therefore the optimization procedure outlined above is not useful and will not be discussed further.

If, however, the target signal is spatially coherent, i.e. has a coherent wavefront, it can simply be described by a vector $\underline{s}$ instead of a covariance matrix as before. In this case Eq. 43 can be optimized by several criteria

(LR-test, maximum signal-to-noise ratio, maximum detection index, see *[1]*) by the choice

$$\underline{h} = \underline{Q}^{-1}\,\underline{b}\ , \qquad \text{[Eq. 46]}$$

which means again whitening and matching in frequency and space. Figure 27 shows the simple block diagram of the spatial part of a general linear array processor. In the optimum case the noise-suppression box contains the matrix $\underline{Q}^{-1}$. Notice that the generalized beamformer matrix in Fig. 14, defined by $\underline{P} = \underline{H}_s \underline{H}_s^*$, has been replaced by the vector $\underline{s}$, so that $\underline{P} = \underline{s}\,\underline{s}^*$ is a dyadic. Therefore the detection performance of the OLP in shallow water will be influenced by the simplification of the beamforming, i.e. the mismatch of the beamforming vector $\underline{b}$ to the actual random wavefront given by a positive, definite, signal covariance matrix $P = E\{\underline{s}\,\underline{s}^*\}$.

For the linear processor, the gain in signal-to-noise ratio of an array compared with a single omnidirectional sensor is

$$G = \frac{\underline{h}^*\,\underline{P}\,\underline{h}}{\underline{h}^*\,\underline{Q}\,\underline{h}} \cdot \frac{P_n}{P_s}\ . \qquad \text{[Eq. 47]}$$

The following two sections evaluate a few examples of application of the OLP. Following the conclusion of Ch. 3, only one set of channel parameters is chosen (Figs. 10 and 11) for all numerical examples given in the rest of the report.

4.2 Numerical Results

Figure 28 and 29 show a comparison of the OQP and the OLP for the same noise configuration as in Ch. 3. For small arrays (e.g. 10λ aperture, Fig. 28) almost no difference in performance can be observed. There is just a little deviation between the curves of OQP and OLP in the direction of the endfire noise source where interference and signal energy are distributed over about 20°. Here the matrix matched filter (MMF) yields some more individual integration of the signal energy because it contains the spatial amplitude distribution of the signal; the OLP, on the other hand, contains only a conventional beamformer, which sums energy without distinguishing between signal and interference.

For large arrays (80λ aperture in Fig. 29) the mismatch between the conventional beamformer in the OLP and the spatial signal spread becomes significant in that the beamwidth becomes narrower than the signal spread. Therefore signal energy is lost. There is, however, a second effect: the signal is always spread between the true bearing and a certain angle towards broadside such that there is usually an offset between the energy maximum and the same position. It was assumed in both the examples that the beam of the OLP points always in the true direction of the target. Consequently, there is some offset between beam direction and energy maximum, which becomes significant for narrow beamwidth.

There is only one point where the gains of the OLP and OQP coincide exactly. At broadside the signal covariance matrix reduces to a dyadic: $P_{90} = \underline{s}\,\underline{s}^*$; therefore, the gain (e.g. Eq. 37) becomes

$$G_{OQP} = \frac{\mathrm{tr}(\underline{H}^*\,\underline{P}\,\underline{H})\,P_n}{\sqrt{\mathrm{tr}(\underline{H}^*\,\underline{Q}\,\underline{H})^2 P_s}} = \frac{\underline{s}^*\,\underline{Q}^{-1}\,\underline{s}\,\underline{s}^*\,\underline{Q}^{-1}\underline{s}}{\sqrt{(\underline{s}^*\,\underline{Q}^{-1}\,\underline{Q}\,\underline{Q}^{-1}\underline{s})^2}} \cdot \frac{P_n}{P_s}$$

$$= \underline{s}^*\,\underline{Q}^{-1}\underline{s} \cdot \frac{P_n}{P_s} \quad . \qquad \text{[Eq. 48]}$$

For the OLP we get

$$G_{OLP} = \frac{\underline{s}^*\,\underline{Q}^{-1}\underline{s}\;\underline{s}^*\,\underline{Q}^{-1}\underline{s}}{\underline{s}^*\,\underline{Q}^{-1}\underline{Q}\,\underline{Q}^{-1}\underline{s}} \cdot \frac{P_n}{P_s} = \underline{s}^*\,\underline{Q}^{-1}\underline{s} \cdot \frac{P_n}{P_s} \, . \qquad \text{[Eq. 49]}$$

Figure 30 shows the application of the OLP to wide angle noise. The conditions are the same as in Fig. 23. The performances of OQP and OLP are almost identical. Some loss in gain may be achieved only for large arrays.

4.3 Conclusions on the Optimum Linear Processor

a. For small arrays (less than 20λ aperture) the OLP gives almost the same gain as the OQP in the white-noise-limited area.

b. For large arrays, losses in gain occur because the beam of the OLP becomes narrower than the signal spread.

c. There is an offset between energy maximum and tone target position due to the spatial spread; this causes some errors in the target bearing when searching with narrow beams. If the spread is approximately known, a rough correction of the bearings of detected targets can be made by adding (for angles < 90°) or subtracting (>90°) about half the angle interval of signal spread.

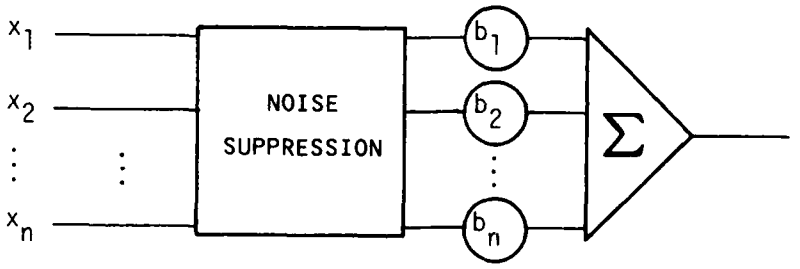

FIG. 27 LINEAR ARRAY PROCESSOR

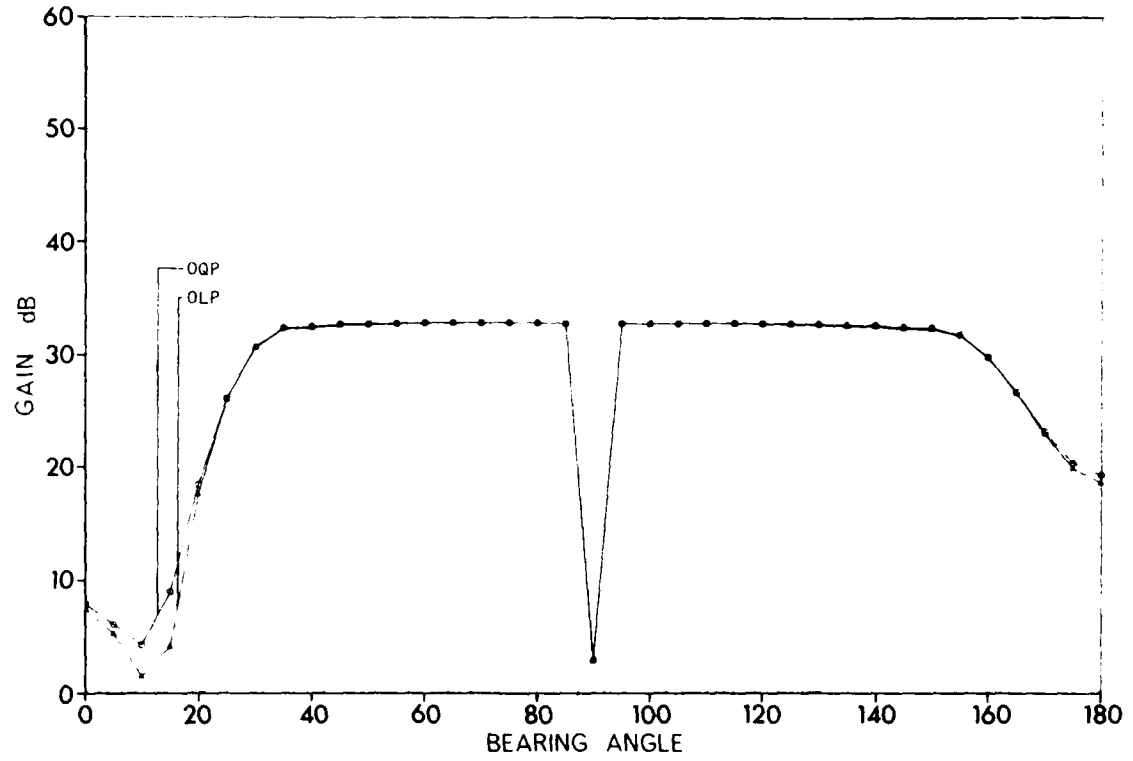

FIG. 28 COMPARISON OF OQP WITH OLP (N = 20, 20 dB I/N)

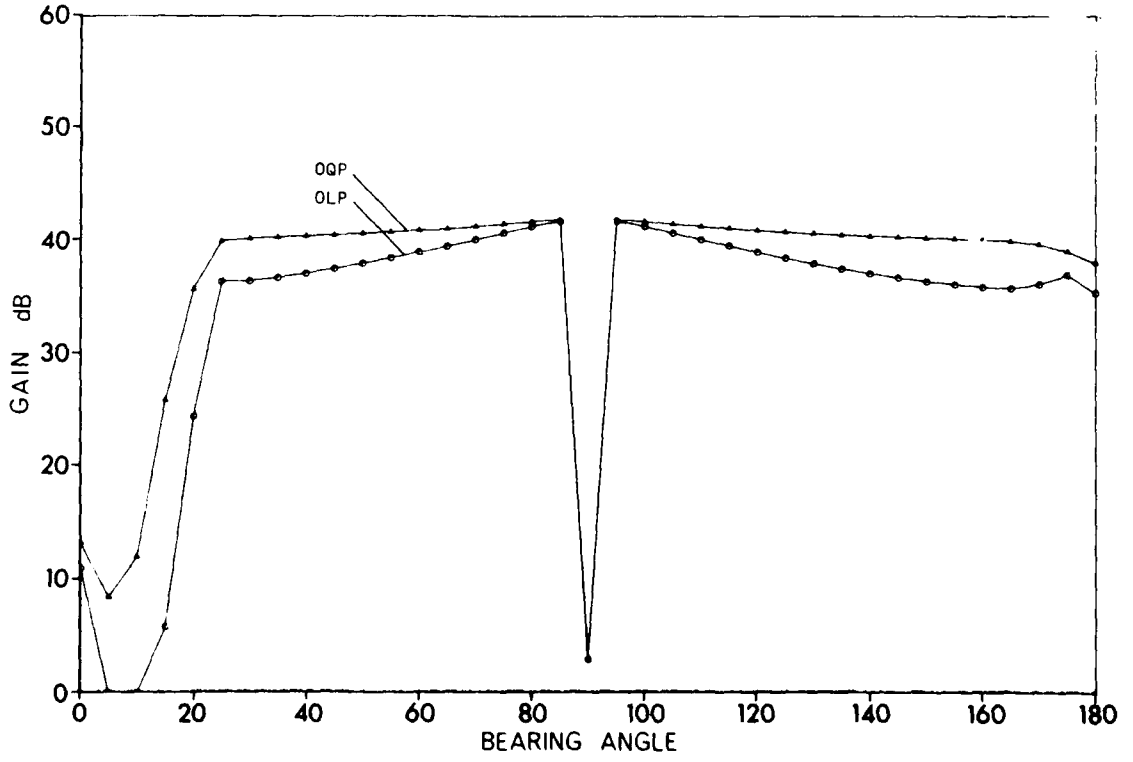

FIG. 29 COMPARISON OF OQP WITH OLP (N = 160, 20 dB I/N)

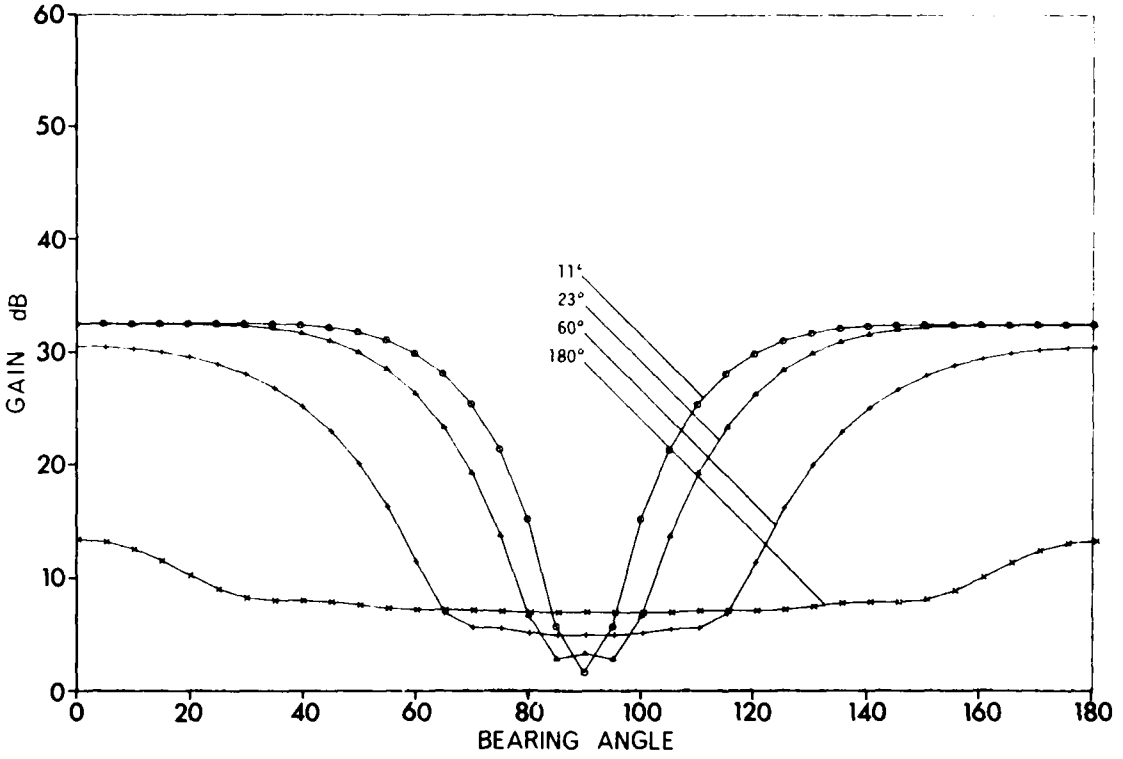

FIG. 30 OLP PERFORMANCE FOR WIDE-ANGLE NOISE (40 dB I/N)

5. SHADING METHODS

5.1 General Remarks

Shading methods are well-known means for reducing the sidelobe level of an array pattern. There are methods for minimizing the beamwidth at a given sidelobe level (Dolph-Tchebycheff). Binomial shading (shading coefficients proportional to binomial coefficients) yield the narrowest, with a total absence of sidelobes. Uniform shading (conventional beamforming) is optimum for detecting deterministic signals (i.e. coherent wavefronts) in white noise or, equivalently, for omnidirectional noise and $\lambda/2$ spacing between sensors. Any kind of shading method is simply achieved by replacing $\underline{Q}^{-1}$ in Eq. 46 and in the noise suppression box in Fig. 27 by a diagonal matrix $\underline{Z}$ containing the shading coefficients in the main diagonal:

$$\ell \equiv \mathrm{Re}\{\underline{x}^* \, \underline{Z} \, \underline{b}\} \gtrless \eta \quad \begin{matrix} \text{target + noise} \\ \text{noise} \end{matrix} \quad \text{decision} \qquad \text{[Eq. 50]}$$

Basically, the coefficients of $\underline{Z}$ can be optimized in the sense of maximum signal-to-noise ratio in the same way as mentioned in Ch. 3. Equation 50 can be written in the following form

$$\ell \equiv \{\underline{x}^* \, \underline{B} \, \underline{z}\} \, , \qquad \text{[Eq. 50a]}$$

where $\underline{z}$ is a vector of shading coefficients and $\underline{B}$ a diagonal matrix that contains the beamformer coefficients. Now we have an optimization problem for the vector of shading coefficients

$$\max_{\underline{z}} \frac{\underline{z}^* \, \underline{B}^* \, \underline{P} \, \underline{B} \, \underline{z}}{\underline{z}^* \, \underline{B}^* \, \underline{Q} \, \underline{B} \, \underline{z}} \, , \qquad \text{[Eq. 51]}$$

which is solved by choosing $\underline{z}$ to be the eigenvector corresponding to the maximum eigenvalue of the generalized eigenvalue problem

$$\underline{B}^*(\underline{P} - \lambda \underline{Q}) \, \underline{B} \, \underline{z} = \underline{0}. \qquad \text{[Eq. 52]}$$

Therefore, in general, optimum shading depends on $\underline{P}$ and $\underline{Q}$ and, hence, is an adaptive process.

Dolph-Tchebcheff optimization could basically be applied by pre-assigning the sidelobe level so that the array-power response to a directional source in the maximum sidelobe is equal to the white-noise power level. As the interference-to-noise ratio has to be known, this optimization is adaptive as well. In the limit, i.e. for the white-noise level approaching zero, the method will approach binomial shading (no sidelobes).

Instead of very complicated optimization procedures, three simple and well-known shading methods (cosine, binomial, uniform) are considered in the following.

5.2 Binomial Shading (B/N)

Figure 31 shows the gain for different array lengths in the presence of one interfering source at 0° and additional white noise 20 dB below the interference level. For arrays greater than N = 40 the subroutine generating the binomial coefficients went out of range of the 32-bit words of the computer used.

There is a completely flat white-noise-limited area around broadside, which is due to the fact that there are no sidelobes at all. However, the main beam is broadened so that there is a quite broad area of main-lobe interference due to the source at 0° and a correspondingly broad grating null entering the visible range from 180°. Another effect of the broadened beam is that even in the white-noise-limited area, i.e. outside the mainlobe interference, there are significant losses compared with the optimum (interference/noise-ratio + N), which are indicated by small horizontal lines on the left.

5.3 Cosine Shading

The shading coefficients have been chosen to be

$$a_n = 0.5 - 0.5 \cos(2\pi \cdot (n-0.5)/N). \quad n = 1...N, \text{ N even.}$$

Figure 32 shows the gain of different lengths for the same noise configuration as before. For small arrays a slight ripple due to some remaining sidelobes can be observed in the white-noise-limited area. For large arrays the white-noise-limited area is quite flat, which is due to the fact that the interfering source (which appears to be distributed between 0° and 20°) does some averaging over several sidelobes when moved over the array pattern. From N = 10 to N = 80, doubling of the aperture gives an additional gain of about 3 dB, which is achieved also by optimum processors, see Fig. 16. A comparison with the optimum gain levels on the left shows that about 3 dB are lost between optimum and cosine-shaded arrays over a broad area around broadside. It can be stated roughly that a 40λ cosine-shaded array has about the same gain as a 20λ optimum array. For smaller arrays the mainlobe interference becomes significant at endfire and backfire directions. For apertures much larger than 40λ the gain is proportional to the aperture only at broadside, where the signal appears to the horizontal array as a discrete line. Apart from broadside, the mismatch between the conventional beamformer and the spatial spread of the signal leads to additional loss (compare with Ch. 4).

The grating null on the right side can be avoided by somewhat smaller spacing of the sensors. Figure 33 shows three curves for an array with 20 sensors spaced at 0.1, 0.3, and 0.5λ. As can be seen, the ambiguity is removed at the cost of poor resolution and, hence, more main-lobe interference.

5.4 Comparison of Shading with OQP

Figures 34 and 35 plot the array gain over one and two noise sources respectively (each of them 20 dB above the white-noise level). As can be seen, the cosine shading is by far the best approximation to the OQP in that the gain in the white-noise-limited area is just about 3 dB below the OQP curve and the area of the main-lobe interference is much smaller than with binomial shading. Conventional beamforming leads to the narrowest beamwidth and thus to the narrowest main-lobe interference zones. It suffers, however, from the hign sidelobe level.

The example in Figs. 36, 37 and 38 show a situation where five noise sources are distributed on a half circle, or, equivalently, nine sources on a full circle. The results confirm once again what has been found before. For small arrays (10λ-aperture in Fig. 36) cosine shading does not work well, especially with a high interference/noise ratio (40 dB in Fig. 37). For the 40λ array, however, reasonable approximation of the OQP is achieved. This also holds for higher interference/noise ratios.

As shown in Fig. 39, cosine shading even works well for smaller arrays if the interference is distributed over a wide angle.

Other kinds of shading *[19]* may be used as well, most of them having a lower side-lobe level at the cost of a larger beamwidth, which leads to larger optimum array length.

5.5 Conclusions on Shading Methods

a. Optimum shading depends on the spatial noise distributions and leads, therefore, to adaptive methods that involve complicated arithmetic operations but are still inferior to the OQP.

b. Binomial shading suffers seriously from main-lobe interference and also from loss in signal gain due to the broadening of the beam outside the main lobe interference.

c. As is well known, conventional beamforming should be applied only if the noise is isotropic or white.

d. Cosine shaded is recommended for array lengths of about 50λ. Compared with the OQP, the loss for the same aperture is about 3 dB. For smaller arrays the performance is degraded heavily by main-lobe interference. For larger arrays (>80λ) the beamwidth becomes narrower than the spatial signal spread, thus causing additional loss in gain. For smaller arrays the influence of the main-lobe interference becomes significant.

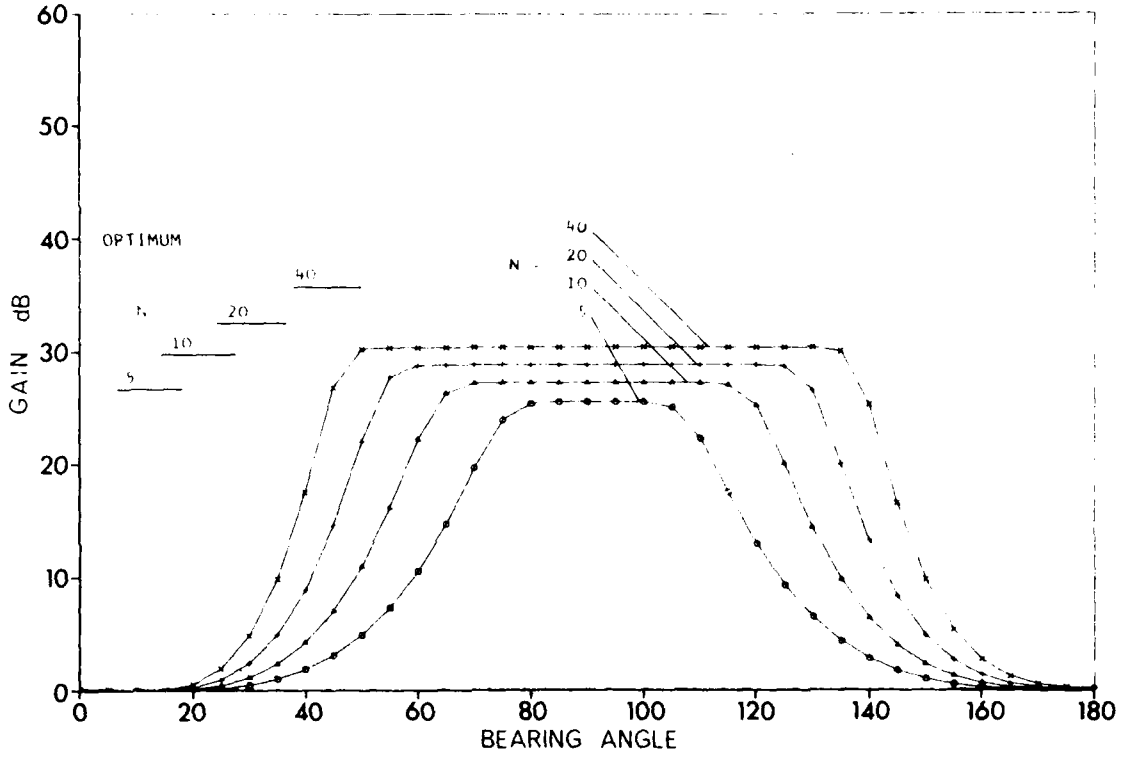

FIG. 31 PERFORMANCE OF ARRAYS WITH BINOMIAL SHADING

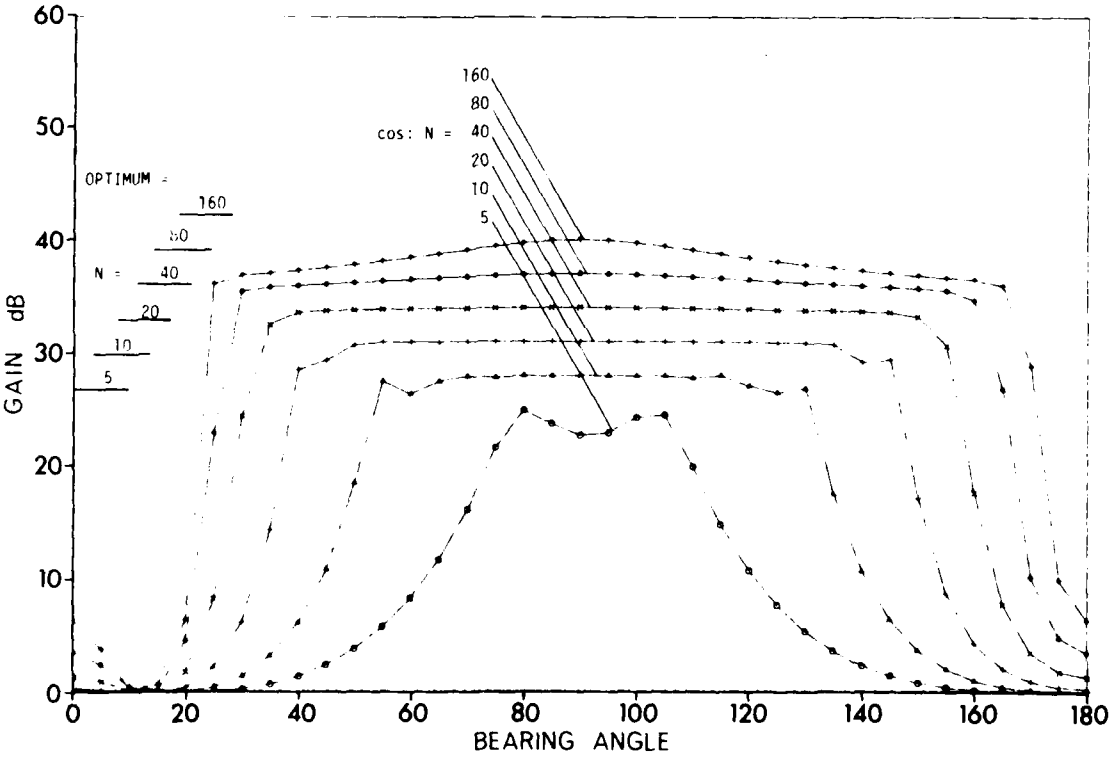

FIG. 32 GAIN OF COSINE-SHADED ARRAYS

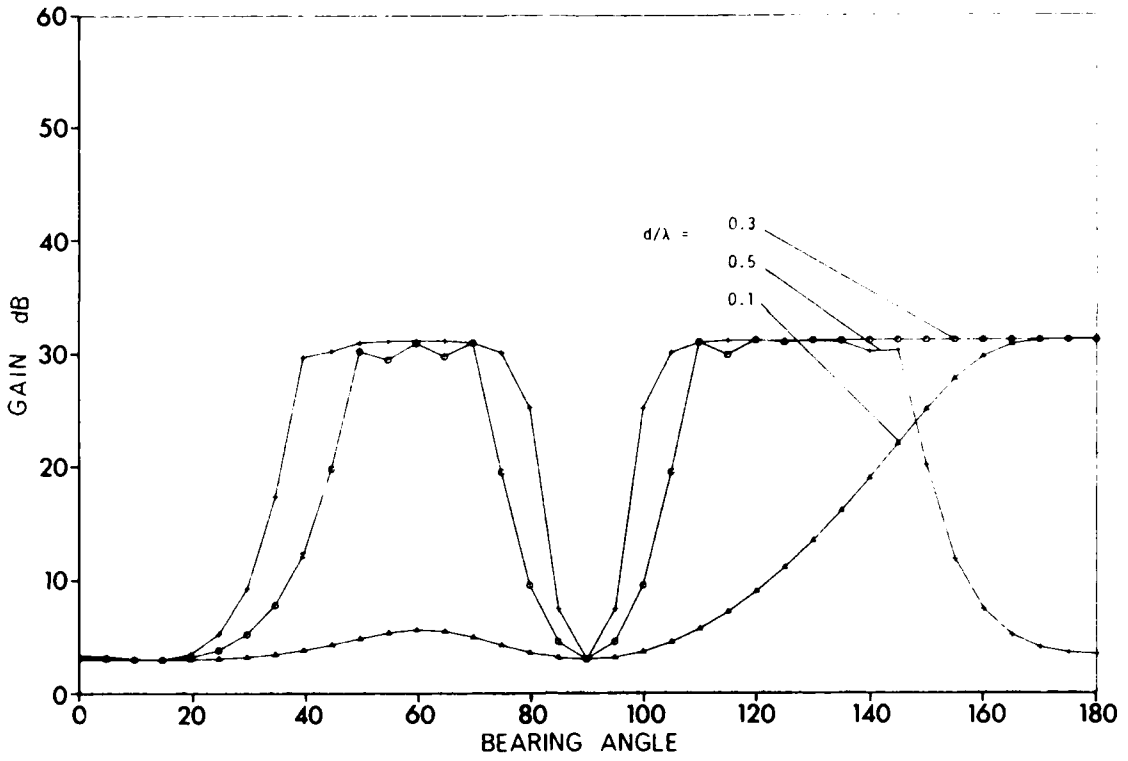

FIG. 33 COSINE-SHADED ARRAY WITH DIFFERENT SPACING (N = 20)

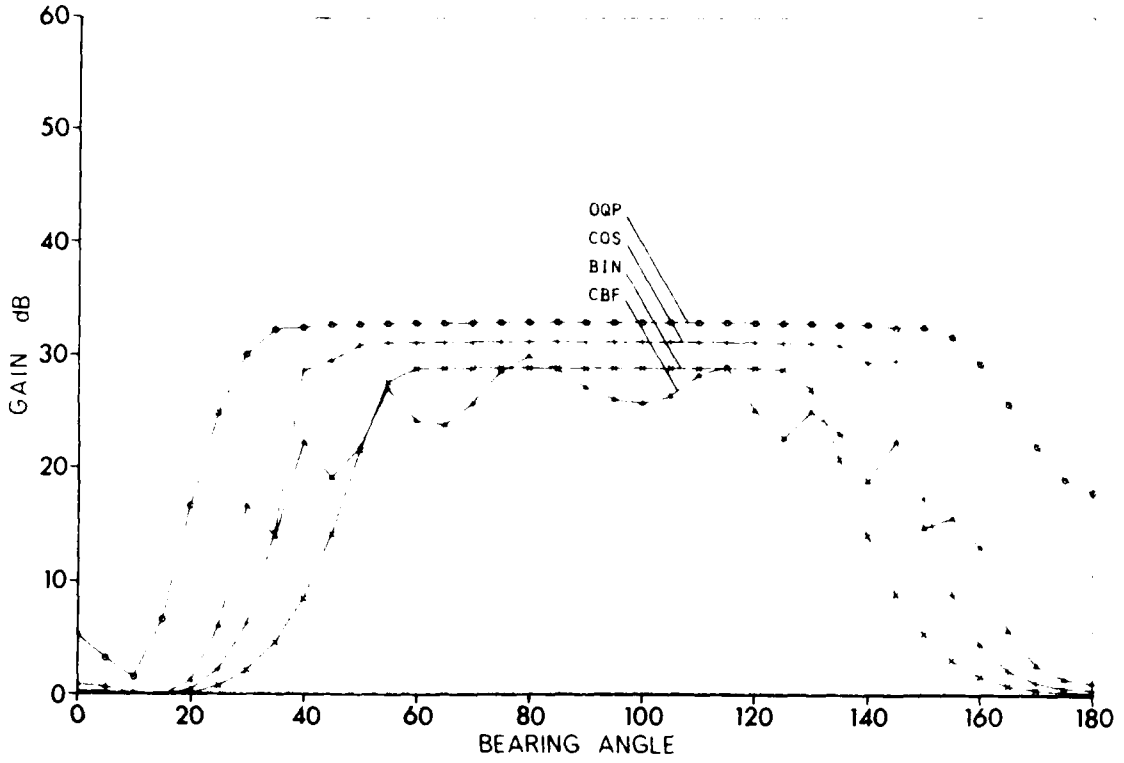

FIG. 34 COMPARISON OF COS-SHADING WITH OQP (N = 20) (one noise source)

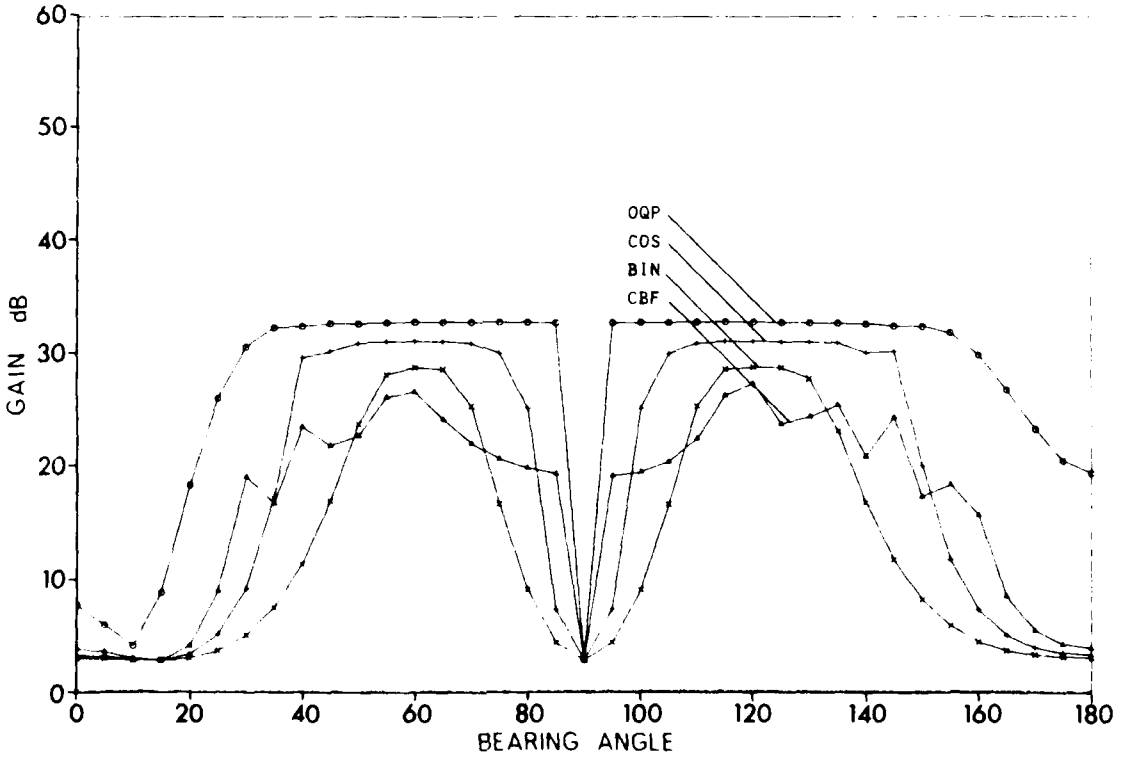

FIG. 35 COMPARISON OF COS-SHADING WITH OQP (N = 20) (two noise sources)

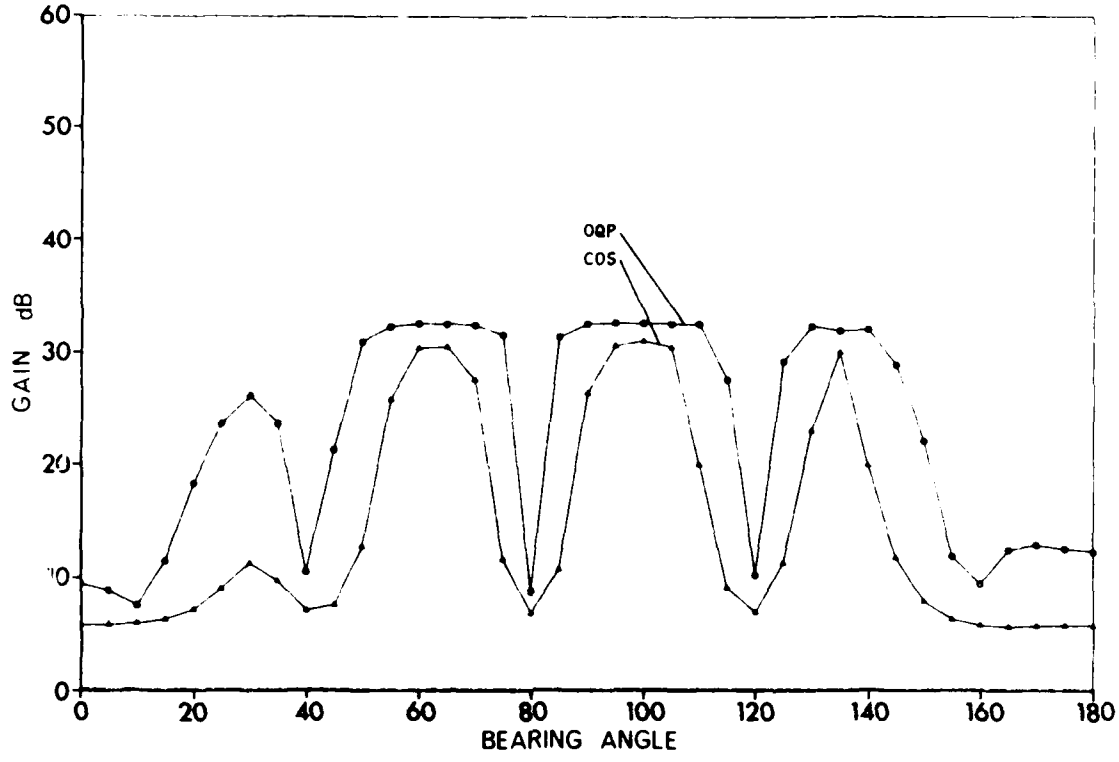

FIG. 36 COMPARISON OF COS-SHADING WITH OQP (five noise sources, 20 dB I/N each)

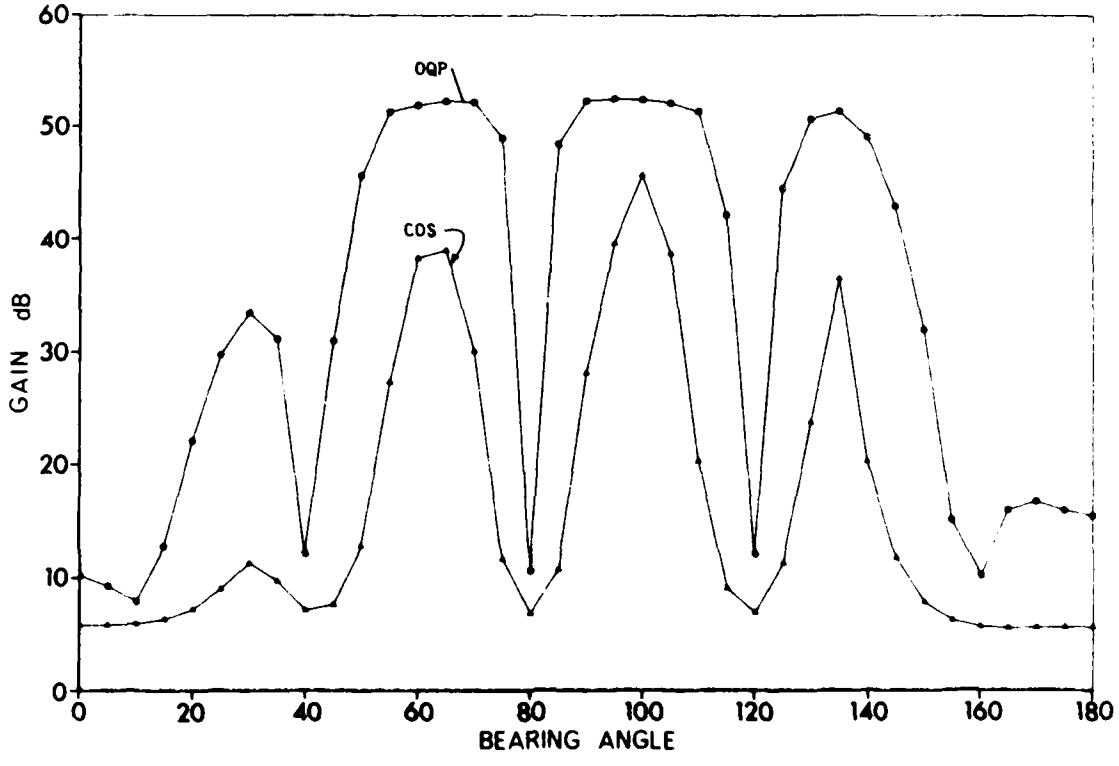

FIG. 37 COMPARISON OF COS-SHADING WITH OQP (40 dB I/N)

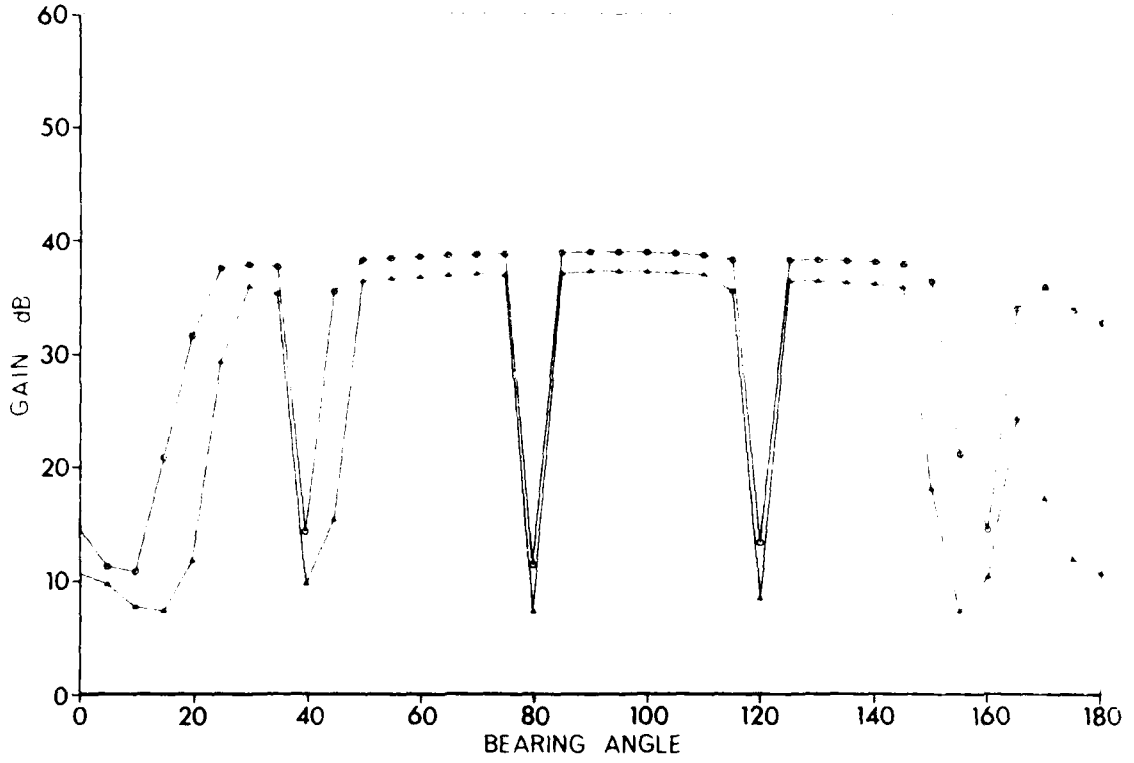

FIG. 38 COMPARISON OF COS-SHADING WITH OQP (N = 80)

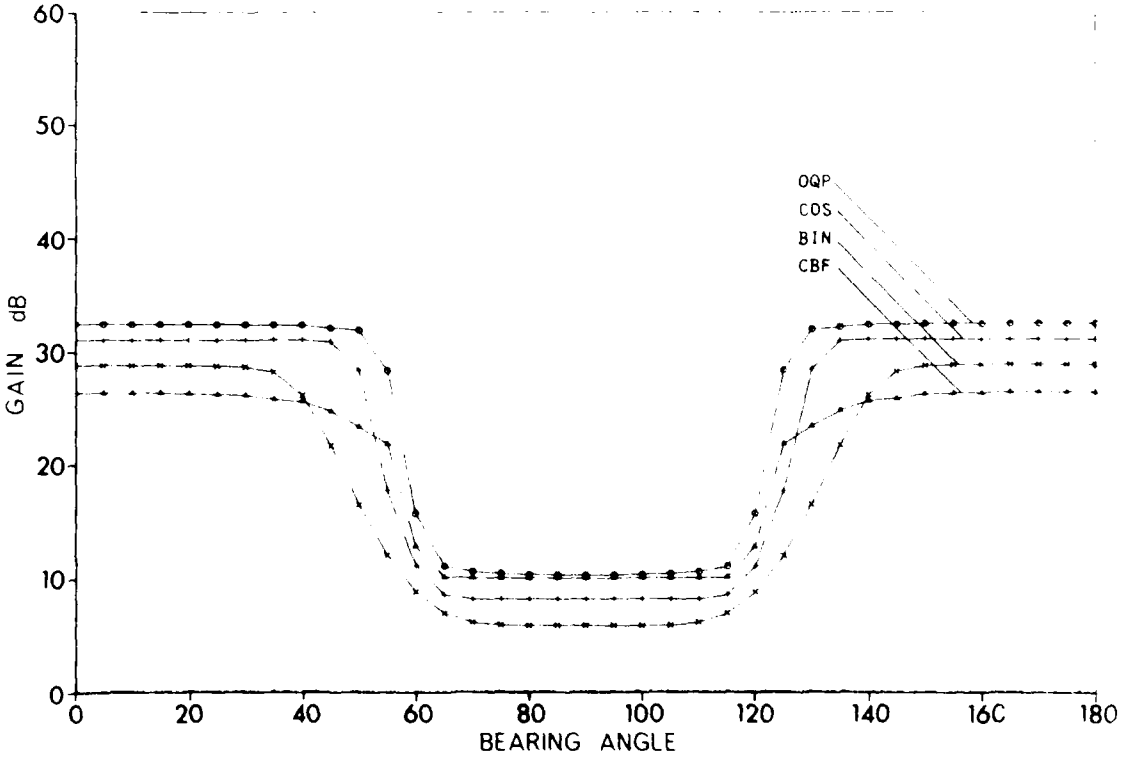

FIG. 39 COMPARISON OF SHADING METHODS WITH OQP (WIDE-ANGLE NOISE)

6 NULL-STEERING METHODS

6.1 General Description

In many cases the direction of a noise source is known *a priori*. For instance, the direction of the towing ship in a towed array sonar is always known. The directions of other ships might be known by means of radar or optical position finding. If this is so, suppression of point-shaped interference may be performed by steering nulls, either of the array pattern or of the individual sensor pattern, in the direction of the interfering sources. Directive sensor patterns (dipole or cardioide patterns) can easily be formed by appropriate combination of adjacent sensors. Both kinds of null-steering are suboptimum because the widths of the nulls are fixed. Adaptive processors like the OQP or the OLP adapt to the individual spatial distribution of the interference and noise, which usually depends on the medium and on the cosine of the bearing. Optimum adaptive processors attempt to achieve an optimum compromise between noise reduction and signal gain rather than to form an accurate null in the direction of the interference without considering the target direction.

A null in the array pattern is achieved by transforming the received data by a so-called projection matrix, defined by

$$\underline{C} = \underline{I} - \frac{\underline{c}\,\underline{c}^*}{\underline{c}^*\underline{c}} \quad , \qquad \text{[Eq. 53]}$$

if only one null is formed. The vector $\underline{c}$ describes the direction of the null. Clearly, the product

$$\underline{C}\,\underline{c} = \left(\underline{I} - \frac{\underline{c}\,\underline{c}^*}{\underline{c}^*\underline{c}}\right)\underline{c} = \underline{o} \quad , \qquad \text{[Eq. 54]}$$

i.e. the array becomes "blind" for the direction $\underline{c}$. For more than one null a multiple constraint matrix is given by

$$\underline{C} = \underline{I} - \underline{H}(\underline{H}^*\,\underline{H})^{-1}\,\underline{H}^* \quad . \qquad \text{[Eq. 55]}$$

such that $\underline{C}\,\underline{H} \equiv \underline{0}$. Notice that the rank of $\underline{H}$ must be less than the order of $\underline{C}$, otherwise Eq. 55 can be written

$$\underline{C} = \underline{I} - \underline{H}\,\underline{H}^{-1}\,\underline{H}^{*-1}\,\underline{H}^{*} = \underline{0} \quad \text{for arbitrary } \underline{H}, \qquad \text{[Eq. 55a]}$$

which means that the array becomes blind for any direction!

Dipole or cardioide patterns may be achieved by combining adjacent sensor outputs so that arrivals from a certain direction are subtracted from one another. The corresponding noise suppression matrix is given by

$$D \equiv \begin{pmatrix} 1 & & & 0 \\ -a & 1 & & \\ & -a & \ddots & \\ & & \ddots & 1 \\ 0 & & & -a \quad 0 \end{pmatrix}, \qquad \text{[Eq. 56]}$$

where a denotes the phase factor corresponding to the interference direction. Notice that one sensor is lost. This can be avoided by combining the n^{th} sensor with the $n\text{-}2^{th}$:

$$D \equiv \begin{pmatrix} 1 & & & 0 \\ -a & 1 & & \\ & -a & \ddots & -b \\ & & 1 & 0 \\ 0 & & -a & 1 \end{pmatrix}. \qquad \text{[Eq. 57]}$$

The schemes of Eqs. 56 or 57 may be generalized to more than one interfering source by cascading several matrices of the same forms, e.g.

$$D = \begin{pmatrix} 1 & & & 0 \\ -a & 1 & & \\ & -a & \ddots & \\ & & \ddots & 1 \\ 0 & & & -a \quad 0 \end{pmatrix} \begin{pmatrix} 1 & & & 0 \\ -b & 1 & & \\ & \ddots & \ddots & \\ & & -b & 1 \\ 0 & & & 0 \quad 0 \end{pmatrix} \cdots \qquad \text{[Eq. 58]}$$

where a and b define the directions of two interfering sources.

6.2 Numerical Results

The following results are achieved by replacing $\underline{Q}^{-1}$ in Eq. 46 by $\underline{C}$ or $\underline{D}$ and evaluating Eq. 47. Figure 40 shows gain curves for the OQP, the dipole processor (Eq. 56), and null-steering in the array pattern (Eq. 53), for an array with 20 hydrophones in the presence of an interfering source at endfire direction. It can be seen that the DIP-processor gives a rather good approximation to the performance of the OQP over a large bearing interval (30° to 150°). Only very close to the interfering source does some loss have to be taken into account. The same is valid for the grating null at 180° bearing. The array considered in this example was supposed to have 0.5λ spacing. Therefore, application of the transform of Eq. 56 leads to dipole sensor patterns, so that there is a second null at 180° that reduces the signal response of the sensors in that direction.

Reducing the spacing results in individual cardioide patterns rather than dipole patterns. Figure 41 shows the gain for different spacings (d/λ = 0.1, 0.3, 0.5) from which it is seen that the optimum spacing is obviously about 0.3λ. In this case the sensor patterns have a minimum instead of a deep null at 180°; in addition, the grating null at 180° is removed. The main lobe interference in the vicinity of the interfering source has not increased significantly.

Steering a null of the array pattern does not work sufficiently well in the example of Fig. 40. Obviously the null is not broad enough to cope with the spatial spread of the endfire interference. For very small arrays (e.g. N = 5, as shown in Fig. 42), however, the width of the null is broad enough to suppress the interference sufficiently. For very large arrays (e.g. N = 160, as shown in Fig. 43) the loss compared with the OQP becomes even higher than for N = 20, as expected. But now even the DIP-processor is significantly inferior to the OQP, except for 90°. This indicates that the DIP-processor works well enough as far as noise suppression is concerned. The loss in gain is again due to the mismatch of the subsequent beamformer to the signal spread. If the interference is at 90° (Fig. 44) both methods (dipole, null steering) work quite well. Null steering is now slightly superior, because there is no signal spread at broadside.

Figure 45 shows the result of a two-stage dipole processor (see Eq. 58) applied for suppression of two interfering sources (0° and 90°). The performance is rather poor. In comparison with the OQP, 10 dB and more are lost. The reason is that cascading of dipole processor matrices leads to products of dipole patterns, as shown qualitatively by the hatched areas in the upper part of Fig. 45. This obviously causes reduction of target signal power.

6.3 Conclusions on Null Steering

a. Dipole or cardioide patterns achieved by subtracting signals of neighbouring sensors with respect to the interference direction yield almost optimum noise suppression for apertures smaller than 40λ, because the width of the null in the sensor pattern copes well with the spatial signal spread. It is useful, in particular, if there is only one noise source with known direction (e.g. towing ship noise). In this case 0.3λ spacing is appropriate [trade-off between too great a width of the null in the interference direction and a minimum (loss of signal power) in the opposite direction].

b. Null steering in the array pattern leads to much narrower nulls than dipoles. It is therefore useful only for interference coming from about broadside or for very small arrays.

c. Cascading of dipole processors for suppression of more than one noise source does not work well due to the reduction of the signal power by the multiplication of different dipole patterns with one another.

d. Application of nonadaptive null-steering methods requires additional information about the noise field, which may be obtained by radar. Therefore, these methods are restricted to the radar range (typically 15 miles).

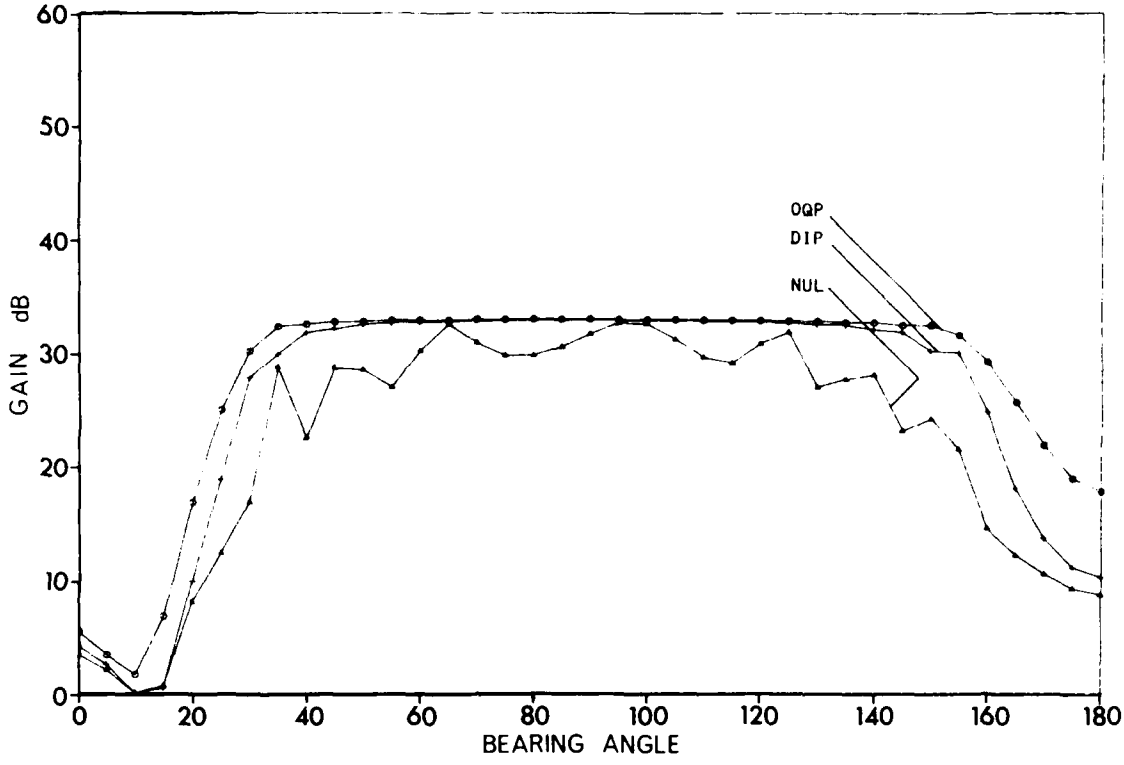

FIG. 40 COMPARISON OF NULL-STEERING WITH OQP (N = 20, 20 dB I/N)

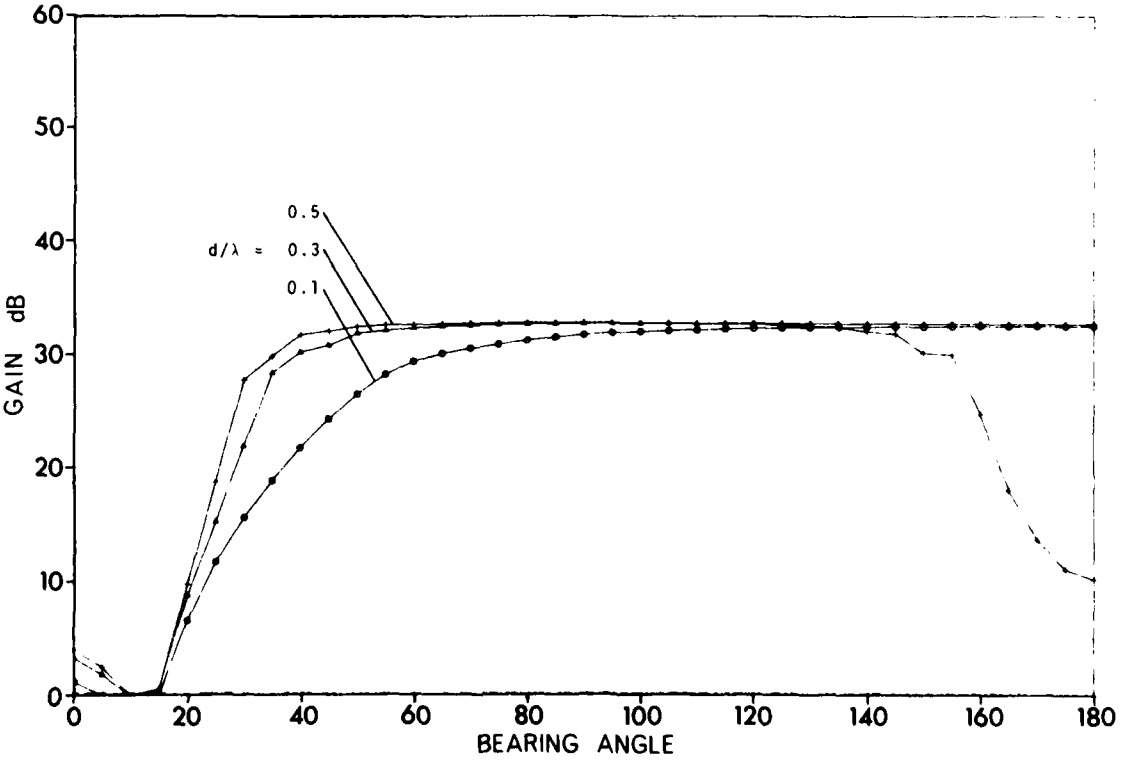

FIG. 41 DIPOLE PROCESSING FOR DIFFERENT SPACING

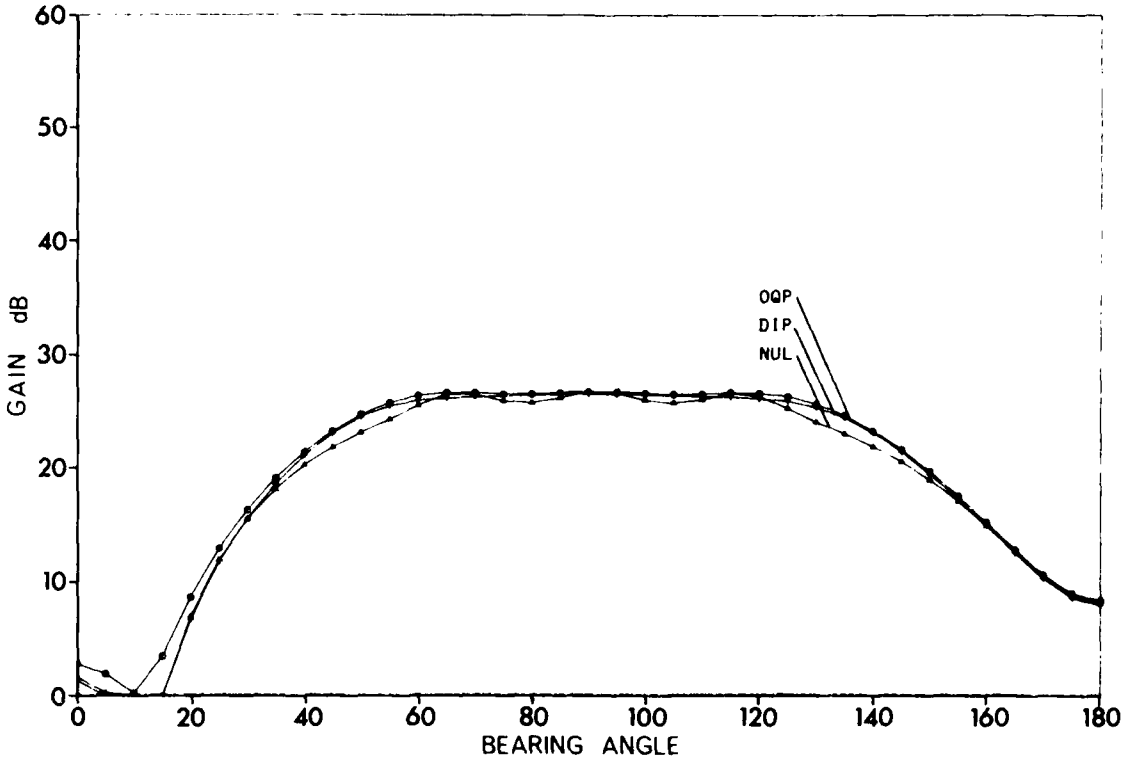

FIG. 42 COMPARISON OF NULL-STEERING WITH OQP (N = 5)

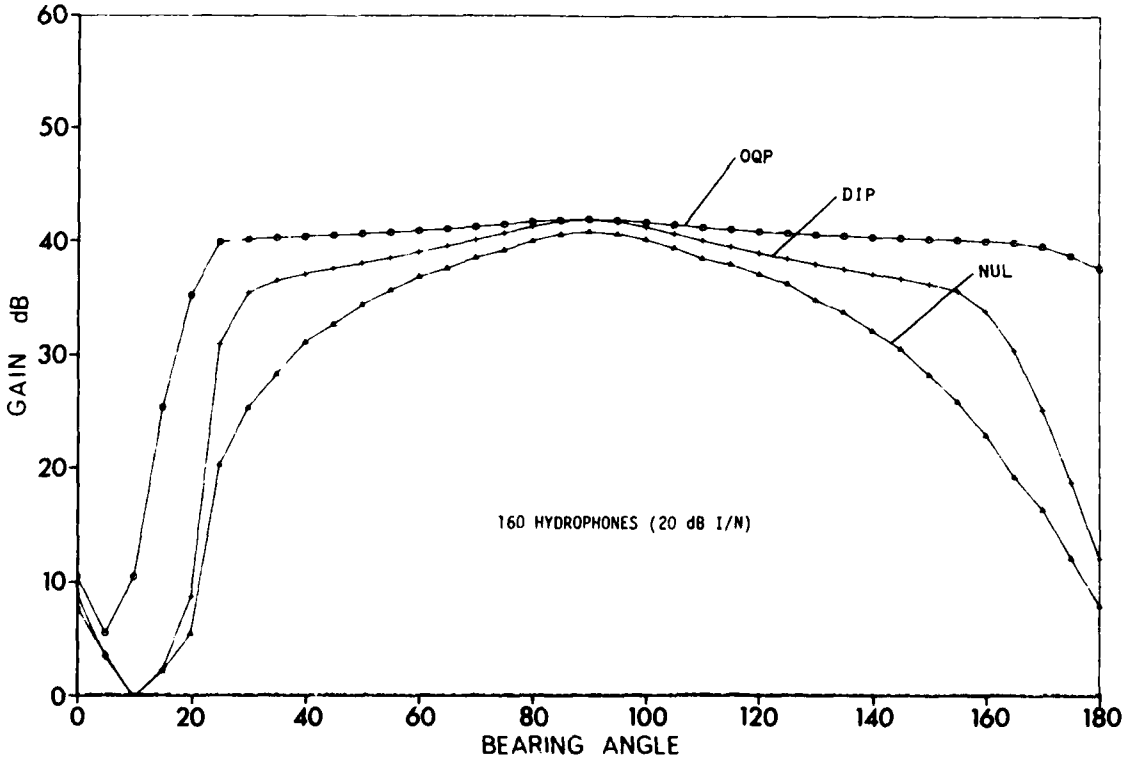

FIG. 43 COMPARISON OF NULL-STEERING METHODS

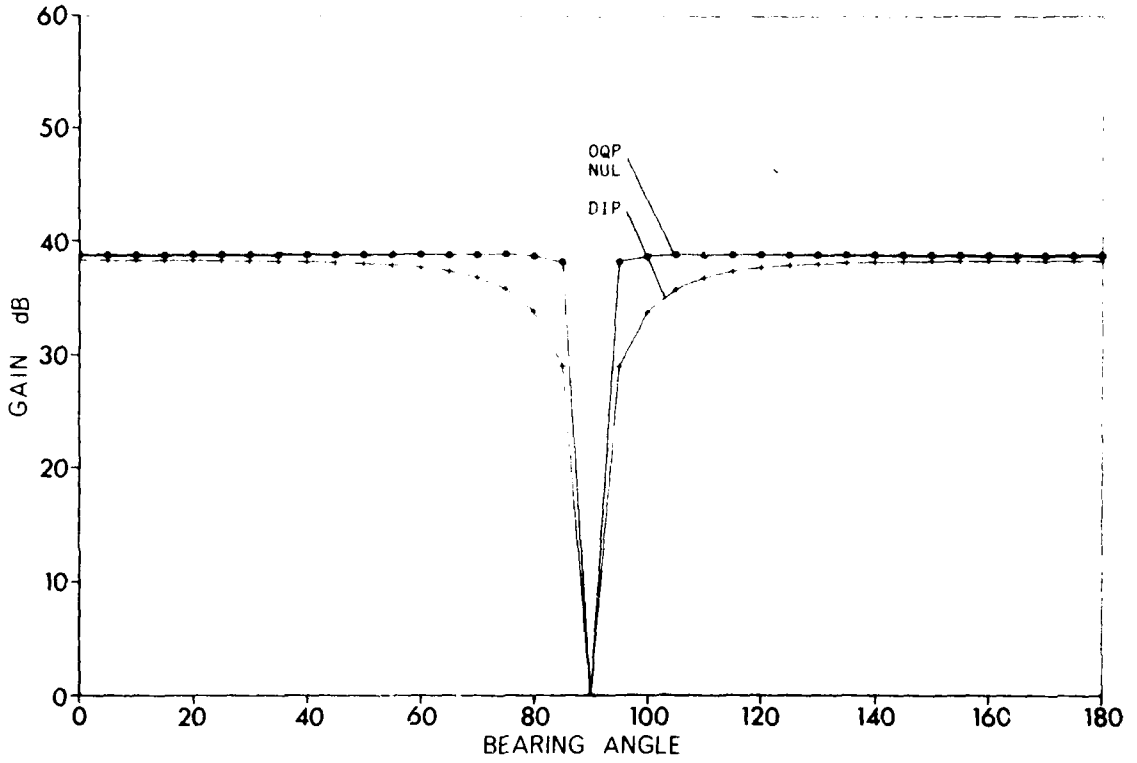

FIG. 44 NULL-STEERING IN BROADSIDE DIRECTION (d/λ = 0.1, N = 80)

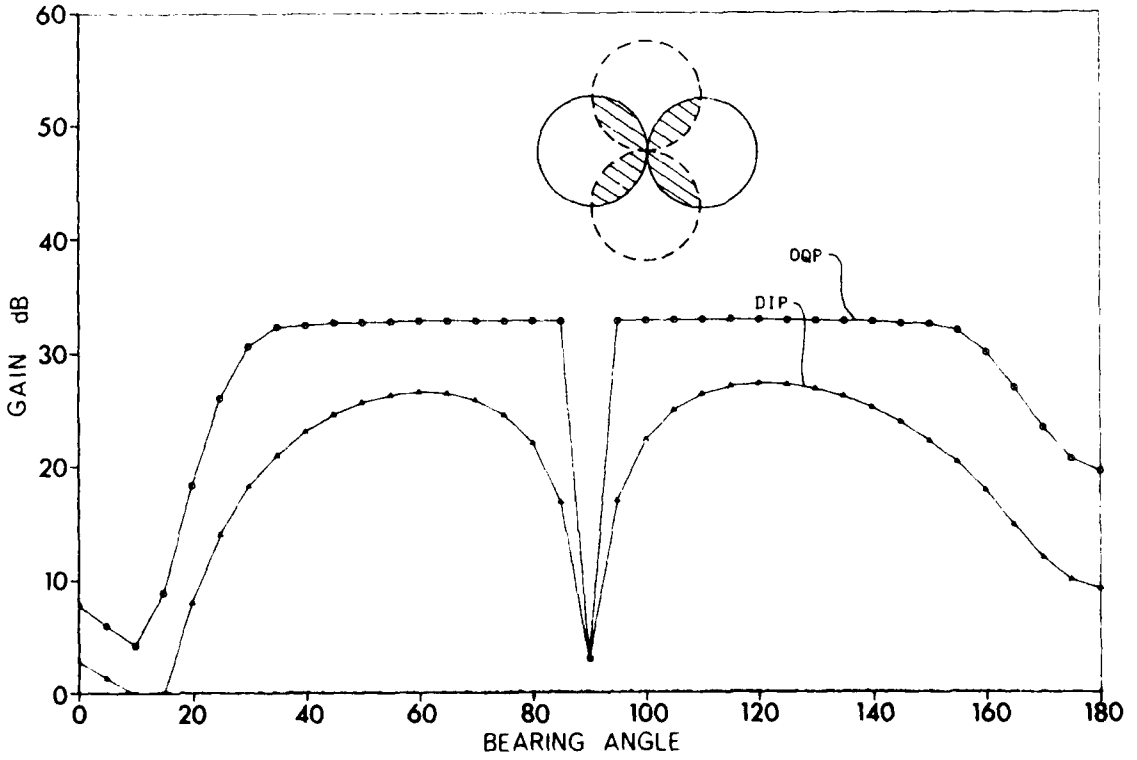

FIG. 45 COMPARISON OF TWO-STAGE DIPOLE PROCESSOR WITH OQP

7 PRE-TRANSFORM ARRAY PROCESSORS

7.1 Introductory

All array processors treated in this chapter differ from the previous ones in that the received signals are first subjected to a pre-transform

$$\underline{y} = \underline{T}\,\underline{x} = \underline{T}(\underline{s} + \underline{n}) \; . \qquad \text{[Eq. 59]}$$

The covariance matrices of signal and noise become

$$\begin{aligned} \underline{S} &= E\{\underline{T}\,\underline{s}\,\underline{s}^*\,\underline{T}^*\} = \underline{T}\,\underline{P}\,\underline{T}^* \\ \underline{N} &= E\{\underline{T}\,\underline{n}\,\underline{n}^*\,\underline{T}^*\} = \underline{T}\,\underline{Q}\,\underline{T}^* \; . \end{aligned} \qquad \text{[Eq. 60]}$$

The quadratic array processor after the pre-transform becomes

$$\ell \equiv \underline{x}^*\,\underline{T}^*\,\underline{N}^{-1}\,\underline{S}\,\underline{N}^{-1}\,\underline{T}\,\underline{x} \gtrless \eta \qquad \text{[Eq. 61]}$$

and the optimum linear pre-transform processor

$$\ell \equiv \mathrm{Re}\{\underline{x}^*\,\underline{T}^*\,\underline{N}^{-1}\,\underline{T}\,\underline{b}\} \; . \qquad \text{[Eq. 62]}$$

As far as $\underline{T}$ is a regular square matrix, Eq. 61 is identical to Eqs. 25 and 27 and Eq. 62 is identical to Eqs. 42 and 45, because

$$(\underline{T}\,\underline{Q}\,\underline{T}^*)^{-1} = (\underline{T}^{*-1}\,\underline{Q}^{-1}\,\underline{T}^{-1}) \; .$$

If, for instance, $\underline{T}$ contains the eigenvectors of the covariance matrix of input signals $E\{\underline{x}\,\underline{x}^*\}$ (Karhunen-Loeve transform), the resulting covariance matrix $E\{\underline{T}\,\underline{x}\,\underline{x}^*\,\underline{T}^*\}$ becomes diagonal, thus obtaining a spectral decomposition in space or, in other words, representing the sound field by N fictive point sources. The eigenvalues denote the source strengths, the eigenvectors the directions. In this case optimum noise suppression reduces to division of the received signal by the spatial power spectrum. However, the spectral decomposition is a quite cumbersome procedure. It has been pointed out in [9] that even a suboptimum iterative approach, considering just the strongest eigenvalues of the noise covariance matrix, does not lead to a simple algorithm for real-time processing.

The transforms considered in the following are LxN-matrices, where L<N. The idea is to reduce the order of the signal vector space such that subsequent processing (pre-whitening and matching) can be carried out in the vector space of low order. Therefore, $\underline{T}$ has to be chosen so that

L<<N, in order to spare arithmetic operations.

L is sufficiently large for adaptive noise suppression, i.e. L > number of interfering sources.

No target energy is lost.

The third requirement can be satisfied by steering one or more beams in the hypothetical target direction. For large arrays a bunch of over-lapping beams should be used to cover the whole area of spatial signal spread. Therefore, in general, the matrix $\underline{T}$ will have the following form

$$\underline{T} \equiv \left(\frac{\text{beamformers}}{\text{noise estimation}} \right) . \qquad \text{[Eq. 63]}$$

That means that all methods discussed below differ basically from all previous ones in that the noise suppression is carried out after the beamforming, instead of before. For example,

$$\underline{T} \equiv \left(\begin{array}{c|ccc} & b^* & & \\ \hline 1 & & & \\ & 1 & & \\ & & 1 & \\ & 0 & & \end{array} \right) \qquad \text{[Eq. 64]}$$

represents a beamformer and, in addition, L-1 auxiliary sensors for estimating the noise in the beam. Consequently, the covariance matrix

$$\underline{N} = \underline{T}\,\underline{Q}\,\underline{T}^*$$

contains the correlation coefficients between auxiliary sensors and beam. For another choice of auxiliary sensors one may get

$$\underline{T} \equiv \left(\begin{array}{c|ccc} & b^* & & \\ \hline 1 & & & \\ & 1 & & 0 \\ & & 1 & \\ & 0 & & 1 \end{array} \right) . \qquad \text{[Eq. 65]}$$

In passive systems, where no target-signal free-noise estimates are available, auxiliary difference patterns may be formed with the null pointing in the hypothetical target direction, e.g.

$$\underline{T} \equiv \left(\begin{array}{c} \underline{b}^* \\ \hline \begin{array}{ccccc} 1 & -b_2^* & & & \\ & 1 & -b_2^* & & \\ 0 & & 1 & -b_2^* & 0 \\ & & & 1 & -b_2^* \end{array} \end{array} \right) . \qquad \text{[Eq. 66]}$$

Instead of difference sensor patterns some kind of difference beam patterns could be used

$$\underline{T} \equiv \left(\begin{array}{c} \underline{b}^* \\ \hline \underline{b}^*(1) \\ \underline{b}^*(2) \\ \vdots \end{array} \right) . \qquad \text{[Eq. 67]}$$

The $\underline{b}^*(i)$ have to be chosen such that they yield a null in the hypothetical target direction, i.e. they have to be orthogonal to the beamformer $\underline{b}$:

$$\underline{b}^*(i)\underline{b} = 0 \qquad i.$$

Such orthogonal vectors can be produced easily by multiplying the coefficients of $\underline{b}$ with orthogonal functions, such as Walsh functions.

Finally, a multibeam transform is given by

$$T \equiv \left(\begin{array}{c} \underline{b}_1^* \\ \underline{b}_2^* \\ \underline{b}_3^* \\ \underline{b}_4^* \\ \vdots \end{array} \right) , \qquad \text{[Eq. 68]}$$

where the $\underline{b}_i^*$ are beams pointing in different directions. Since in sonar systems all beams are usually pre-formed, the use of multiple beams does not mean an additional expense as it does, for example, in radar systems. The question still arises of which beams should be taken. One possibility is to steer some beams in the target direction (slightly overlapping) and

steer one beam on each interfering source. This has been proved to be almost optimum for the use in a multiple beam-phased array radar [37]. The disadvantage is that the positions of the interference have to be known [illegible], i.e. by some other means, such as radar. Another possibility is to centre all beams orthogonally overlapping around the hypothetical target direction and to make noise suppression in the "signal-beam domain". Orthogonal overlapping guarantees well-conditioned covariance matrices, which is important for numerical reasons.

The gains of the processors of Eqs. 61 and 62 are found by replacing $\underline{Q}$ by $\underline{N}$ and $\underline{P}$ by $\underline{S}$ in Eqs. 37 and 47:

$$G_{QP} = \frac{\mathrm{tr}(\underline{F}^* \underline{S} \underline{F})}{\sqrt{\mathrm{tr}(\underline{F}^* \underline{N} \underline{F})^2}} \cdot \frac{P_n}{P_s} \quad , \qquad \text{[Eq. 69]}$$

where $\underline{F} = \underline{N}^{-1} \underline{H}$ [Eq. 70]

and $\underline{S} = \underline{H} \underline{H}^*$. [Eq. 71]

$$G_{LP} = \frac{\underline{k}^* \underline{N}^{-1} \underline{S} \underline{N}^{-1} \underline{k}}{\underline{k}^* \underline{N}^{-1} \underline{N} \underline{N}^{-1} \underline{k}} \cdot \frac{P_n}{P_s} = \frac{\underline{k}^* \underline{N}^{-1} \underline{S} \underline{N}^{-1} \underline{k}}{\underline{k}^* \underline{N}^{-1} \underline{k}} \cdot \frac{P_n}{P_s} \quad , \qquad \text{[Eq. 72]}$$

where $\underline{k} = \underline{T} \underline{b}$ denotes the beamformer vector after the pre-transform. Replacing $\underline{k}$ by a unity vector $\underline{e}$ causes only the beamformer output of the pre-transform to be considered, e.g. for the pre-transform of Eq. 64 the unity vector

$$\underline{e}_1 = \begin{pmatrix} 1 \\ 0 \\ \vdots \\ 0 \end{pmatrix} + j \, \underline{0} \qquad \text{[Eq. 73]}$$

is chosen. The contributions of the auxiliary sensors or beams are omitted.

7.2 Calculation of the Generalized Beamformer

The role of optimum and suboptimum quadratic beamformers has been discussed in Ch. 3. The generalized beamformer is a matrix $\underline{H}$ defined by

$$\underline{L} = \underline{H} \underline{H}^* \, , \qquad \text{[Eq. 74]}$$

where $\underline{L}$ may be the signal covariance $\underline{P}$ or the transformed matrix $\underline{S} = \underline{T}\,\underline{P}\,\underline{T}^*$. If $\underline{P}$ is not known, it has to be replaced by some matrix $\underline{G}$ that describes an equivalent angle interval with uniform energy distribution as an approximation for the actual signal spread. For the gain calculation in Eqs. 37 and 47, the factorization of Eq. 74 is not necessary. The gain formula can be rewritten as follows:

$$G = \frac{\mathrm{tr}(\underline{F}^*\,\underline{P}\,\underline{F})}{\sqrt{\mathrm{tr}(\underline{F}^*\,\underline{Q}\,\underline{F})^2}} \cdot \frac{P_n}{P_s}$$

$$= \frac{\mathrm{tr}(\underline{P}\,\underline{F}\,\underline{F}^*)}{\sqrt{\mathrm{tr}(\underline{Q}\,\underline{F}\,\underline{F}^*)^2}} \cdot \frac{P_n}{P_s} = \frac{\mathrm{tr}(\underline{P}\,\underline{Q}^{-1}\,\underline{H}\,\underline{H}^*\,\underline{Q}^{-1})}{\sqrt{\mathrm{tr}(\underline{Q}\,\underline{Q}^{-1}\,\underline{H}\,\underline{H}^*\,\underline{Q}^{-1})^2}} \cdot \frac{P_n}{P_s} \quad .$$

That means that for the gain calculation the unfactored matrix, $\underline{H}\,\underline{H}^* = \underline{P}$ or $\underline{H}\,\underline{H}^* = \underline{G}$ respectively, is needed. The same is true of course for the transformed matrix $\underline{T}\,\underline{H}\,\underline{H}^*\,\underline{T}^*$ in Eq. 69.

One is, however, faced with the problem of factorization in order to design the quadratic array processor. If a modelling program is run in order to get some *a priori* knowledge about the signal covariance matrix $\underline{P}$, the beamformer matrix $\underline{H}$ is given explicitly without factorization by

$$\underline{H} = \underline{M}^*\,\underline{A}\,\underline{W} \ ,$$

which follows direct from Eq. 17. $\underline{W}$ is defined by

$$\underline{V} = \underline{W}\,\underline{W}^* \ ,$$

i.e. the factorized normalized covariance matrix among modes. This factorization has to be carried out only once. In the trivial case of uncorrelated modes one has

$$\underline{W} = \underline{I}.$$

$\underline{M}^*$ and $\underline{A}$ are given by the modelling program.

If, however, the signal covariance matrix is given, e.g. by measurement or by assuming an equivalent angle interval with uniform energy distribution, the factorization must be carried out by means of the Cholesky-algorithm, see [21], for example. Some numerical problems will arise for $\cos\beta = 0$,

i.e. broadside direction. Corresponding to Eq. 20 the covariance matrix becomes singular, which means that the factorization can no longer be carried out. One way to avoid that is to add some "artificial noise", which means adding a certain small number, δ, to the elements of the main diagonal of the covariance matrix

$$r'_{ii} = r_{ii}(1 + \delta) \qquad i = 1...N \qquad \text{[Eq. 75]}$$

If δ is small the influence on the array gain is negligible.

An alternative approach is to use the Cholesky-algorithm until break-off. The algorithm is given by

$$r_{ik} = \left(a_{ik} - \sum_{j=1}^{i-1} r_{ji}\, r_{jk}\right) / r_{ii}$$

$$r_{ii} = a_{ii} - \sum_{j=1}^{i-1} r_{ji}^2 \qquad \begin{matrix} i = 1...N \\ k = i...N, \end{matrix} \qquad \text{[Eq. 76]}$$

where a_{ik} are the elements of the original matrix and r_{ik} the elements of the triangular matrix after factorization. The algorithm breaks off if the elements r_{ii} become smaller than the arithmetic accuracy used. To illustrate this let us consider the case of a 3×3 Toeplitz-matrix:

$$\underline{A} = \begin{pmatrix} 1 & a & b \\ a & 1 & a \\ b & a & 1 \end{pmatrix} .$$

After factorization the result is

$$\underline{R} = \begin{pmatrix} 1 & a & b \\ 0 & \sqrt{1-a^2} & \dfrac{a(1-b)}{\sqrt{1-a^2}} \\ 0 & 0 & 1-b^2 - \dfrac{a^2(1-b^2)}{1-a^2} \end{pmatrix}$$

The algorithm calculates the values of the first row column by column, then the second row, and so on. If a approaches +1 or -1 the value $r_{22} = \sqrt{1 - a^2}$ becomes 0 and the algorithm breaks off when calculating r_{23}.

If $a = 1$, the algorithm breaks off if $b = 1$ or $b = 2a^{-1}$. In this case the first two rows are calculated correctly and the rest have to be omitted. If $|a| = 1$, one finishes up just with a vector (first row of $\underline{A}$), so that the Toeplitz-matrix $\underline{R}^* \underline{R}$ is just a dyadic. This happens at broadside, as pointed out above. That means that the result of the interrupted factorization is the conventional beamformer, which is in fact optimum at broadside.

The only point to be observed is that after break-off the rest of the matrix has to be zero. As the Cholesky decomposition is usually carried out "in place" the algorithm has to be modified such that after break-off the part of the matrix not yet computed is made zero.

7.3 Nonadaptive Null-steering

A pre-transform array processor involving nonadaptive nullsteering can be achieved just by replacing $\underline{N}^{-1}$ in Eq. 69 by a constraint matrix of the kind given by Eqs. 53 and 55. After the pre-transform the interference direction is given by $\underline{T}\,\underline{c}$. Therefore, the projection matrix in the reduced vector space becomes

$$\underline{C} = \underline{I} - \frac{\underline{T}\,\underline{c}\,\underline{c}^*\,\underline{T}^*}{\underline{c}^*\,\underline{T}^*\,\underline{T}\,\underline{c}} \qquad \text{[Eq. 77]}$$

or, with more than one interfering source,

$$\underline{C} = \underline{I} - \underline{I}\,\underline{H}(\underline{H}^*\,\underline{T}^*\,\underline{T}^*\,\underline{H})^{-1}\,\underline{H}^*\,\underline{T}^* \,, \qquad \text{[Eq. 78]}$$

so that $\underline{C}\,\underline{T}\,\underline{H} = \underline{0}$.

The corresponding quadratic array processor becomes

$$\ldots \underline{x}^*\,\underline{T}^*\,\underline{C}^*\,\underline{S}\,\underline{C}\,\underline{T}\,\underline{x} \gtrless \eta \qquad \text{[Eq. 79]}$$

and the linear one

$$\ldots \mathrm{Re}\{\underline{x}^*\,\underline{T}^*\,\underline{C}\,\underline{T}\,\underline{b}\} \gtrless \eta \,. \qquad \text{[Eq. 80]}$$

However, this kind of processing leads to similar results to those achieved by processors using the noise-suppression matrices of Eqs. 53 or 54,

because the constraint matrices of Eqs. 77 and 78 do the same as Eqs. 53 and 54, i.e. move a null of the array pattern in the direction of the interference. The only difference is that for large arrays less arithmetic operations are required to implement Eq. 77 than Eq. 53. Nevertheless, steering of nulls in the array pattern does not work well enough for bearing angles close to endfire and will, therefore, not be discussed further.

.4 The Choice of the Pre-transform

Figures 46 to 49 present some numerical results on array gain to show the performance of different kinds of pre-transform array processors. Figures 46 and 47 show two different choices of auxiliary sensors. In Fig. 46 the sensors are chosen (1, 4, 7) to be widely but equally spaced, (see Eq. 65). In Fig. 46, the 1, 2, 3 sensor are chosen (see Eq. 64). In both cases many auxiliary sensors are required in order to approximate the performance of the optimum quadratic processor (OQP). It is not even possible to make a statement on whether it is better to use closely or widely spaced auxiliary sensors. For two, three, or four auxiliary sensors obviously small spacing is advantageous, for six auxiliary sensors, however, large spacing seems to be better. In any case, except for six widely spaced auxiliary sensors, all curves show more or less some kind of ripple due to the sidelobes of the beam when moved over the interfering sources. The reason is that for the auxiliary sensors the interference-to-noise ratio is always constant for all directions, whereas in the main beam it changes with bearing according to the sidelobe pattern.

For the simple example of two sensors, it can be shown that the array becomes maximum if the interference-to-noise ratio in both channels is equal. The signals are $x_1 = q_1 + n_1$ and $x_2 = q_2 + n_2$, where q is the interference, n the noise portion, and the indices refer to the corresponding channels. The covariance matrix becomes

$$\underline{X} = E\{\underline{x}\ \underline{x}^*\} = \begin{pmatrix} Q_1+N_1 & Q_{12} \\ Q_{12}^* & Q_2+N_2 \end{pmatrix}$$

The inverse becomes

$$\underline{X}^{-1} = \frac{1}{\det \underline{X}} \begin{pmatrix} Q_2+N_2 & -Q_{12} \\ -Q_{12}^* & Q_1+N_1 \end{pmatrix}$$

Q_1 and Q_2 are the interference powers in channel 1 and 2, N_1 and N_2 are the noise powers, and Q_{12} is the crosscorrelation term $E\{x_1 x_2^*\} = E\{q_1 q_2^*\}$. Let us consider, for convenience, the array gain in endfire direction in the presence of a broadside interference, and let us introduce the conditions

$$Q_2 + N_2 = 1$$

$$Q_1 + N_1 = 1$$

$$N_0 = N_1 + N_2.$$

The inverse covariance matrix is

$$\underline{X}^{-1} = \frac{1}{\det \underline{X}} \begin{pmatrix} 1 & -Q_{12} \\ -Q_{12} & 1 \end{pmatrix}$$

The array gain in endfire direction is, for a $\lambda/2$-spaced array (see Eq. 49),

$$G = \underline{s}^* \underline{Q}^{-1} \underline{s} \frac{P_n}{P_s},$$

which becomes, for this example,

$$G = (1 \ , \ -1) \begin{pmatrix} 1 & -Q_{12} \\ -Q_{12} & 1 \end{pmatrix} \begin{pmatrix} 1 \\ -1 \end{pmatrix} = 2(1 + Q_{12})$$

The crosscorrelation coefficient is simply

$$Q_{12} = \sqrt{1 - N_1} \ \sqrt{1 - N_2},$$

so that the gain becomes

$$G = 2(1 + \sqrt{(1 - N_1)(1 - N_2)}).$$

For example, if there is no interference, we get $N_1 = N_2 = 1$ and $G = 2$, which is the white noise gain for two sensors. For $N_1, N_2 < 1$ let us write $N_2 = N_0 - N_1$ in order to keep the total power constant:

$$G = 2(1 + \sqrt{(1 - N_1)(1-(N_0 - N_1)}\ ),$$

which becomes maximum if $N_1 = \frac{1}{2} N_0 = N_2$. Therefore, the gain of an array is maximum if (for a given total interference-to-noise ratio) the interference-to-noise ratios of all channels are the same. This is verified for adaptive processors like the OQP or OLP that perform interference rejection before beamforming. The interpretation of the inverse covariance matrix between sensors is that arbitrary N-1 sensors are used to estimate the interference in the remaining channel and to subtract it. In this case, of course, all channels have the same interference-to-noise ratio.

Consequently, for a pre-transform-type processor (i.e. interference rejection after beamforming) the auxiliary channels should be chosen such that the interference-to-noise ratio is about the same as in the main beam, i.e. the auxiliary channels have about the same beam pattern as the main beam. Of course, they must not be exactly the same, otherwise the rows of the pre-transform matrix $\underline{T}$ become linearly dependent, causing all transformed matrices (e.g. $\underline{N} = \underline{T}\ \underline{Q}\ \underline{T}^*$) to be singular.

Consequently, the best choice is a bunch of orthogonally overlapping beams centred around the beam looking in the hypothetical target direction. The same principle has proved to be quite efficient for adaptive clutter suppression in step-scan radars *[22]*. Orthogonal overlap of beams guarantees well-conditioned covariance matrices as far as the pre-transform is concerned. Figure 48 shows the same example as before but for the multibeam processor (MBP) described above. The performance is significantly better than the results achieved in the two previous examples. In particular, almost no sidelobe ripple can be observed.

The multibeam processor described above has another property that is quite useful for application in shallow water. If the signal energy is spread in space, it has to be spatially integrated. If the number of orthogonally

overlapping beams is such that the whole area of the signal is covered, appropriate integration (such as the quadratic pre-transform processors of Eqs. 59 and 60) of the beam outputs can be expected to be an almost optimum generalized beamformer. Considering furthermore the good interference rejection properties discussed above, the quadratic multibeam processor promises to be an efficient means for target detection by large arrays.

As an example, Fig. 49 shows the quadratic MBP applied to an array with 160 sensors (80λ aperture). As can be seen, for NB = 5 a remarkable approximation to the OQP is achieved. For NB = 3 some loss in gain is observed. This is because the number of degrees of freedom of the noise-cancelling system (NB-1) is too small. Basically, the number of degrees of freedom has to be equal to or greater than the number of different eigenvalues of the interference-covariance matrix different from zero. For coherent plane waves this is identical to the number of distinct interfering sources. In our example the spread of the endfire source causes a spread of the source energy over more than one eigenvalue, thus increasing the number of degrees of freedom required for cancellation. This effect increases with an increase in the number of sensors, i.e. with increasing resolution of the array, as can be seen by comparing Figs. 48 and 49.

Figure 50 shows the same conditions as Fig. 49. However, two of the curves show the situation in which two of the beams are steered permanently on the interfering sources (which, in practice, requires a knowledge of their positions). If there are just two noise beams and one signal beam (NB = 3) the gain decreases because of the lack of degrees of freedom in the system. A system with three signal beams and two interference beams is slightly superior to the MBP with five signal beams. However, the difference is so small that there is no reason for designing a system that needs *a priori* knowledge of the interference geometry.

Figure 51 shows that in certain, less-complicated situations (e.g. one broadside source) different kinds of pre-transform methods (auxiliary sensors, MBP) yield about the same good approximation to the OQP.

A comparison of Figs. 52 and 53 shows that the MBP is significantly superior to the auxiliary sensor processor when applied to wide-angle noise.

7.5 Linear versus Quadratic Processing

In the following, only the multiple beam processor (MBP) is considered. As pointed out in the introduction to this chapter (Sect. 7.1), a considerable number of arithmetic operations can be saved if the number of beams is small compared with the number of sensors. However, the optimum quadratic pre-transform processor still contains the covariance matrix of the signal, which is usually not known *a priori*. Of course, an estimate can be achieved by measurement if there is only one sound source around, or alternatively, by running a modelling program. However, these results are still range-dependent, and it is quite cumbersome to carry out the calculation of the quadratic beamformer for all ranges. It is desirable to have a simple, robust beamformer that does not depend on range but gives satisfactory approximation to the optimum performance.

The simplest approximation is the conventional linear beamformer (see Ch. 5 and Eq. 73), which is supposed to operate well enough for relatively small arrays in which the beamwidth is larger than the spatial energy distribution of the signal.

Figure 54 shows a comparison of quadratic (QP) and linear (LP) multiple beam processing for different numbers of sensors, N. For N = 10, QP and LP coincide almost perfectly. For N = 40, little loss in gain between QP and LP can be recognized apart from broadside. For large arrays (N = 160) the loss between LP and QP becomes significant. Notice that for bearing angles less than 60° and greater than 120° the gain becomes even smaller than when N = 40.

7.6 Suboptimum Quadratic Beamforming

The idea of suboptimum quadratic beamforming is to replace the actual spatial signal distribution by a rectangular window, thus assuming the

signal energy to be distributed uniformly over this interval. The principle has been pointed out in Sects. 3.4 and 7.2. Figure 55 shows some numerical results. The upper curve again shows the QP and the lowest one the LP. The three curves between them show the gain of suboptimum, quadratic, multiple beam processers with different window widths u_0 as defined in Sect. 3.4. If the window is too narrow ($u_0 = 0.01$) the processor behaves like the LP. For other values of u_0($u_0 = 0.05...0.25$) the gain depends on u_0 only when very close to broadside. Obviously the beamwidth causes a significant decrease in gain if it is smaller, rather than greater, than the actual size of the spatial signal spread. This statement was made already in the conclusion to Ch. 3 (Sect. 3.5).

7.7 Incoherent Beam Integration

Suboptimum quadratic processing can be simplified even more by replacing the spatial filter matrix $\underline{H}$ in Eq. 74 by the unity matrix $\underline{I}$. This promises to give a good approximation to the optimum quadratic multiple beam processor if the beams cover just the area of signal spread; Fig. 56 gives a numerical example. Apart from broadside, incoherent integration leads to the same results as the suboptimum quadratic beamformer discussed in the previous section. At broadside even the linear processor is superior to quadratic beam integration, which can be explained as follows: at broadside the signal appears to the linear array to be a single line. As the beams of the multiple beam processor are chosen to be orthogonal, only the middle beam contains the signal whereas the others contain just noise. Consequently, the signal-to-noise ratio in the middle beam is higher than that achieved by integration over all beams. However, compared with the optimum quadratic multiple beam processor, the loss is not greater than 3 dB. The small lack in gain compared with the LP can be avoided by switching off the auxiliary beams when steered in the area around broadside, i.e. using the linear processor.

7.8 Comparison with OQP and COS-shading

Figures 57 and 58 show a comparison between optimum quadratic processing (OQP), quadratic multi-beam processor (SIB), and cosine shading in a multi-

noise-source environment. It can be observed that for small arrays (in this case N = 20) the SIB is much superior to the linear cos-shading processor due to main-lobe interference of the shading method. For certain array lengths (N 80) however, cosine shading will yield a sufficient approximation (loss 3 dB) to the optimum. For much larger arrays (N >> 80) nonadaptive cosine shading should be combined with quadratic beam integration, as described in the previous section.

7.9 Conclusions on Pre-transform Array Processors

a. The multiple-beam transform (steering a bunch of orthogonally overlapping beams in the hypothetical target direction) is superior to all other pre-transforms, e.g. auxiliary sensor transform.

b. For arrays smaller than 20λ aperture, the linear, adaptive, multiple beam processor is almost optimum.

c. A suboptimum, quadratic, multiple beam processor can be obtained by replacing the signal covariance matrix used for calculating the generalized beamformer [Eq. 70] by a matrix that describes the spatial covariance of an angle interval with uniformly distributed energy. The loss in gain compared with the OQP is about 3 dB.

d. An even simpler method than (c) is given by incoherent integration of the signal energy contained in orthogonally overlapping beams. Except for broadside, the gain achieved is the same.

e. For practical application the adaptive, linear, multiple beam processor is recommended for array apertures up to 20λ. For large arrays (>40λ), incoherent integration (summation of squared outputs) of overlapping beams should be applied after cos-shading.

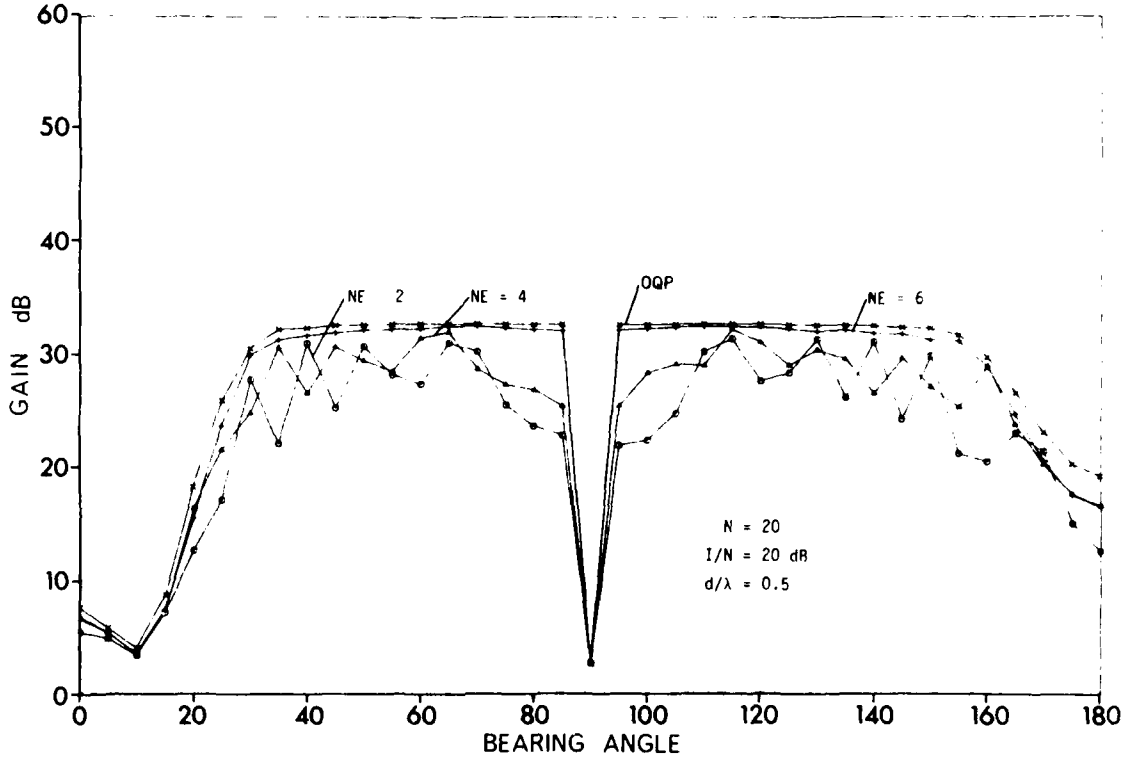

FIG. 46 WIDELY-SPACED AUXILIARY ELEMENTS

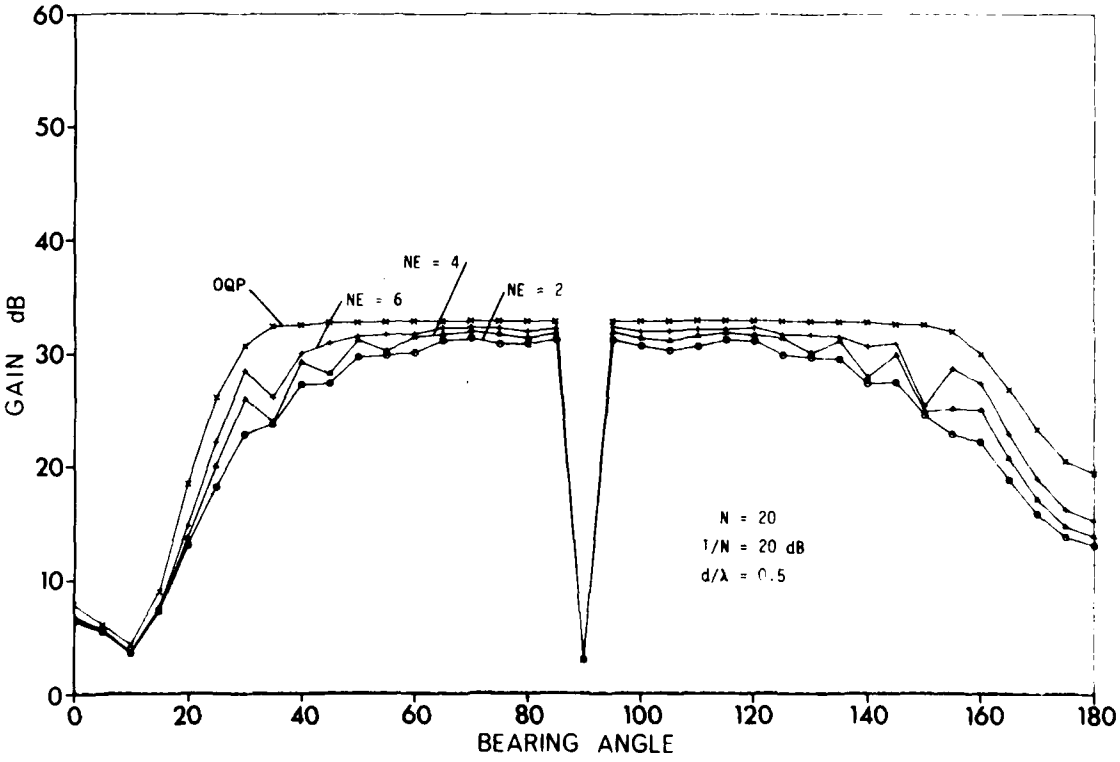

FIG. 47 CLOSELY-SPACED AUXILIARY SENSORS

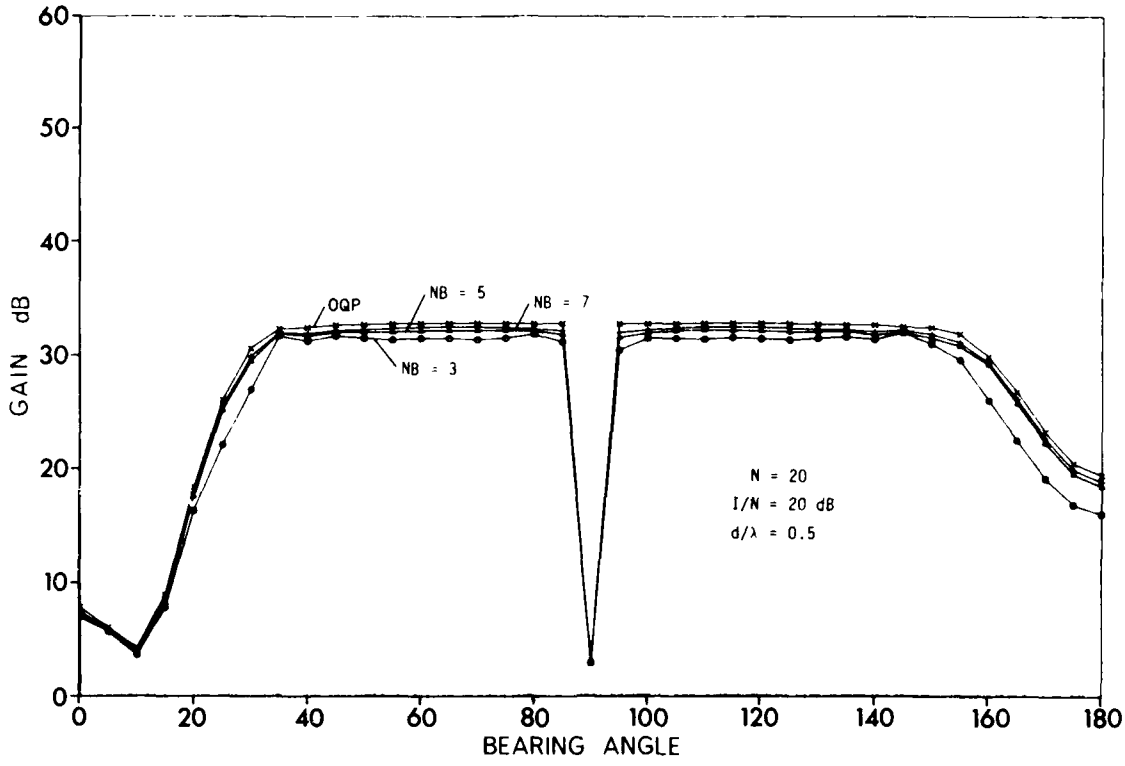

FIG. 48 SIGNAL BEAMS (20 sensors)

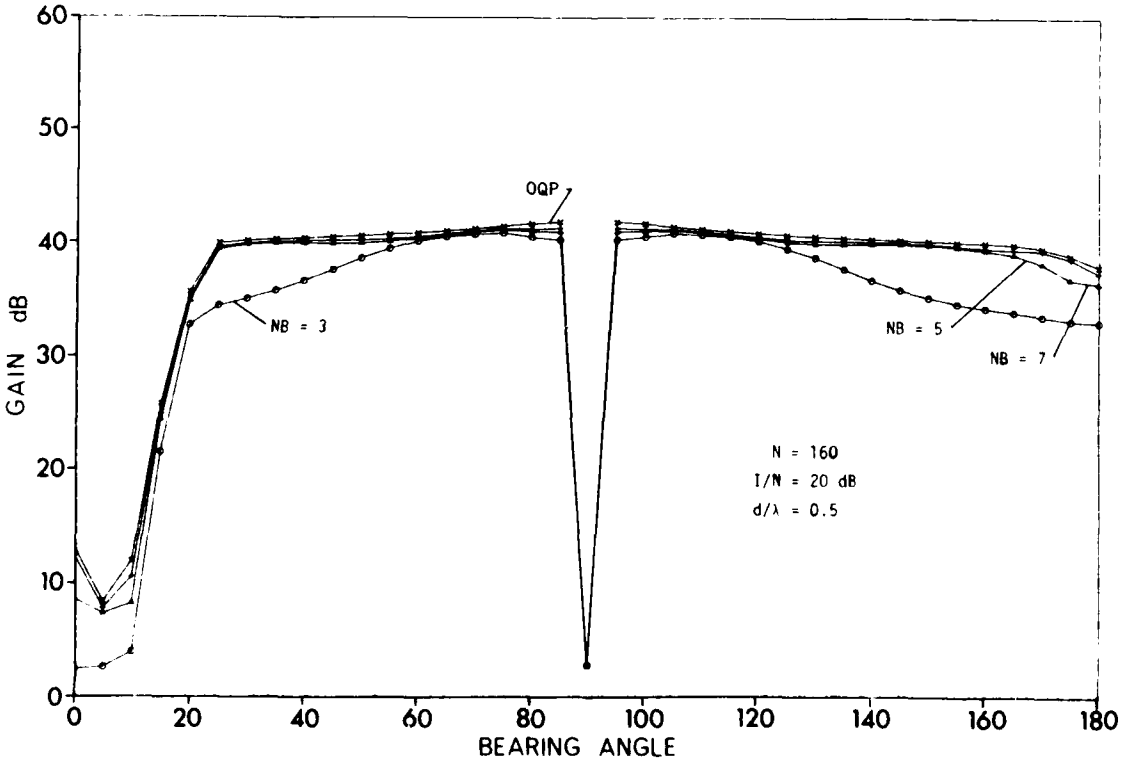

FIG. 49 SIGNAL BEAMS (160 sensors)

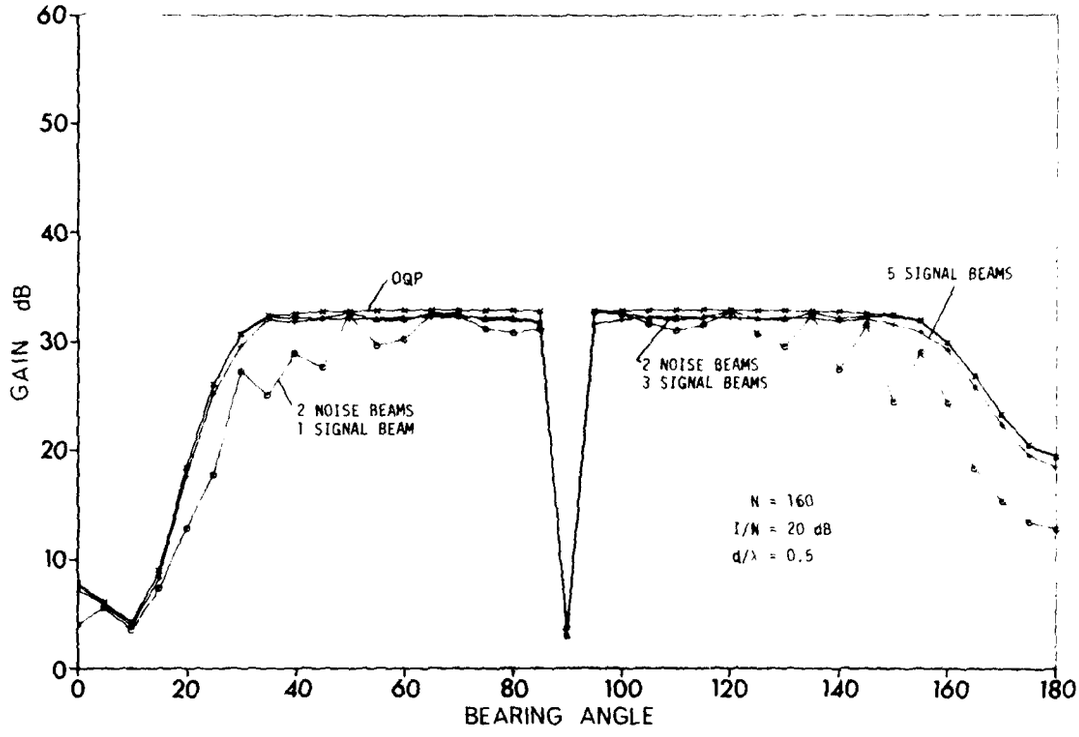

FIG. 50 NOISE BEAMS (160 sensors)

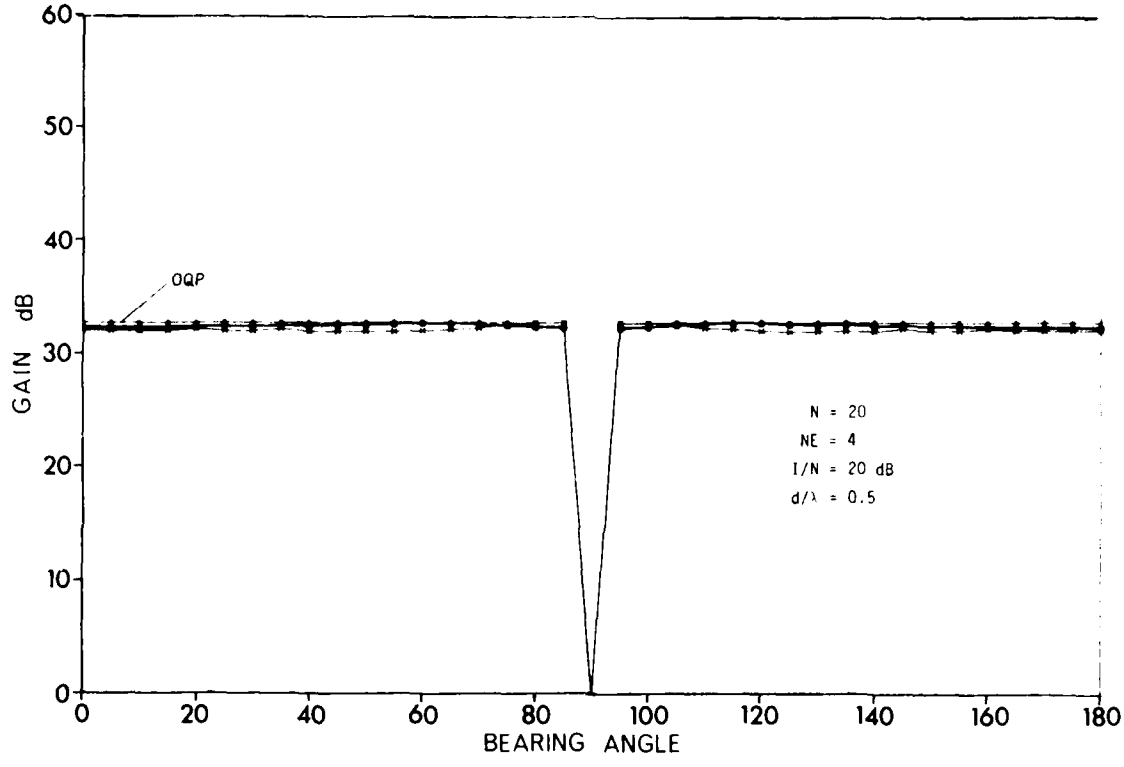

FIG. 51 COMPARISON OF PRE-TRANSFORMS FOR BROADSIDE INTERFERENCE

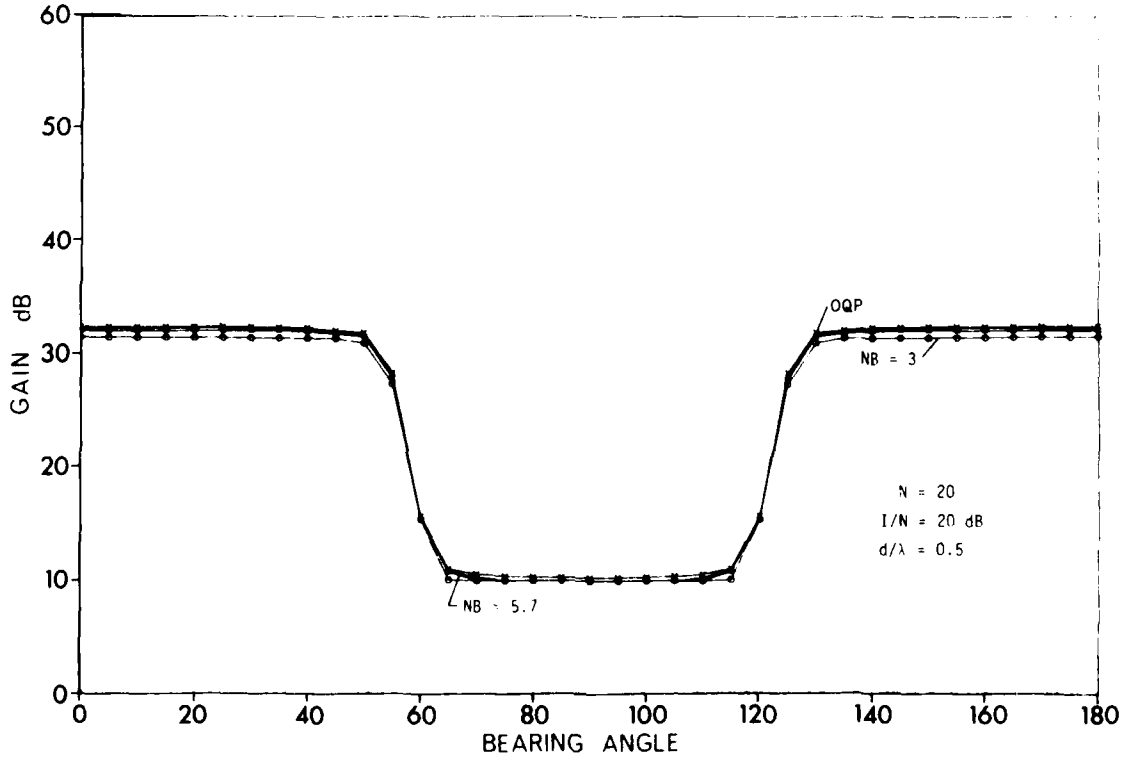

FIG. 52 SIGNAL BEAMS: BROAD-ANGLE NOISE

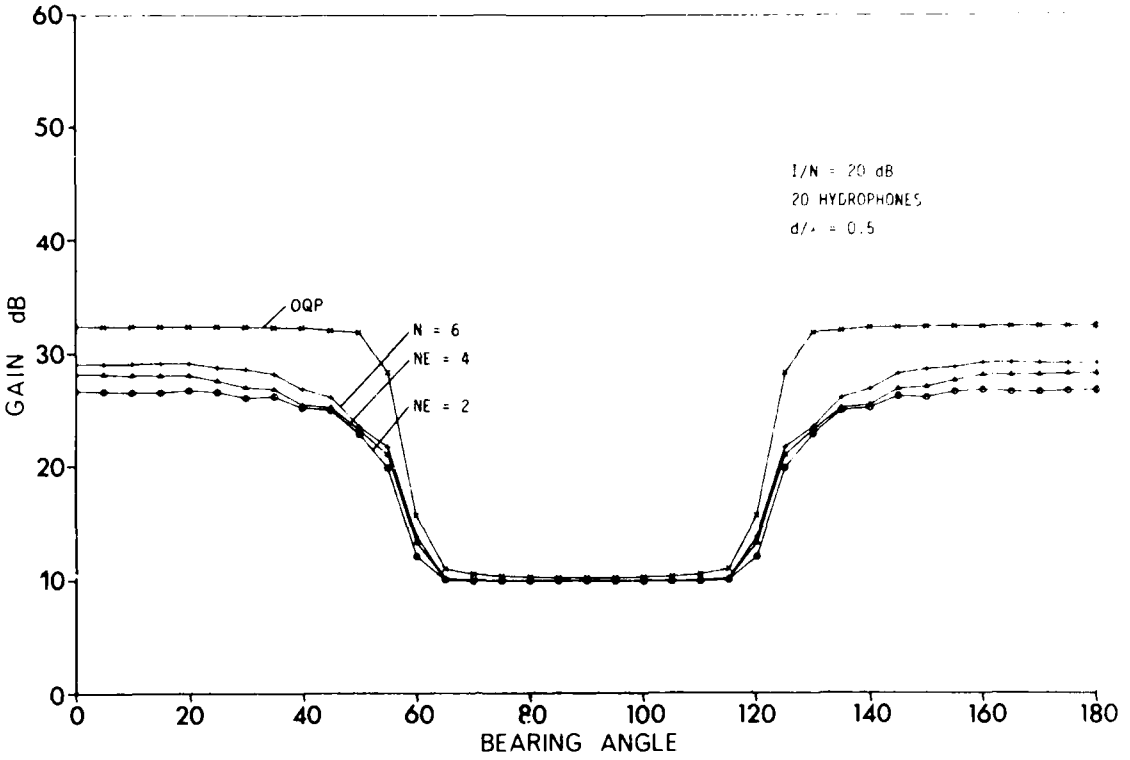

FIG. 53 CLOSELY-SPACED AUXILIARY SENSORS: BROAD-ANGLE NOISE

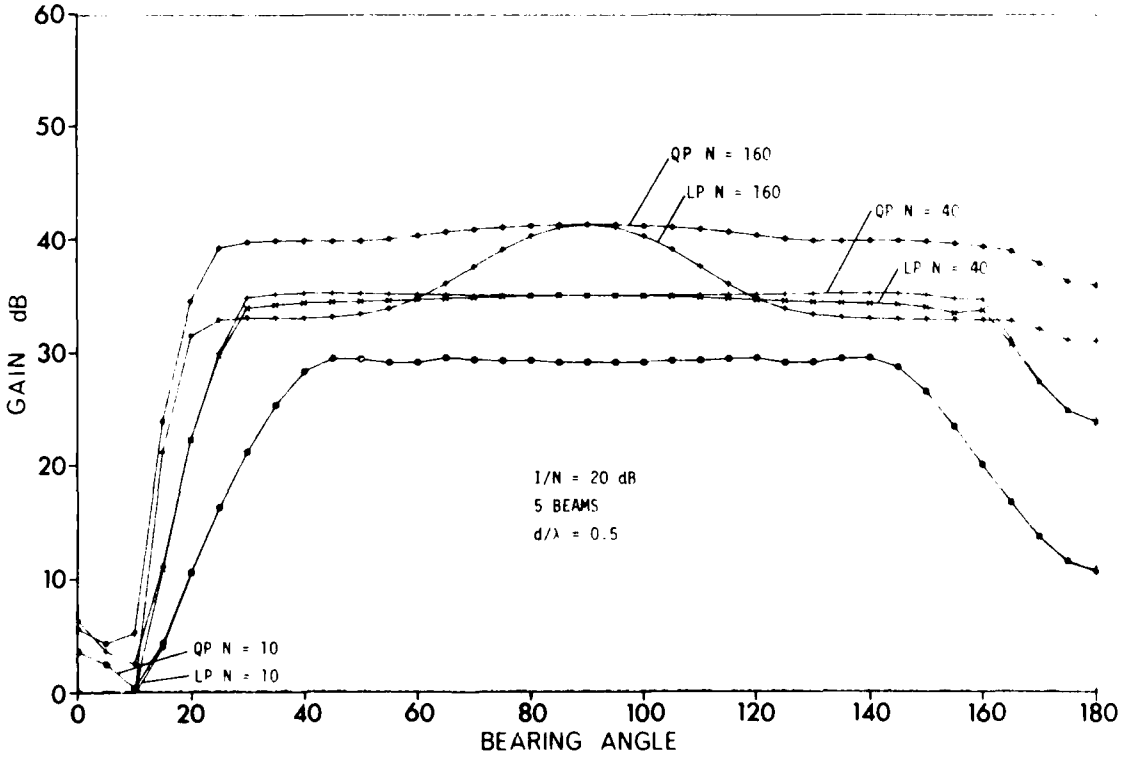

FIG. 54 COMPARISON OF LINEAR AND QUADRATIC MULTIBEAM PROCESSING

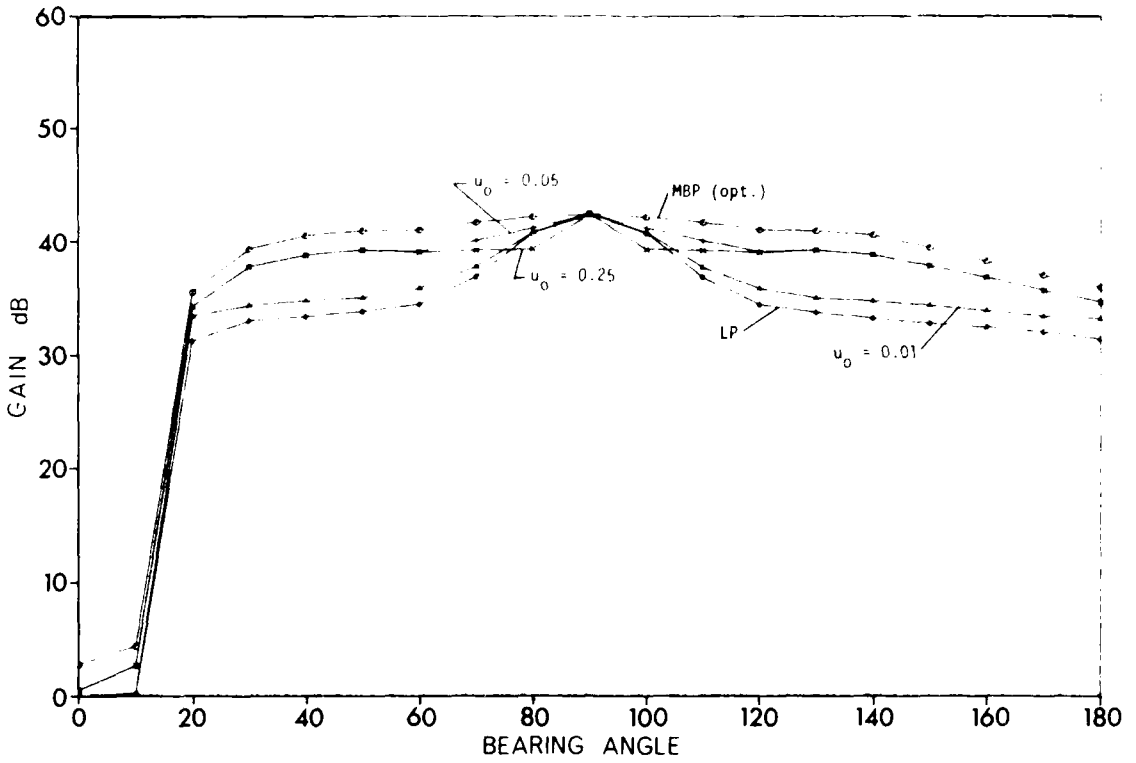

FIG. 55 OPTIMUM AND SUBOPTIMUM QUADRATIC BEAMFORMING

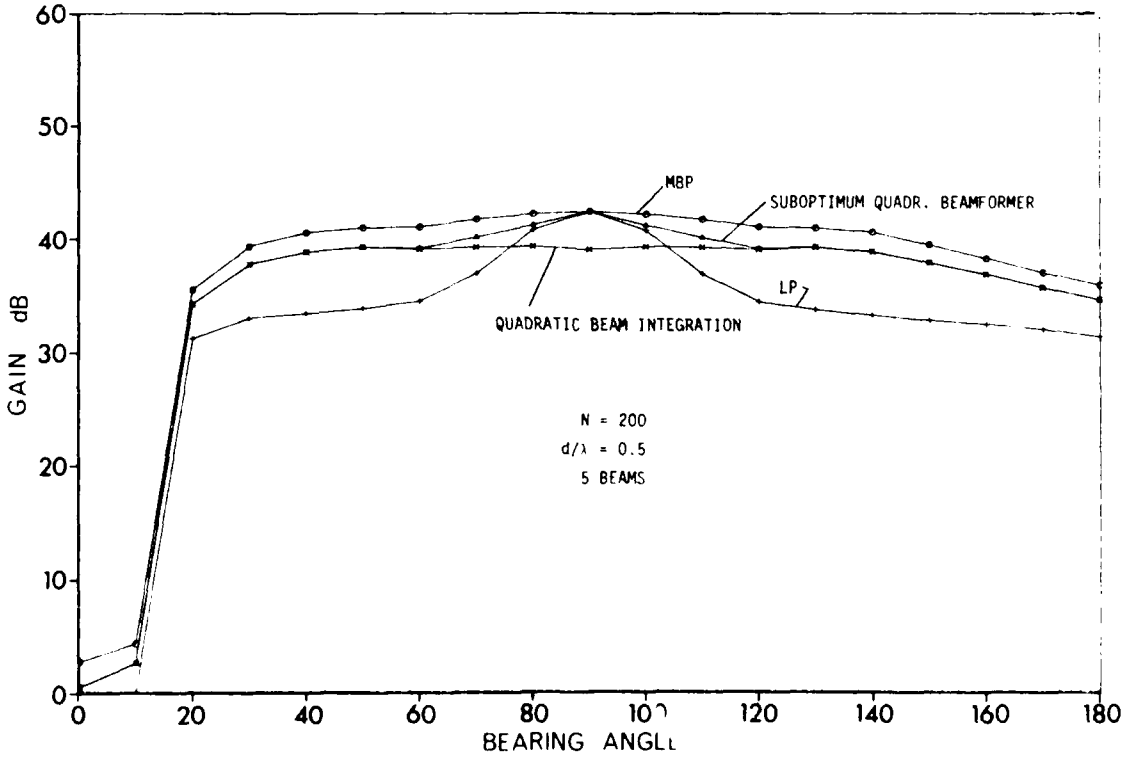

FIG. 56 DIFFERENT KINDS OF BEAMFORMING

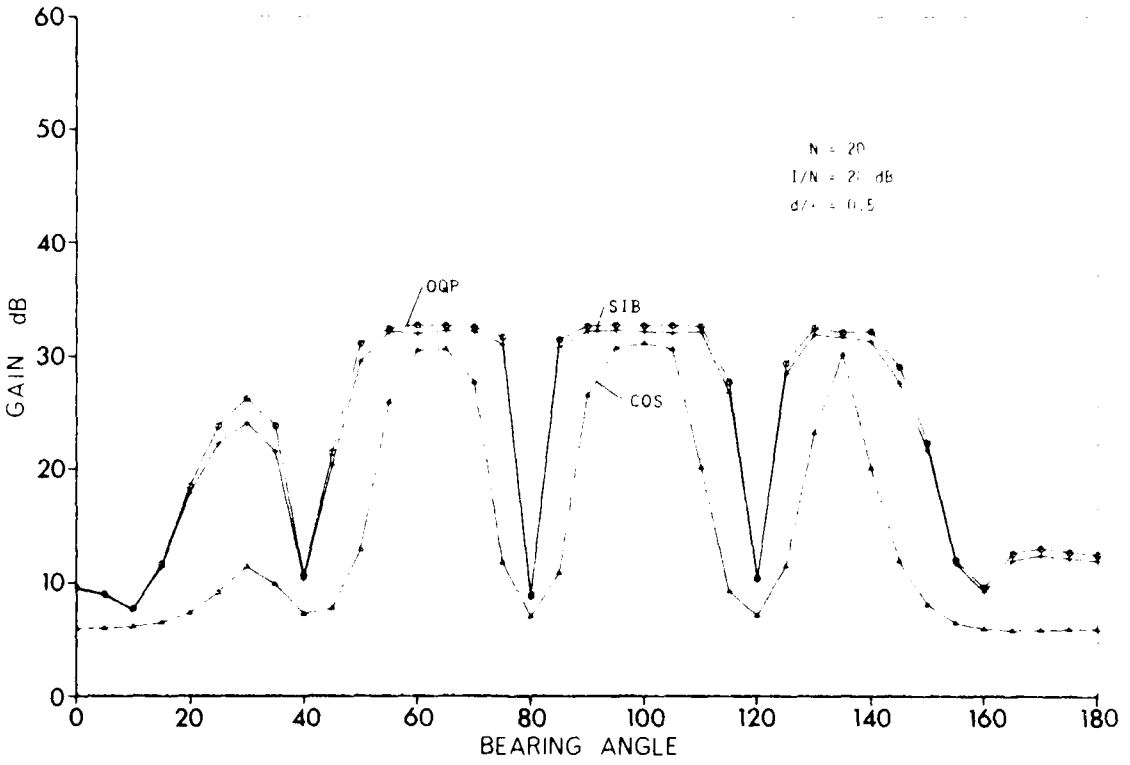

FIG. 57 COMPARISON OF OQP, SIB AND COS-PROCESSOR (N = 20)

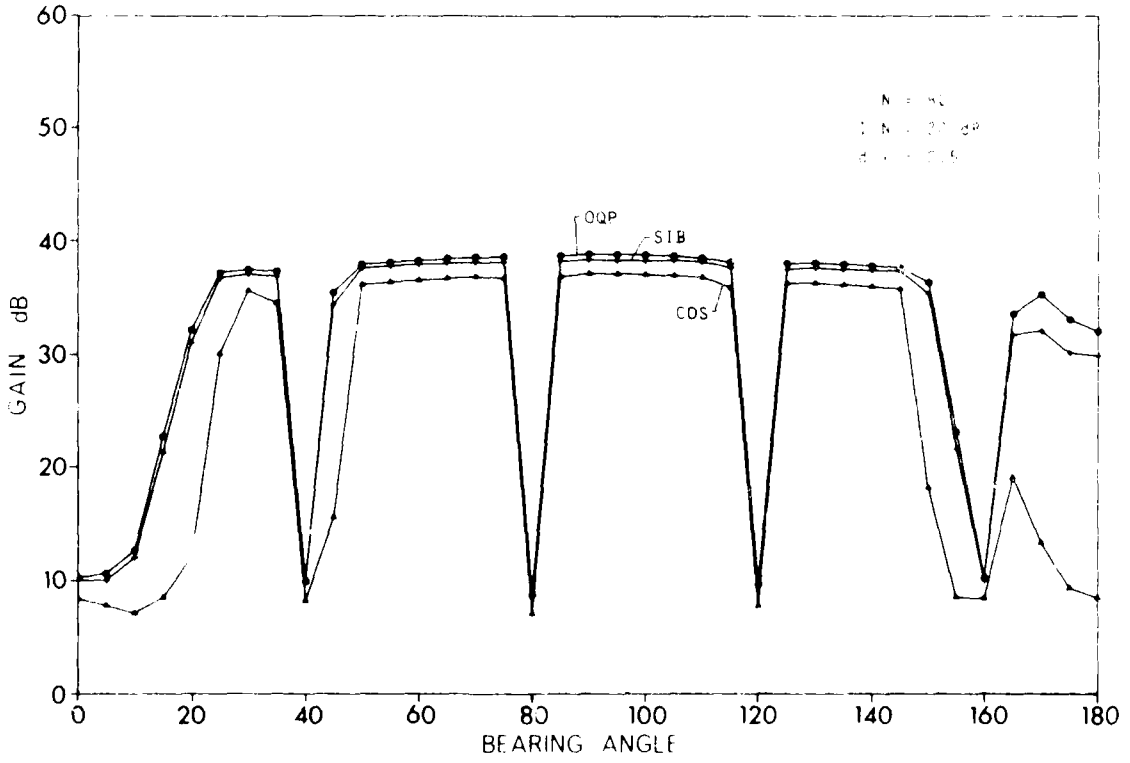

FIG. 58 COMPARISON OF OQP, SIB AND COS-PROCESSOR (N = 80)

AD-A097 948 SACLANT ASW RESEARCH CENTRE LA SPEZIA (ITALY) F/G 17/1
DETECTION PERFORMANCE OF HORIZONTAL LINEAR HYDROPHONE ARRAYS IN--ETC(U)
DEC 80 R KLEMM

UNCLASSIFIED SACLANTCEN-SR-43 NL

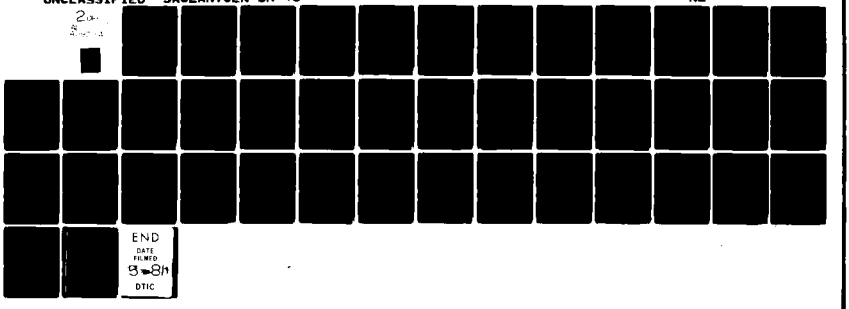

END
DATE FILMED
3-81
DTIC

8 INFLUENCE OF THE SENSOR BANDWIDTH

8.1 Introductory

For all results achieved so far it was assumed that signals and noise are monochromatic or, equivalently, that the input channels have zero bandwidth. This assumption enables us to use a normal-mode program to model point sources, which gives essentially the solution of the wave equation for one single frequency (Helmholtz-equation).

In practice, however, the channel bandwidth will never be zero. Otherwise, no signal energy can be received. Any signal or noise wave arriving at the array from directions other than broadside appears more or less delayed between the sensors. If the received wave is a random time function (as is particularly the case for interference) the received signal will be correlated, because the correlation response of the narrowband filter $\rho = h * h^*$, h is the impulse response of the filter. Consequently the cross-correlation between sensors will be given by the correlation response of the filters, thus causing degradation of noise-suppression performance and of signal gain well (compared with the monochromatic case).

The purpose of the following investigation is to find out the degradation of array gain that depends on the receiver bandwidth for some of the processor structures discussed in the previous chapters. Two kinds of narrowband filters are considered:

1. The rectangular time-response filter, which is equivalent to one channel of the DFT. It is of special importance because the spectral analysis in Fig. 14 can be carried out by the FFT.
2. The rectangular frequency response.

For a simple approach to the problem's solution, an additional assumption is made, which is justified by the conclusion given in Sect. 3.5a.

It is supposed that the mode structure, i.e. the spatial energy distribution,

is constant within the bandwidth considered. This is not exactly the case: any change in frequency will cause a change in the energy distribution. In particular, a continuous spectrum will cause a continuous energy distribution instead of a discrete one such as those in Figs. 3 and 4. However, for small relative bandwidths it is supposed that no significant changes in the signal distribution will occur. On the other hand, the results achieved in Ch. 3 have shown that the array gain basically does not depend very much on the individual channel and source parameters (in particular, not on the frequency).

The rectangular time-response filter is

$$h(t) = e^{-j\omega t} \Big/_{t=0}^{T} .$$

The correlation response of this filter is achieved by convolving h(t) with its conjugate complex h*(t)

$$\rho(\tau) = (1 - \frac{|\tau|}{T})\, e^{j\omega t} , \qquad \text{[Eq. 81]}$$

the well-known triangular correlation function.

Now the delay τ has to be expressed in terms of the array geometry. Recalling Eq. 12, the delay of any plane wave between the i^{th} and the ℓ^{th} sensor is determined by the distance

$$r_{i,\ell} = d(i - \ell)\cdot\cos\beta . \qquad \text{[Eq. 82]}$$

Multiplying $r_{i,\ell}$ by the wavenumber k gives

$$k\, r_{i,\ell} = \frac{\omega}{c} \cdot r_{i,\ell} = \omega\tau .$$

Consequently,

$$\omega\tau = d(i - \ell)\cdot\cos\beta \cdot k$$

$$\tau = k\cdot d\cdot(i - \ell)\, \cos\beta \,/\, \omega \qquad \text{[Eq. 83]}$$

Defining the bandwidth of the rectangular time response filter to be

$$b = \frac{1}{T} ,$$

one gets

$$\frac{\tau}{T} = \frac{1}{2\pi} \cdot d(i - \ell)\cdot\cos\beta \cdot \frac{b}{f} \cdot k \quad . \qquad \text{[Eq. 84]}$$

Inserting Eqs. 83 and 84 in Eq. 81 yields

$$\rho(i - \ell) = \left(1 - \frac{k}{2\pi} \cdot d \cdot (i - \ell) \cdot \cos\beta \cdot \frac{b}{f}\right) \cdot \exp(jkd \cdot (i - \ell) \cdot \cos\beta) \qquad \text{[Eq. 85]}$$

Replacing the wavenumber k by the modal wavenumbers k_n and taking the sum over all arrivals (observing the assumption of Sect. 1.6) gives

$$\rho(i-\ell) = \sum_{n=1}^{M} \left(1 - \frac{k_n}{2} \cdot d \cdot (i-\ell) \cdot \cos\beta \cdot \frac{b}{f}\right) \cdot \exp(jk_n \cdot d \cdot (i-\ell)\cos\beta), \qquad \text{[Eq. 86]}$$

which is now the spatial correlation as achieved at the outputs of the array.

The correlation response of a narrowband filter with rectangular frequency response is given by

$$\rho(\tau) = \int_{f_o - \frac{b}{2}}^{f_o + \frac{b}{2}} \cdot \frac{1}{b} e^{j\omega t} \, df$$

$$= \frac{\sin \pi b \tau}{\pi b \tau} \cdot e^{j\omega\tau} \, . \qquad \text{[Eq. 87]}$$

By means of Eq. 83 one gets for the correlation

$$\rho(i - \ell) = \sum_{n=1}^{M} \frac{\sin\pi\, \Theta_n}{\pi\, \Theta_n} \, e^{jdk_n(i-\ell)\cos\beta} \, , \qquad \text{[Eq. 88]}$$

where

$$\Theta_n = d \cdot k_n \cdot (i - \ell) \cos\beta \cdot \frac{b}{f_o} \, .$$

In the following examples it is assumed that the modification of the covariance matrices by the receiver bandwidth, as given in Eqs. 86 and 87 respectively, is known *a priori* wherever covariance matrices are used in the processing (adaptive noise suppression, matrix matched filter).

8.2 The Optimum Quadratic Processor (OQP)

Figures 59, 60 and 61 show the array gain when the received signals have passed rectangular time-response filters (i.e. FFT channels) before spatial processing. Different curves correspond to different ratios τ/T, where τ is now the travel time over the whole aperture and T is the inverse bandwidth of the input filter. Different plots are due to different interference-to-noise ratios (30, 20, 10 dB). A considerable sensitivity to the decorrelation due to the bandwidth is observed. The sensitivity depends on the interference-to-noise ratio. For 30 dB I/N even a τ/T-ratio of 0.01 yields considerable losses in gain (2 to 10 dB). If the I/N-ratio is just 10 dB, $\tau/T = 0.1$ is tolerable.

Figure 62 shows the same situation except that the interference is at broadside. In this case all arrivals at the array occur at the same time at different sensors, so no decorrelation occurs. For $\tau/T = 1$, however, a slight decrease in gain is observed. The reason for this behaviour is some loss in signal gain rather than imperfect noise suppression as in the previous examples. Consider the white-noise gain

$$G_W = \frac{\mathrm{tr}(\underline{H}^* \underline{P} \underline{H})}{\sqrt{\mathrm{tr}(H^*H)^2}} = \frac{\mathrm{tr}\ \underline{P}^2}{\sqrt{\mathrm{tr}\ P^2}} \ .$$

So the white-noise gain (signal gain) depends on the nature of the signal covariance matrix. If the signal is spatially white, i.e. $\underline{P} = \underline{I}$ the gain becomes $G_W = \frac{N}{\sqrt{N}} = \sqrt{N}$. If $\underline{P} = \underline{s}\,\underline{s}^*$, i.e. a coherent wavefront, the gain becomes $G_W = N^2/N = N$. The second case we have at 90°, therefore the gain is maximum. At all directions different from broadside the signal covariance matrix is influenced by both the relative bandwidth and the signal spread. As the signal spread becomes significant for array apertures greater than 40λ the little reduction in gain shown in Fig. 62 is mainly due to the bandwidth.

Figure 63 shows the same conditions as Fig. 60 but for rectangular frequency-response filters. As can be seen, the gain is now much less sensitive to the input bandwidth than for the case of a rectangular impulse-response filter. There are significant losses only when $\tau/T > 1$.

8.3 Suboptimum Systems

Figures 64 to 69 consider the same conditions as in Sect. 8.2 and Fig. 60. Figures 64 and 65 show the performance of the cos-shading processor for rectangular impulse-response and frequency-response filters respectively. Figures 66 and 67 show the infuence of the bandwidth on the dipole processor, Figs. 68 and 69 its influence on the adaptive multibeam processor. The general impression is that all kinds of processors (adaptive and nonadaptive) have almost the same sensitivity to decorrelation by the input channel bandwidth.

Figure 70 shows a multibeam processor with rectangular frequency response at each beamformer output for the case of a 80-hydrophone array. A comparison with Fig. 69 shows that the effects of sensitivity to non-zero bandwidth increase with array length.

8.4 Conclusions on the Influence of Sensor Bandwidth

In conclusion we find the following points:

a. Rectangular impulse-response filters are attractive for spectral analysis in broadband arrays because they can be implemented by means of the FFT. They yield, however, serious degradation of the crosscorrelation between different sensors. The ratio of travel time over aperture/filter response duration should not exceed 0.01.

b. Rectangular frequency-response filters are more difficult to implement; however, the ratio $\tau/T = 1$ is tolerable.

c. The loss in gain due to the decorrelation by non-zero input bandwidth increases with array length and interference-to-noise ratio.

d. The results achieved can be used for the design of broadband systems by subdividing the band into narrow sub-bands along the guidelines given above. The final processor structure was shown in Fig. 14.

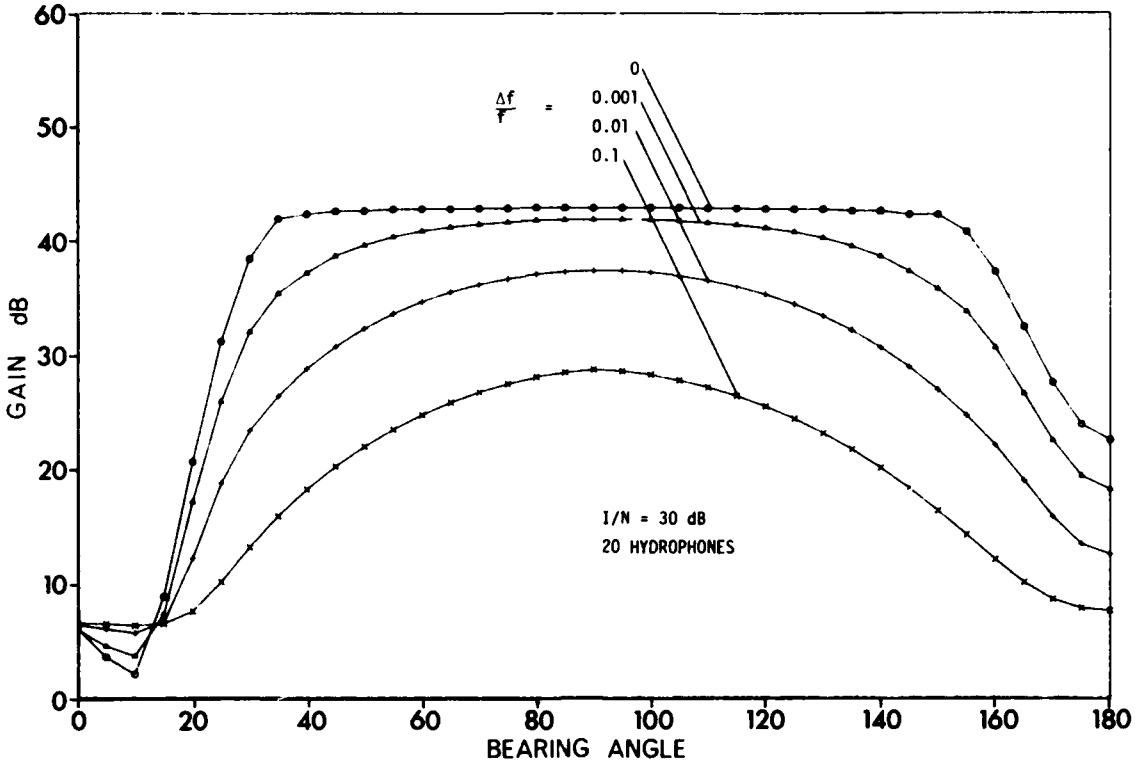

FIG. 59 OQP: INFLUENCE OF RECTANGULAR TIME-RESPONSE FILTER (I/N = 30, N = 20)

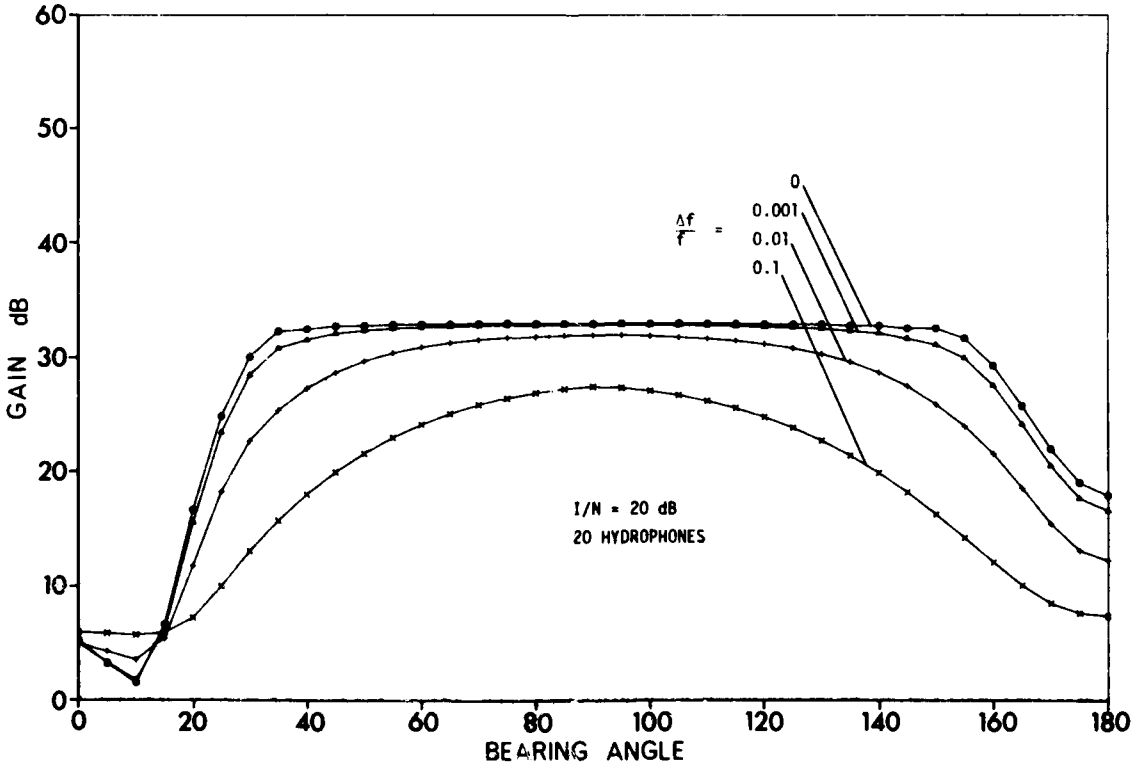

FIG. 60 OQP: INFLUENCE OF RECTANGULAR TIME-RESPONSE FILTER (I/N = 20, N = 20)

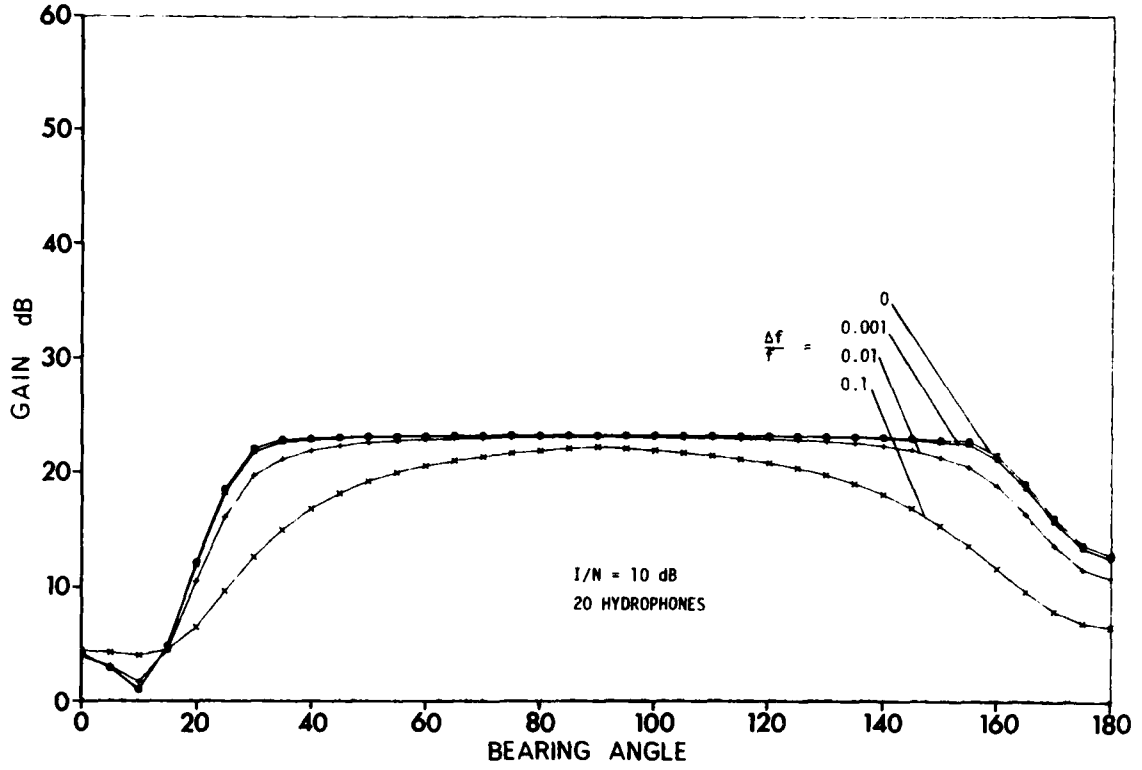

FIG. 61 OQP: INFLUENCE OF RECTANGULAR IMPULSE-RESPONSE FILTER (I/N = 10, N = 20)

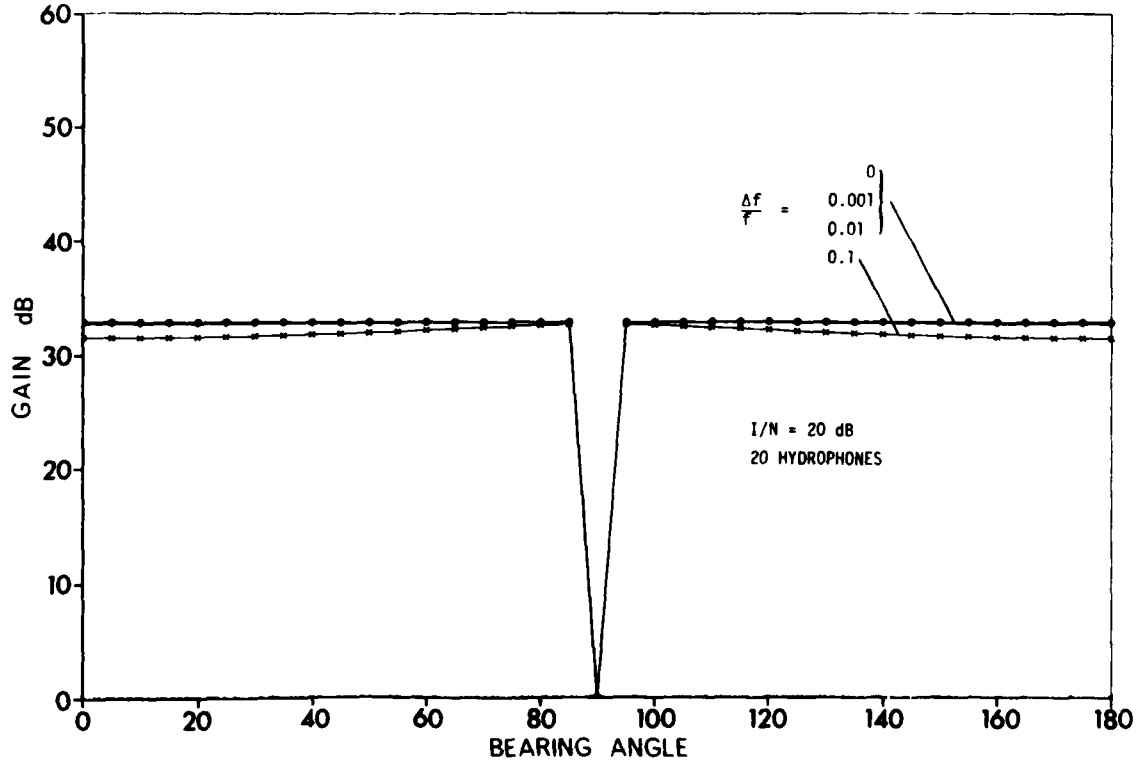

FIG. 62 OQP: INFLUENCE OF RECTANGULAR IMPULSE-RESPONSE FILTER (I/N = 20, N = 20) (Interference at 90°)

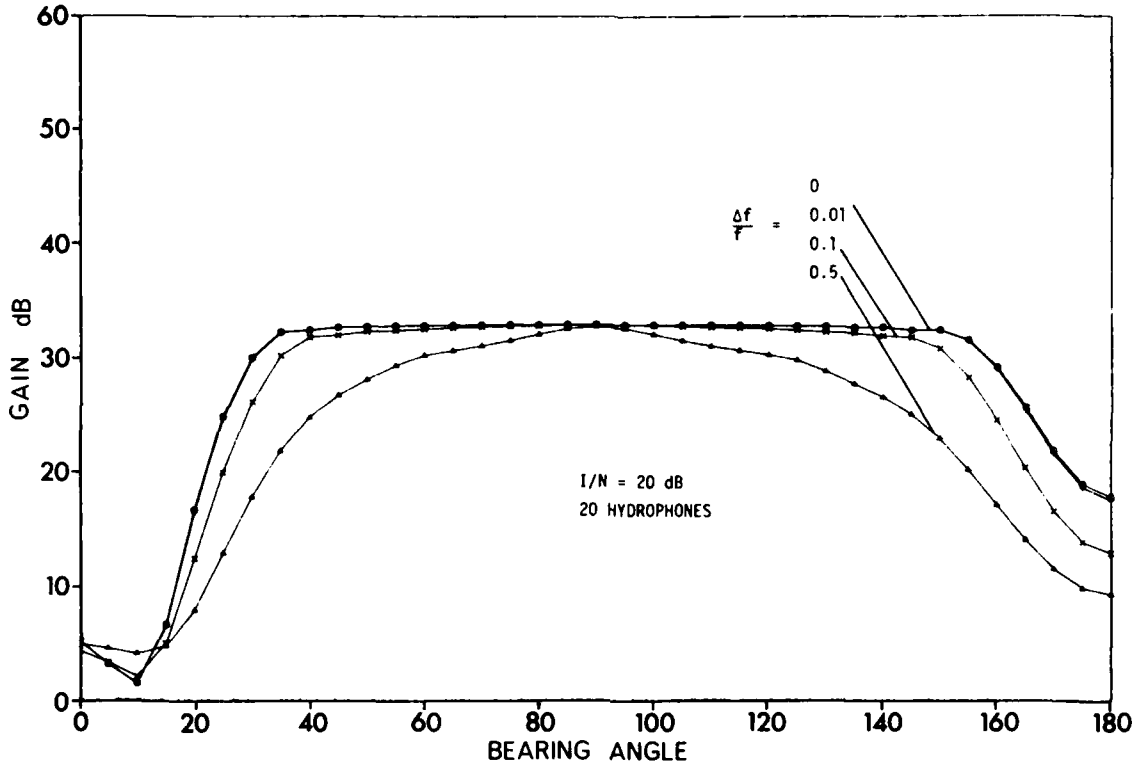

FIG. 63 OQP: RECTANGULAR FREQUENCY-RESPONSE FILTER

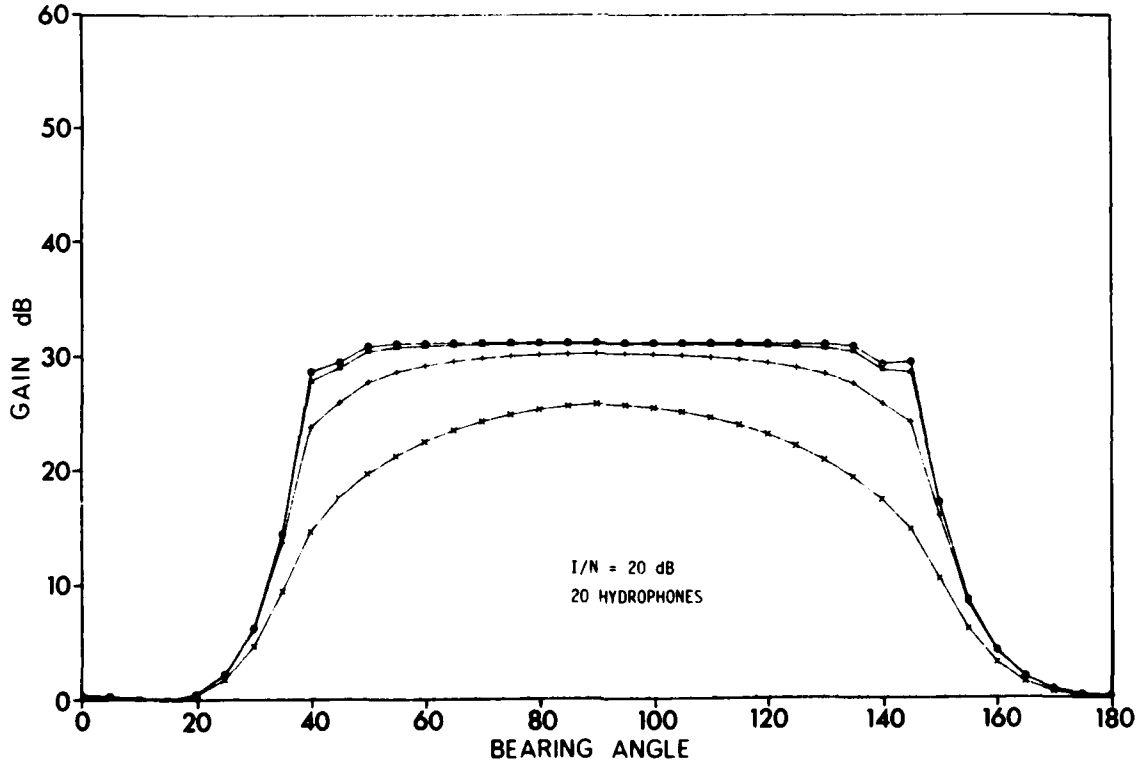

FIG. 64 COS-SHADING AND RECTANGULAR IMPULSE-RESPONSE FILTERS

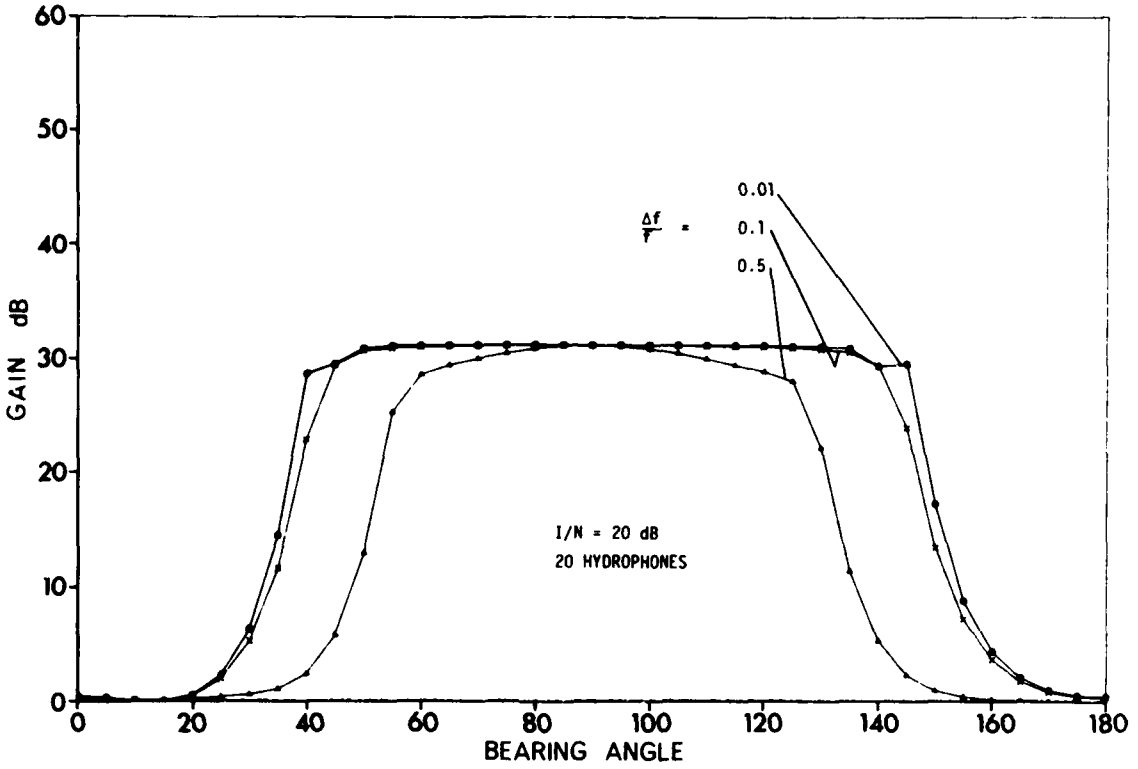

FIG. 65 COS-SHADING WITH RFF

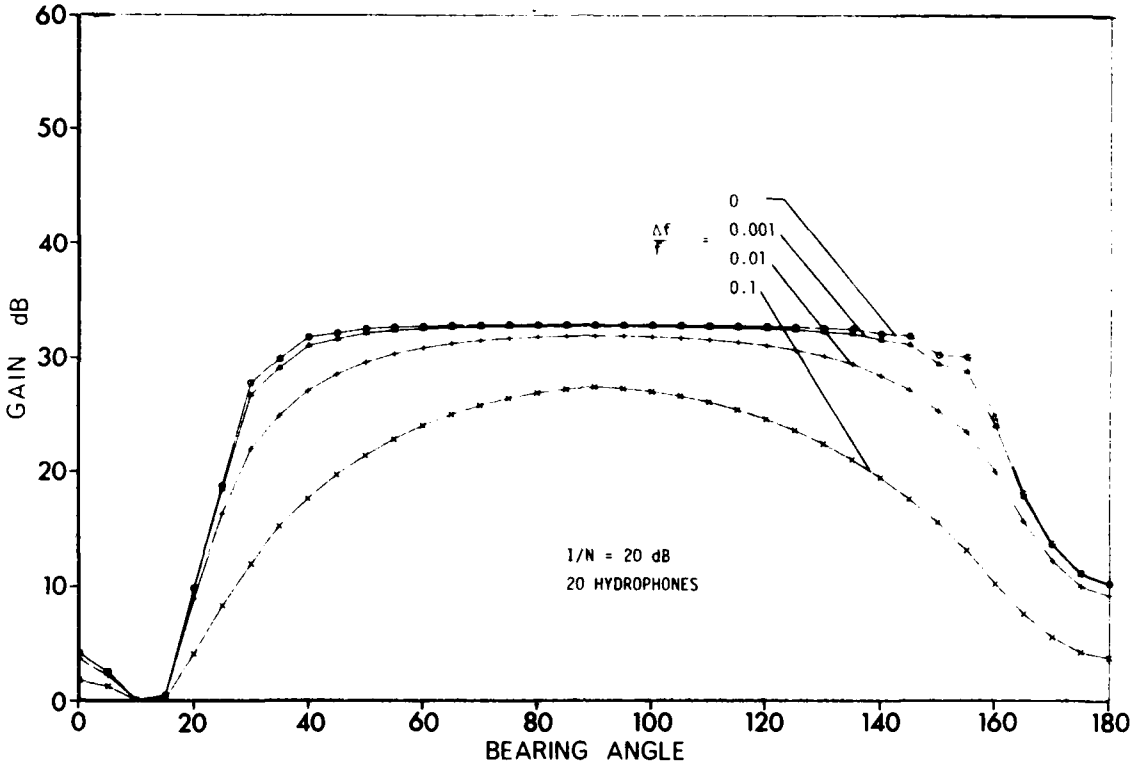

FIG. 66 DIP: RECTANGULAR IMPULSE RESPONSE FILTERS

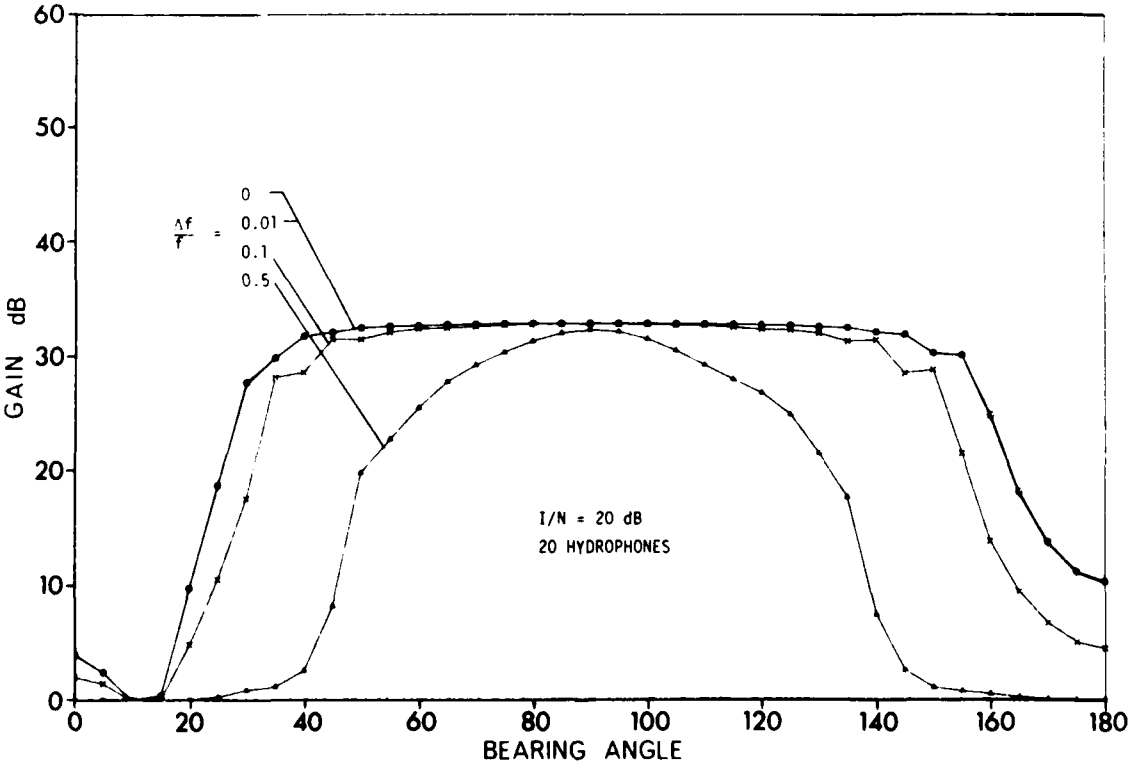

FIG. 67 DIPOLE PROCESSING WITH RECTANGULAR FREQUENCY FILTERS

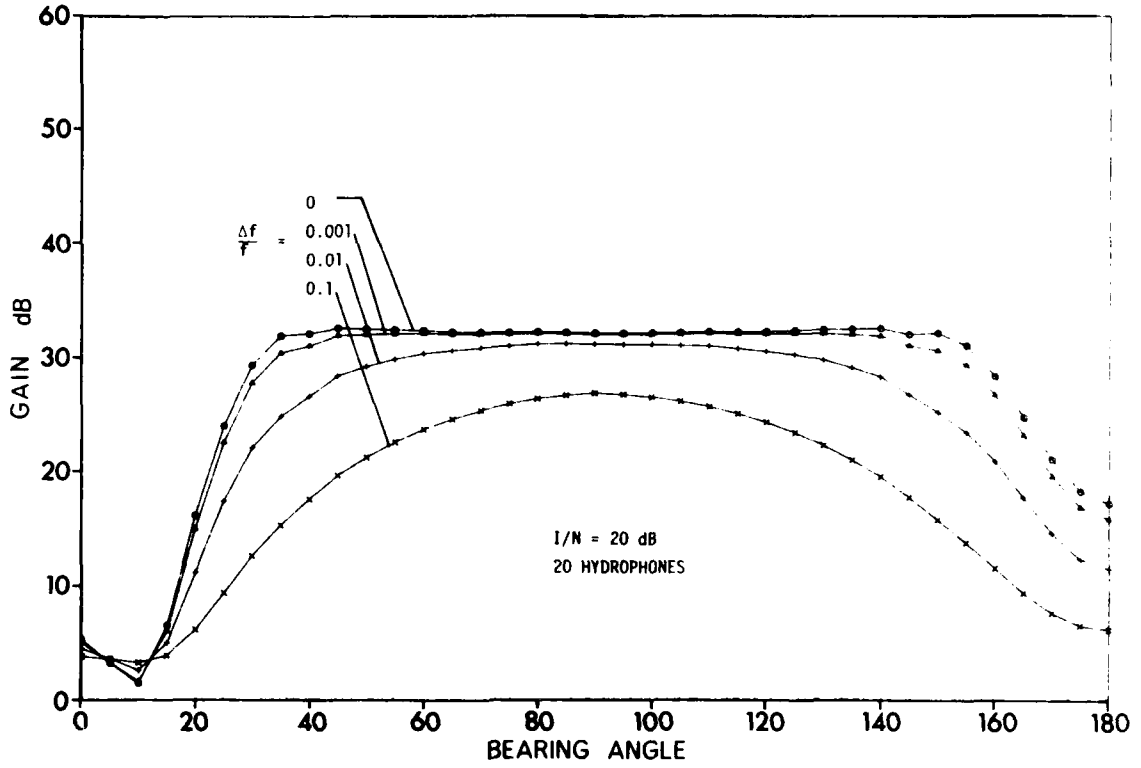

FIG. 68 MULTIBEAM PROCESSOR: RECTANGULAR TIME RESPONSE FILTERS

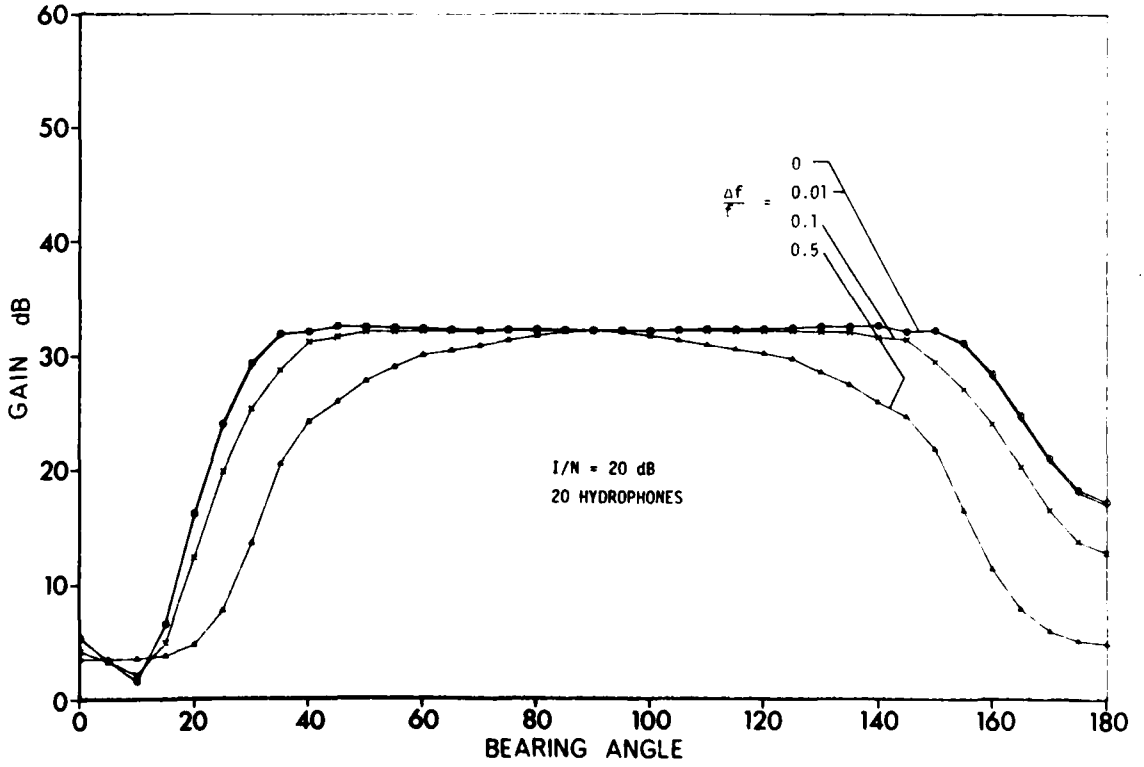

FIG. 69 MULTIBEAM PROCESSOR: RECTANGULAR FREQUENCY RESPONSE FILTER

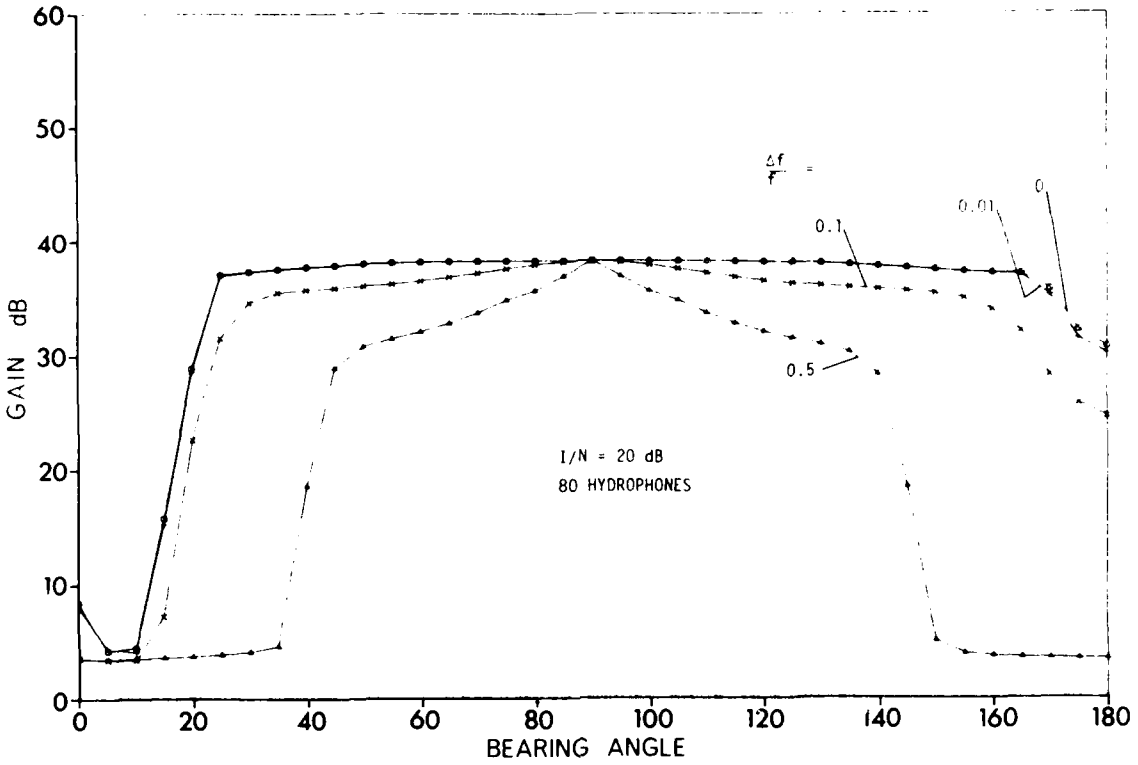

FIG. 70 MBP: RECTANGULAR FREQUENCY RESPONSE FILTER

9 DEVIATION OF THE ARRAY SHAPE FROM A STRAIGHT LINE

9.1 General Remarks

Towed arrays are quite useful for the operation of relatively low frequencies, because they satisfy both the requirements of large aperture and easy handling in mobile systems. However, as this kind of array is a flexible cable, some motion of the sensors may be excited, mainly by the vertical motion of the towing ship and, in very shallow water, by surface waves.

Generally, the motion of each sensor will be three-dimensional. Furthermore, due to a certain stiffness of the array, the motion of neighbouring sensors will not be independent, i.e. there will be some correlation among sensors. It seems to be very difficult to build a statistical model for the motion of a towed cable since it involves the knowledge of the excitation, i.e. the statistics of the motion of the towing ship, of the motion of the surface waves, and of the mechanics of the array cable. On the other hand, suppose that the motion of the array is slower than any time needed for spatial signal processing; it should then be considered to be a trend rather than a stochastic influence on the received signals. As far as noise suppression is concerned, such a trend can be overcome by adaptive signal-processing techniques.

The following takes a very simple approach to solving the problem. As the array is usually pulled at both ends in opposite directions, it will behave more or less like a string. Therefore, for simplicity, a simple, horizontal, sinusoidal deviation of the straight line is supposed. Any motion in the vertical makes the calculation much more complicated because the vertical pressure dependence, i.e. the normal modes, have to be taken into account. On the other hand, sound waves in the shallow-water channel are travelling horizontally rather than vertically. Therefore, any mismatch of the array shape to the wave front will be more serious in the horizontal than in the vertical direction.

The geometry of sensor deviation is shown in Fig. 71. The original positions of the two sensors are A and B. In this case a plane wave arriving from direction β is delayed between B and A by the distance

$$s = r + t = d \cdot \cos\beta. \qquad \text{[Eq. 89]}$$

Suppose that the position of sensor 2 is now C instead of B. The distance between A and C projected on the normal vector of the wavefront is then

$$r = s - t = d \cdot \cos\beta - t. \qquad \text{[Eq. 90]}$$

An additional simplification is made by setting AC = d, i.e. the distance between neighbouring hydrophones remains unchanged. The next step is to express r by z, d and β. One easily gets the equations:

$$t = \ell \cdot \cos(\gamma - \beta) \qquad \text{[Eq. 91]}$$

$$\ell = z/\sin\gamma \qquad \text{[Eq. 92]}$$

$$\ell/2 = d \sin\frac{\alpha}{2} = d \cos\gamma \qquad \text{[Eq. 93]}$$

$$\gamma = (180° - \alpha)/2 = 90° - \alpha/2 \qquad \text{[Eq. 94]}$$

$$\ell^2 = e^2 + z^2 \qquad \text{[Eq. 95]}$$

$$d^2 = z^2 + (d-e)^2 \qquad \text{[Eq. 96]}$$

From Eqs. 93 and 94 one gets

$$\sin\gamma = \sin(90° - \alpha/2) = \cos\frac{\alpha}{2}$$

$$= \sqrt{1 - \sin^2\frac{\alpha}{2}} = \sqrt{1 - \frac{\ell^2}{4d^2}} \quad . \qquad \text{[Eq. 97]}$$

Inserting Eqs. 91 and 95 in Eq. 90 gives

$$r = d \cdot \cos\beta - \frac{z \cdot \cos(\gamma - \beta)}{1 - \frac{\ell^2}{4d^2}} \quad .$$

or, after some manipulations, using Eq. 97,

$$r = d \cdot \cos\beta - z \frac{\ell \cos\beta}{2d\sqrt{1 - \frac{\ell^2}{4d^2}}} - \sin\beta \qquad \text{[Eq. 98]}$$

Eliminating e in Eqs. 95 and 96 and solving for ℓ gives

$$\ell^2 = 2d(d - \sqrt{d^2 - z^2}) \; . \qquad \text{[Eq. 99]}$$

Inverting Eq. 99 in Eq. 98 gives the delay r between sensors 1 and 2 in position C:

$$r = d\cos\beta - z\left(\sqrt{\frac{d - \sqrt{d^2 - z^2}}{d + \sqrt{d^2 - z^2}}}\cos\beta + \sin\beta\right) \qquad \text{[Eq. 100]}$$

At the i^{th} sensor, therefore, a single plane wave with modal wavenumber k_n will be received as follows

$$x_i(f) = \exp[j(k_n r_i - \omega t)],$$

and the cross-correlation coefficient between the i^{th} and the ℓ^{th} sensor

$$E\{x_i(f)\, x_\ell^*(f)\} = \exp[jk_n(r_i - r_\ell)],$$

where

$$r_i = d\cos\beta - z_i\left(\sqrt{\frac{d - \sqrt{d^2 - z_i^2}}{d + \sqrt{d^2 - z_i^2}}}\cos\beta + \sin\beta\right). \qquad \text{[Eq. 101]}$$

9.2 Numerical Results

For the numerical evaluation it is assumed that the array is distorted due to a horizontal sine function

$$z_i = \delta \cdot \sin(2\pi f_a \cdot i/N), \qquad \text{[Eq. 102]}$$

where δ is the amplitude of the deviation of the straight line. Results are shown in Figs. 72 to 75. Different curves are plotted for different deviations, δ. Figures 72 and 73 show the performance of the OLP when the array is distorted in accordance with Eq. 102. On the processing side it is assumed that the array is still a straight line. Obviously, the array is more sensitive to mismatch between processing and array distortion when a source is broadside than when it is at endfire. This follows direct from Eq. 101. As can be seen, the factor of the cos-term is smaller than

unity: $\cos\beta = 1$ means endfire direction whereas $\sin\beta = 1$ means broadside. Consequently, the deviation is more transversal than longitudinal. Figures 74 and 75 show the same conditions, but for the linear cos-shading processor. The results are very similar to those achieved for the optimum linear processor.

9.3 Conclusions on Deviations

a. The transversal deviation of the sensors from a straight line should not exceed 0.1λ.

b. With spatially white noise (no interference) the conventional beamformer turns out to be less sensitive to mismatch than it is with directive noise. Consequently, with directive noise the noise suppression part of the processing is the sensitive point.

c. The sensitivity is the same for adaptive and non-adaptive methods.

d. If the motion of an array cable is slow compared with the time required for adaptation the noise suppression part of any adaptive processor may follow the motion of the sensors, thus leaving just the mismatch between the distorted array and the CBF, which is less serious.

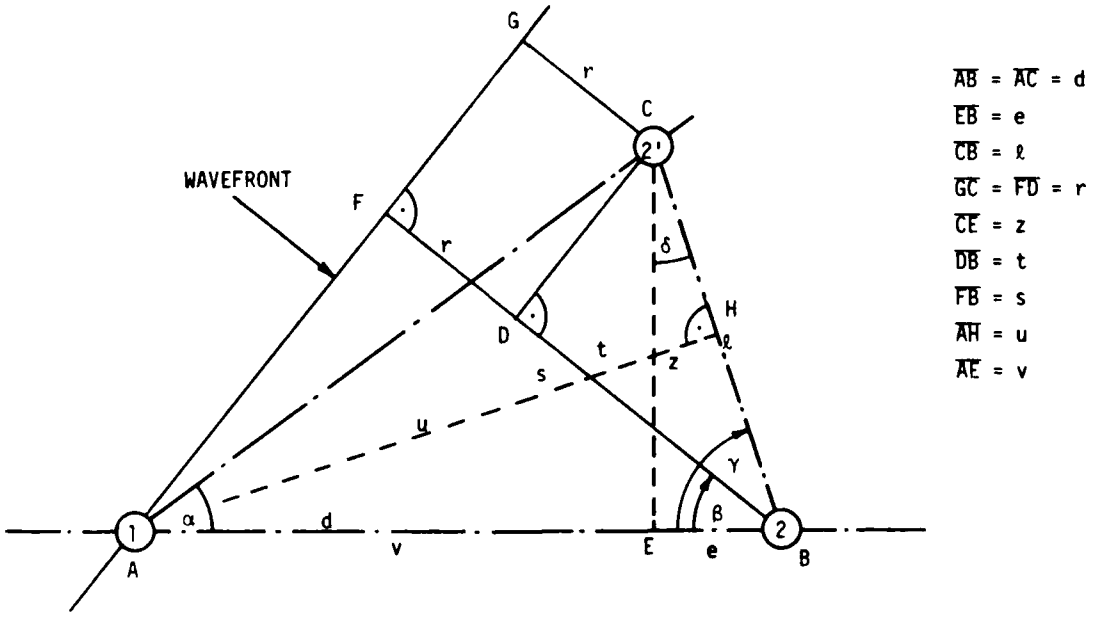

FIG. 71 GEOMETRY OF SENSOR DEVIATION

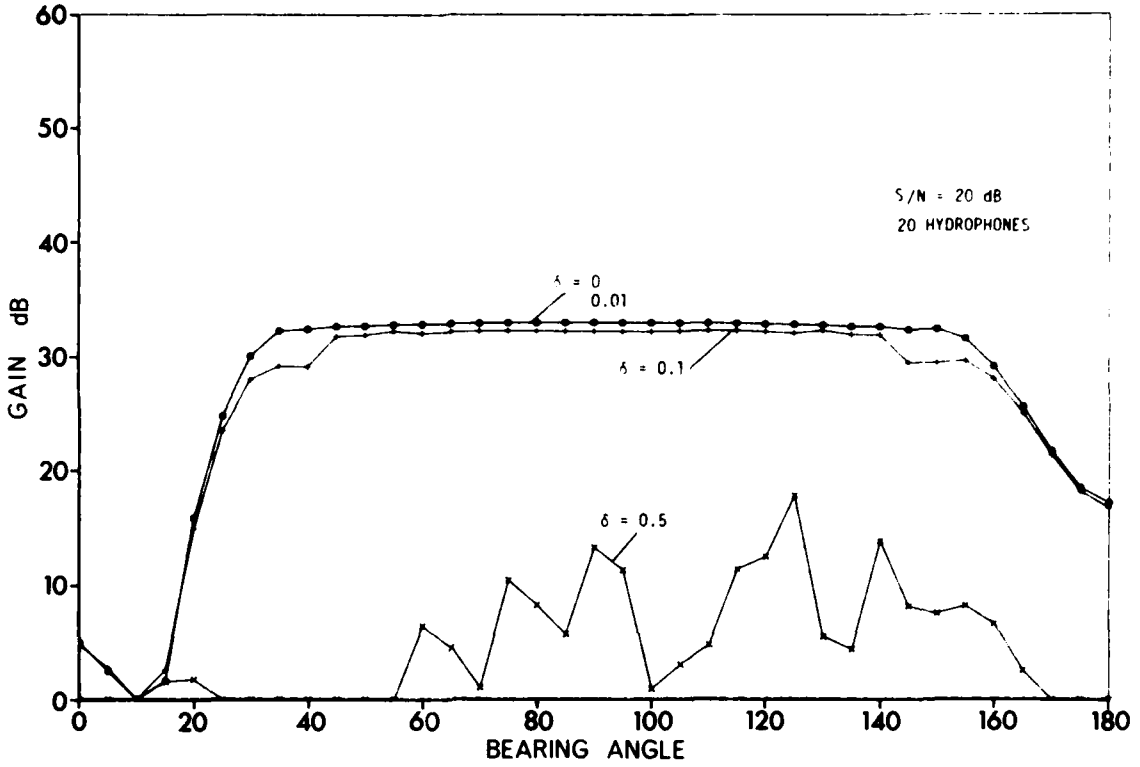

FIG. 72 OLP GAIN AS A FUNCTION OF DEVIATION FROM A STRAIGHT LINE

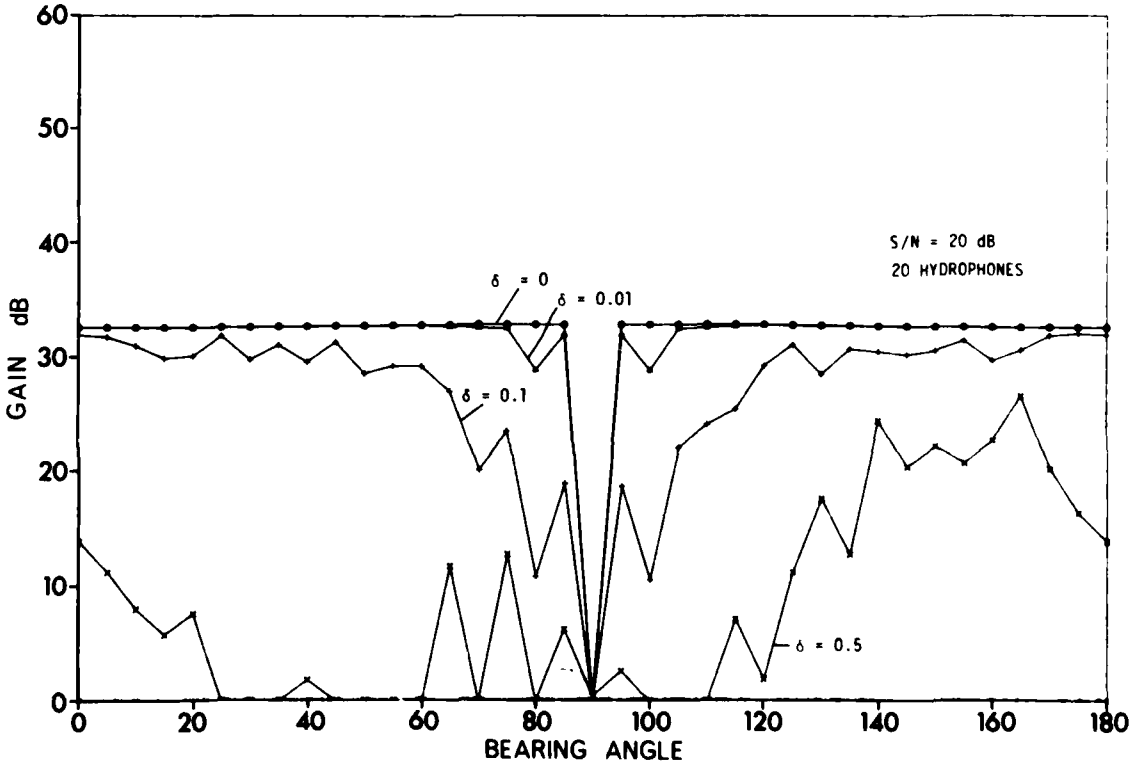

FIG. 73 OLP GAIN AS A FUNCTION OF DEVIATION FROM A STRAIGHT LINE (broadside source)

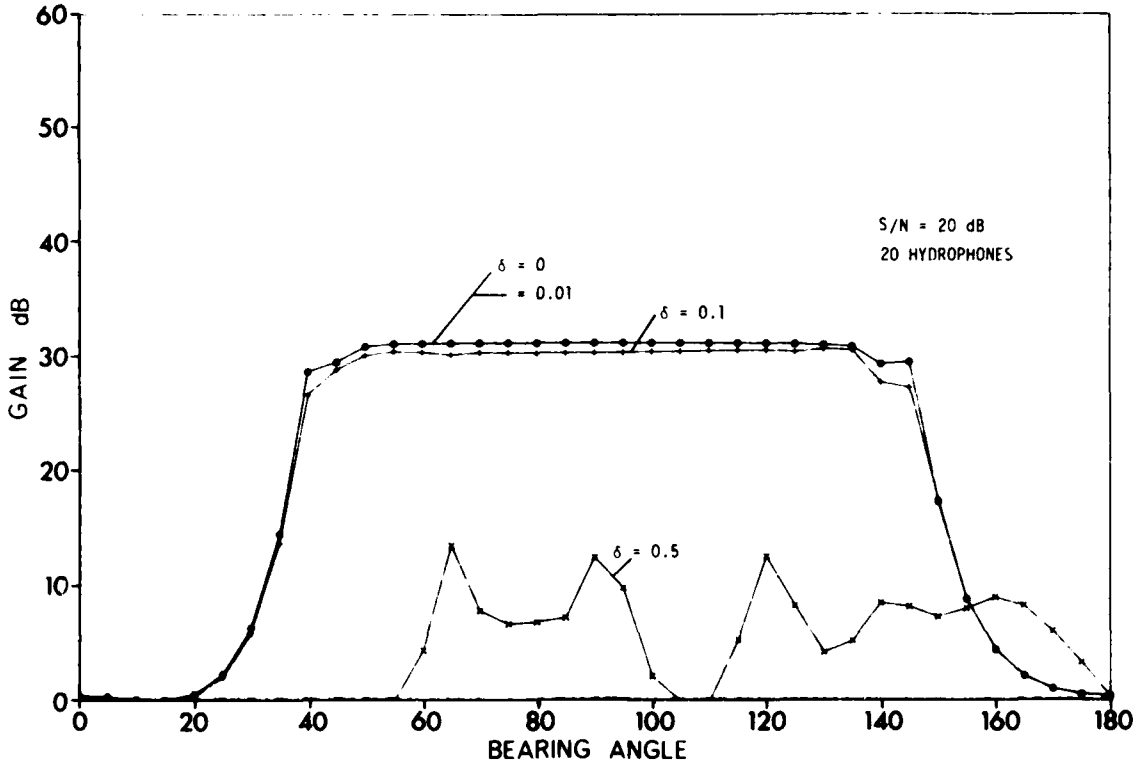

FIG. 74 LINEAR COS-SHADING GAIN AS A FUNCTION OF DEVIATION FROM A STRAIGHT LINE

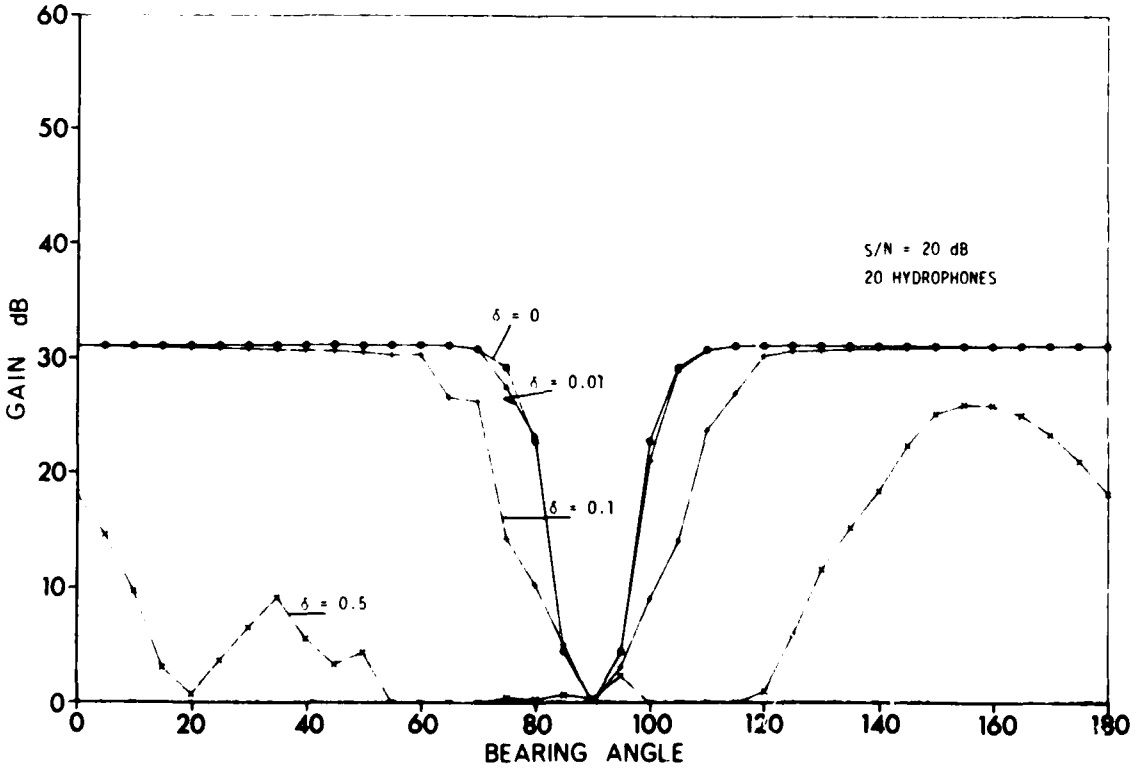

FIG. 75 LINEAR COS-SHADING GAIN AS A FUNCTION OF DEVIATION FROM A STRAIGHT LINE (broadside source)

10 PASSIVE ADAPTIVE ARRAYS: DEGRADATION DUE TO INCLUSION OF TARGET IN ADAPTATION

10.1 Introductory

All kinds of adaptive array processors contain the inverse spatial covariance matrix of the noise, see Sects. 3.2, 3.3, 4.2, 4.6, 7.3, 7.4. In all previous considerations it was assumed that the noise covariance matrix (or an estimate of it) is available. This condition can be satisfied in active systems where the estimation of the noise covariance (or equivalently, the adaptation of an adaptive noise-suppression algorithm) can be carried out before transmitting the pulse, thus achieving a noise estimate that is free of the target signal. In passive systems the signal cannot be switched off; therefore only a noise-plus-signal estimate is available.

The effect of including the signal in the noise estimation has been discussed in *[4]* for the OLP. The following formula is derived

$$\frac{z(\underline{k}_2)}{z(\underline{k}_3)} = 1 + \frac{(S/N)^2 \max \sin^2[2(\underline{m}, \underline{d}, \underline{Q}^{-1})]}{4[1 + (S/N)_{max}]} , \qquad \text{[Eq. 103]}$$

where $\sin^2[\ ]$ describes the mismatch between the target direction $\underline{d}$ and the OLP $\underline{Q}^{-1}\underline{m}$. In particular, $\sin^2(2(\underline{d}, \underline{d}, \underline{Q}^{-1})) = 0$. $z(k_2)$ is the output power of the OLP without the signal included in $\underline{Q}$; $z(k_3)$ is the output power when $\underline{Q}$ contains both signal and noise. $(S/N)_{max}$ is the maximum gain achievable by the OLP:

$$(S/N)_{max} = \underline{d}^* \underline{Q}^{-1} \underline{d} \cdot \frac{P_s}{P_n} .$$

Interpreting Eq. 103 leads to the conclusion that, if there is no mismatch, the inclusion of the signal in the noise suppression part $\underline{Q}^{-1}$ has no influence on the output power, i.e. $z(\underline{k}_3) = z(\underline{k}_2)$. Furthermore the ratio $z(\underline{k}_2) / z(\underline{k}_3)$ depends on the signal-to-noise ratio at the output of the OLP

when perfectly matched to the signal source. Therefore, if either the signal/white-noise ratio is high and/or the array has high gain, the ratio becomes very sensitive to any mismatch between the OLP transformer and the actual target direction. In other words, inclusion of the signal causes a rather narrow beam, which may be desirable for position-finding purposes. In detection systems used for target search, however, a very narrow beam might cause an undesirable increase in scanning rate and hence in operation time and data rate. The usual strategy is first to detect targets with the normal array resolution and secondly to apply high-resolution or split-beam techniques for high-accuracy position-finding only to targets already detected.

Now let us generalize the sensitivity result [Eq. 103] to random wavefronts and quadratic processing by means of the following consideration: suppose the random wavefront to be described by a covariance matrix $\underline{P}$. As $\underline{P}$ is hermitian and positive definite, it can be factored in the following way:

$$\underline{P} = \underline{E}\,\underline{\Lambda}\,\underline{E}^* \ ,$$

where $\underline{E}$ is the unitary matrix of eigenvectors and $\underline{\Lambda}$ the diagonal matrix of *real positive eigenvalues.*

Considering just one eigenvalue gives

$$\underline{P}_i = \underline{E} \begin{pmatrix} 0 & & & & \\ & \ddots & & & \\ & & 0 & & 0 \\ & & & \lambda_i & \\ & 0 & & & 0 \\ & & & & \ddots \\ & & & & & 0 \end{pmatrix} E^*,$$

which is obviously a dyadic of the i^{th} eigenvector with its conjugate complex transpose

$$\underline{P}_i = \lambda_i\, \underline{e}_i\, \underline{e}_i^* \ .$$

The total matrix is given by

$$\underline{P} = \sum_{i=1}^{N} \underline{P}_i \ .$$

In other words, any random wavefront, sampled at N points in space, can be described in the mean as a sum of N fictive coherent waves $\underline{e}_i$ with powers λ_i. Now the sensitivity result [Eq. 103] can be applied direct to the OQP because its output appears to be just a sum of the output signals of N perfectly matched beamformers. Therefore the gain of the OQP is not degraded by inclusion of the signal in the noise estimation (or adaptation) when perfectly matched.

Linear processors, however, are mismatched to the target signal for all directions except broadside. Therefore a peak in the gain curves can be expected at broadside, whereas some decrease in gain is unavoidable for all other directions. The quadratic multiple beam processor, which is some approximation to the OQP, is supposed to yield array gain somewhere between OQP and OLP.

10.2 Constrained Adaptation

One way of avoiding the gain degradation of adaptive array processors due to inclusion of the signal direction in the adaptation is given by the so-called constrained array processors [1,5,6,7,8,23]. The idea of these processors is to superimpose a constraint on the adaptation process such that the signal (i.e. the beam direction) does not influence the adaptation. There are basically two ways of implementation. One way is to include the constraint (e.g. a set of weights such that the noise estimator is blind for the target direction) directly in the adaptive algorithm [6,7]. Alternatively, a fixed pre-transform has to be chosen such that the target direction is eliminated out of the noise estimation. The pre-transform may be of the form of Eqs. 53 or 56 for processors like OQP and OLP. For processors of the pre-transform type, Eqs. 66 or 67 represent constrained pre-transforms. It has been pointed out in [8] that algorithms of the first type (constrained adaptive algorithms) converge in the mean to certain processors of the second kind. In the following, only a few pre-transform type processors are considered.

Two basic kinds of constrained pre-transform processors have been described already in Ch. 7 (see Eq. 46 and 67). Equation 66 describes just dipoles

with the null steered in the direction of the beam. Weightings as shown in Eq. 67 yield some arbitrary array pattern with a null in the beam direction. The nulls of the array patterns given by Eq. 67 are much narrower than those of a dipole, thus causing a processor that is very sensitive to mismatch of the beam direction to the target position. In addition, as discussed already in Ch. 6, for shallow-water application, dipoles appear to be much more useful for signal or noise suppression than nulls in the array pattern (see the conclusion of Sect. 6.3a,b). Consequently only a processor of the type of Eq. 66 will be considered in the numerical evaluation.

A more general approach is suggested in the following. It has, however, not yet been investigated in detail, therefore no prediction on the performance of this method can be made at present. All the constrained adaptive processors mentioned above are more or less sensitive to mismatch between signal direction and beamformer, i.e. between signal direction and null of auxiliary patterns. There is always a certain insensitive angle that is determined by the signal-to-noise ratio, see Fig. 76. If the noise level is far below the signal level the constraint processor becomes very sensitive to mismatch between beam and target direction.

For target search an insensitive angle interval of about the same width as the beamwidth is desired (see Fig. 76). The idea is now to describe the interval statistically, i.e. to try to approximate the angle interval by a B × B-covariance matrix, B being the number of auxiliary channels. The covariance matrix is used to design a "target suppression filter" that has to be inserted in the noise suppression part of the pre-transform. Suppose that there are random plane waves uniformly distributed over the angle interval 2δ. Then the spatial correlation becomes

$$\rho(\Theta) = \frac{1}{\Theta} \int_{\delta_o-\delta}^{\delta_o+\delta} e^{j\Theta u}\, du = \frac{\sin\Theta\delta}{\Theta\delta}\, e^{j\Theta\delta_o} \quad , \qquad \text{[Eq. 104]}$$

where $\Theta = k \cdot d \cdot (i - \ell)$

$\delta_o = \cos\beta$.

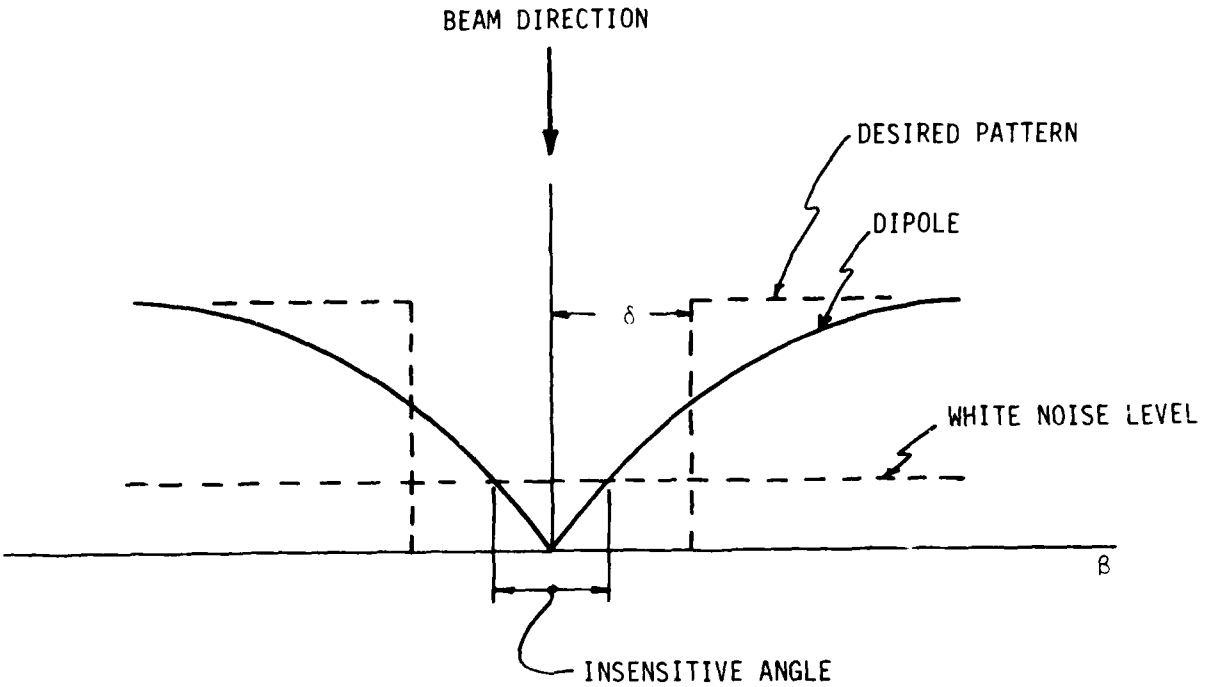

FIG. 76 CONSTRAINT SENSOR PATTERNS

Taking into account the white-noise level with power P_w, the interval covariance matrix $\underline{R}$ contains the values

$$\rho(i - \ell) = \rho(\Theta) \qquad i \neq \ell$$
$$= 1 + P_w \qquad i = \ell.$$

As $\underline{R}$ is positive it can be factorized

$$\underline{R} = \underline{C}^* \underline{C} ,$$

where $\underline{C}$ may be the Cholesky-factorized triangular matrix or any unitary transform of it. Suppose a vector $\underline{a}$ such that $E\{\underline{a}\ \underline{a}^*\} = \underline{R}$. Then the transform

$$\underline{y} = \underline{C}^{*-1} \underline{a}$$

decorrelates $\underline{a}$ such that

$$E\{\underline{y}\ \underline{y}^*\} = \underline{C}^{*-1} \underline{R}\ \underline{C} = \underline{C}^{*-1} \underline{C}^*\ \underline{C}\ \underline{C}^{-1} = \underline{I}.$$

Hence multiplying the vector of auxiliary sensor outputs chosen for noise estimation by C^{*-1} gives the desired transform for suppression of any signal arriving from the interval 2δ.

For a noise-cancellation system for auxiliary sensors one gets the constrained transform

$$y = \underline{K}^*\ \underline{T}\ \underline{x} , \qquad \text{[Eq. 105]}$$

where $\underline{x}$ is the vector of sensor output signals,

$$T \equiv \begin{pmatrix} & \underline{b}^* & \\ \hline 1 & & \\ & 1 & \\ & & \ddots \\ & & 1 \end{pmatrix} \quad \begin{matrix} \\ \\ \text{choice of} \\ \text{auxiliary} \\ \text{sensors} \end{matrix}$$

and

$$\underline{K}^* \equiv \begin{pmatrix} 1 & 0 \ldots\ldots 0 \\ 0 & \\ \vdots & \underline{C}^{*-1} \\ \vdots & \\ 0 & \end{pmatrix} ,$$

A simple example may clarify up matters. Suppose the number of auxiliary sensors to be 2. The normalized 2×2-covariance matrix of the interval becomes

$$\underline{R} = \begin{pmatrix} 1 & a \\ a^* & 1 \end{pmatrix}, \quad |a| < 1,$$

and the inverse

$$\underline{R}^{-1} \sim \begin{pmatrix} 1 & -a \\ -a^* & 1 \end{pmatrix}.$$

Factorization gives

$$\underline{C}^{*-1} \sim \begin{pmatrix} 1 & 0 \\ -a^* & \sqrt{1 - aa^*} \end{pmatrix},$$

such that $\underline{C}^{*-1}\,\underline{C}^{-1} = \underline{R}^{-1}$. Let us now consider the case $|a| = 1$, which happens if the width of the interval $\delta = 0$ and no white noise is assumed. Now the constraint matrix converges to

$$\underline{C}^{*-1} = \begin{pmatrix} 1 & 0 \\ -e^{j\delta_o} & 0 \end{pmatrix}, \qquad \text{[Eq. 106]}$$

i.e. in the limit we again get a dipole pattern with the null steered in the direction $\delta_o = \frac{2\pi}{\lambda} \cos\beta$, i.e. the target direction.

To obtain proper performance of a constrained array processor as described above, the interval width, the interval noise, and the number of auxiliary sensors should be carefully chosen. Furthermore, a certain scaling of $\underline{C}^{*-1}$ should be made in order to avoid numerical problems in the subsequent processing, particularly for the subsequent inversion of the noise covariance matrix $\underline{N} = \underline{T}\,\underline{Q}\,\underline{T}^*$. Some more work should be done on that subject, which would exceed the limits of this report.

10.3 The Optimum Linear Processor (OLP)

Figures 77, 78 and 79 show numerical examples for the case in which the signal is included when adapting the OLP to the noise field. There are

three different curves for different ranges of the target (1, 5, 25 km). The range of the interference is 1 km, as before. There is just one point where all curves coincide: 90° (broadside). This is the only direction where the conventional beamformer contained in the OLP is perfectly matched to the target signal. For all other directions we have some mismatch, for the two reasons mentioned in Ch. 4: on the one hand there is a mismatch in that the signal appears to be spread in the horizontal whereas the beamformer assumes a coherent plane wave; on the other hand the beamformer was always steered in the true position of the target, which causes some off-set for bearing angles distant from broadside. As can be seen in the example in Fig. 77, the gain reduction is greater as the target approaches. At 25 km range almost the optimum gain is achieved. This depends, however, on many different parameters that influence the sound propagation, and, furthermore, on the target strength.

As all these parameters are usually unknown in practice and may change considerably, a general prediction of the performance of the OLP cannot be made. The example in Fig. 78 shows the same conditions except for the noise (I/N = 40 dB). The results are similar to the previous ones. If, however, the array length increases (Fig. 79), e.g. N = 80, even a target at 25 km range causes considerable decrease in gain.

10.4 Pre-transform Array Processors

Figures 80 to 83 show three numerical comparisons of different pre-transform processors with the OQP. Figure 80 shows the performance of the quadratic multi-beam processor (MBP) for different target ranges. The parameters are the same as before. As the beams of the MBP have been chosen to be orthogonal to each other the auxiliary beams are orthogonal to the target direction. Therefore, at broadside, only the middle beam contains the signal whereas the other gives a signal-free noise estimate. For all other directions, however, the signal is no longer orthogonal to the auxiliary beams, i.e. the spread signal cannot be suppressed by a null in the beam pattern. Consequently we get a peak in the gain curves at 90° and a considerable decrease elsewhere, depending on the range of the

target. Figure 82 shows the same curves for an auxiliary sensor processor. Here the signal energy is always contained in the auxiliary channels, so that the gain decreases everywhere. Figure 82 shows the performance of an auxiliary difference element processor as described by Eq. 66. The results are quite similar to those achieved in Fig. 81. In fact, both the processors are similar to each other in that the MBP has auxiliary beam patterns with a null steered in the target direction, whereas the other uses dipole patterns with the null steered in the target direction. The decrease is less serious for very short arrays (see Fig. 83) and for a low interference-to-noise ratio (see Fig. 84) which corresponds again to the result of Cox *[1]*.

It was assumed in the examples in this chapter, that target and interference have equal strength and that differences in the power level are just given by the transmission loss of the channel. In general, however, the strength of a target will be somewhat less than the strength of interfering sources, which leads to a better performance of the array processor.

10.5 Conclusions on Passive Adaptive Arrays

a. In passive systems the spatial signal spread of the signal causes any kind of beamformer (linear, quadratic) to be more or less mismatched to the signal. Furthermore, due to the signal spread it is not possible to achieve a signal-free interference estimate by conventional methods, such as steering a null of auxiliary dipole patterns or auxiliary beam patterns in the target direction.

b. Both effects mentioned under (a) occur for all bearing angles except broadside.

c. As a consequence of (a), the performance of adaptive array processors in passive systems depends very much on the usually unknown signal-to-interference ratio.

d. For very small arrays an array processor using auxiliary dipole patterns may yield satisfactory performance. For large arrays nonadaptive methods (dipole null-steering, shading, see Chs. 5 and 6) should be applied.

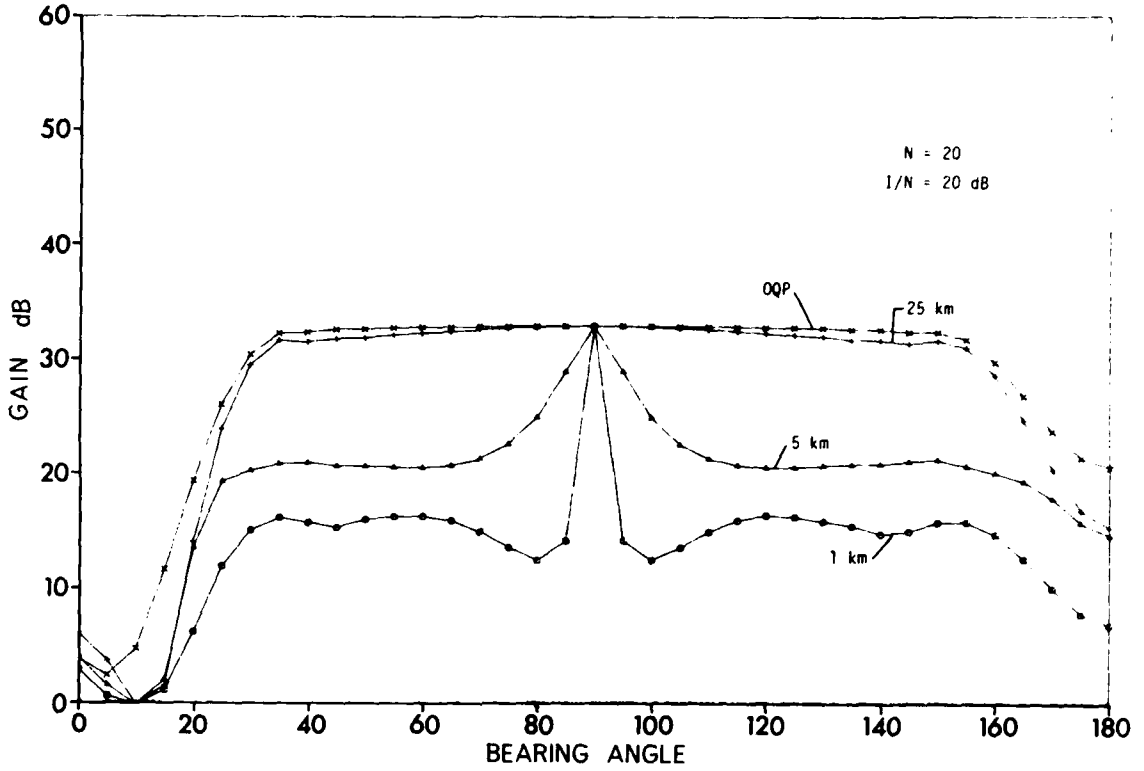

FIG. 77 OLP: INCLUSION OF SIGNAL IN ADAPTATION (N = 20, I/N = 20 dB)

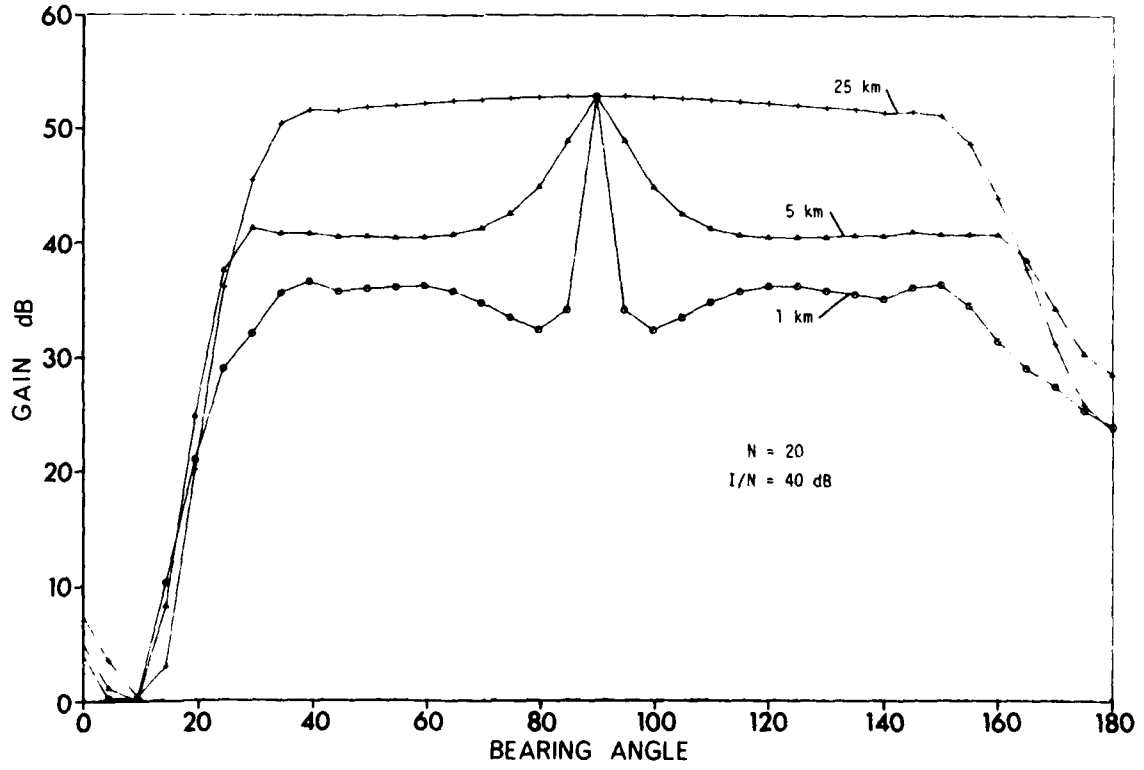

FIG. 78 OLP: INCLUSION OF SIGNAL IN ADAPTATION (N = 20, I/N = 40 dB)

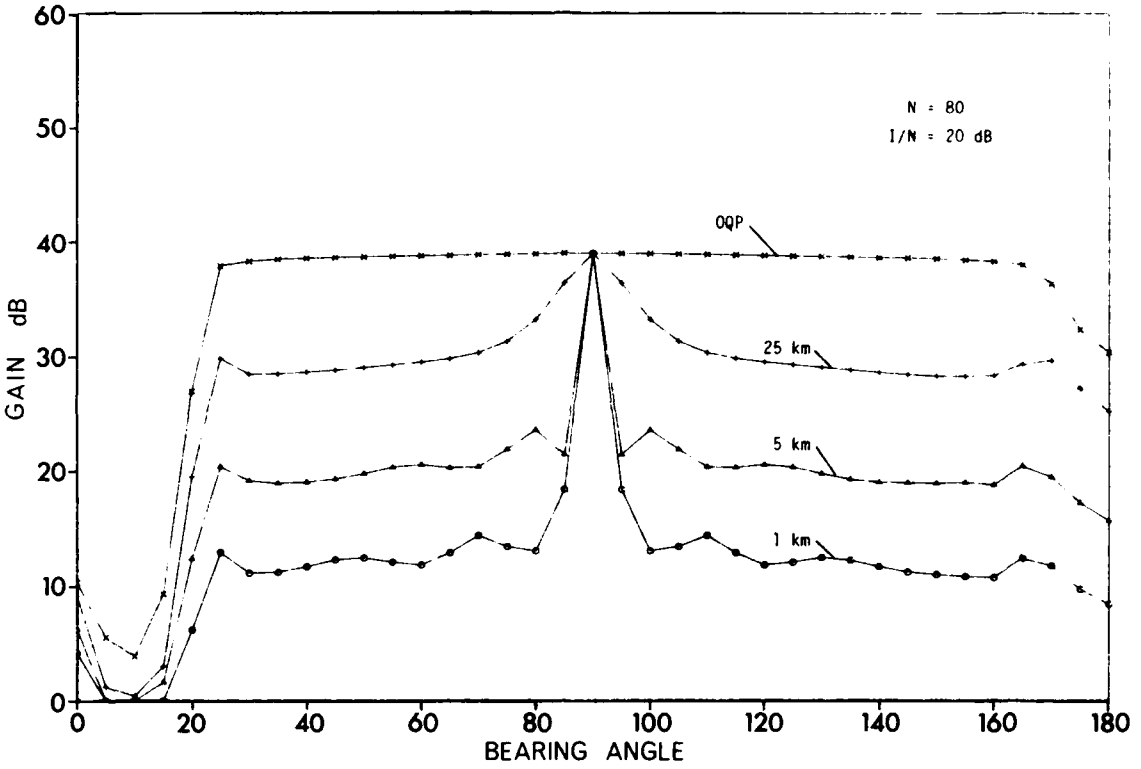

FIG. 79 OLP: INCLUSION OF SIGNAL IN ADAPTATION (N = 80, I/N = 20 dB)

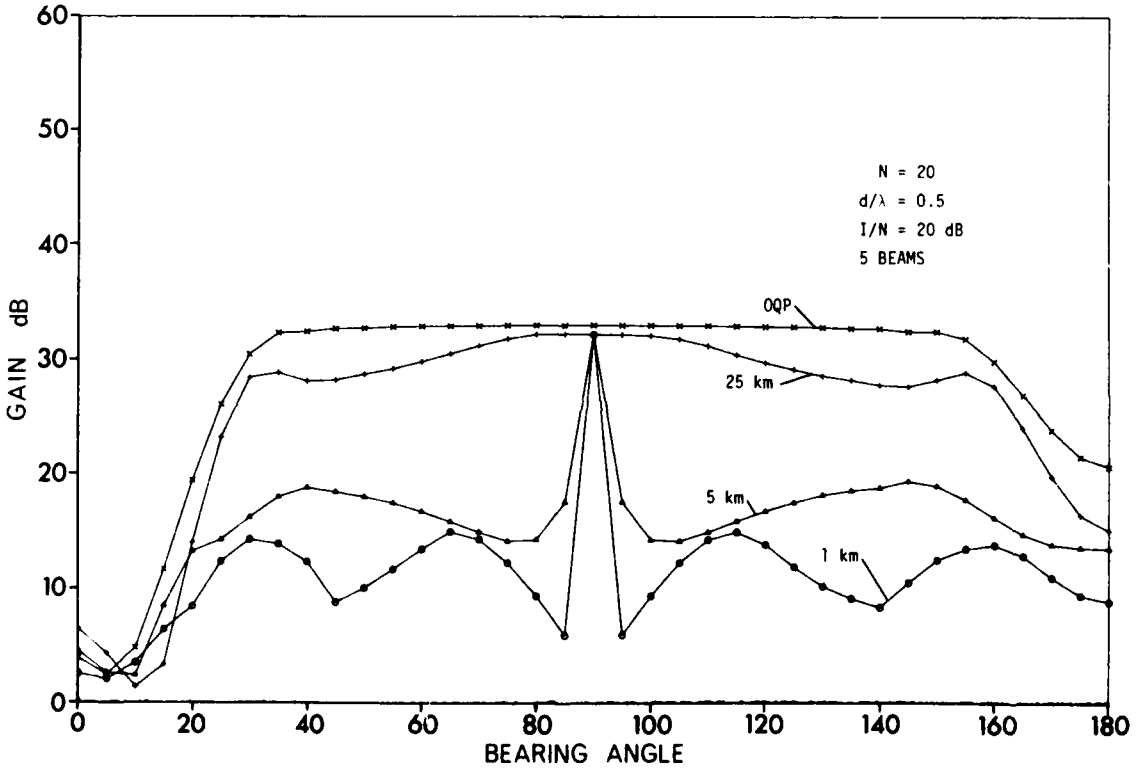

FIG. 80 QUADRATIC MBP: INCLUSION OF SIGNAL IN ADAPTATION

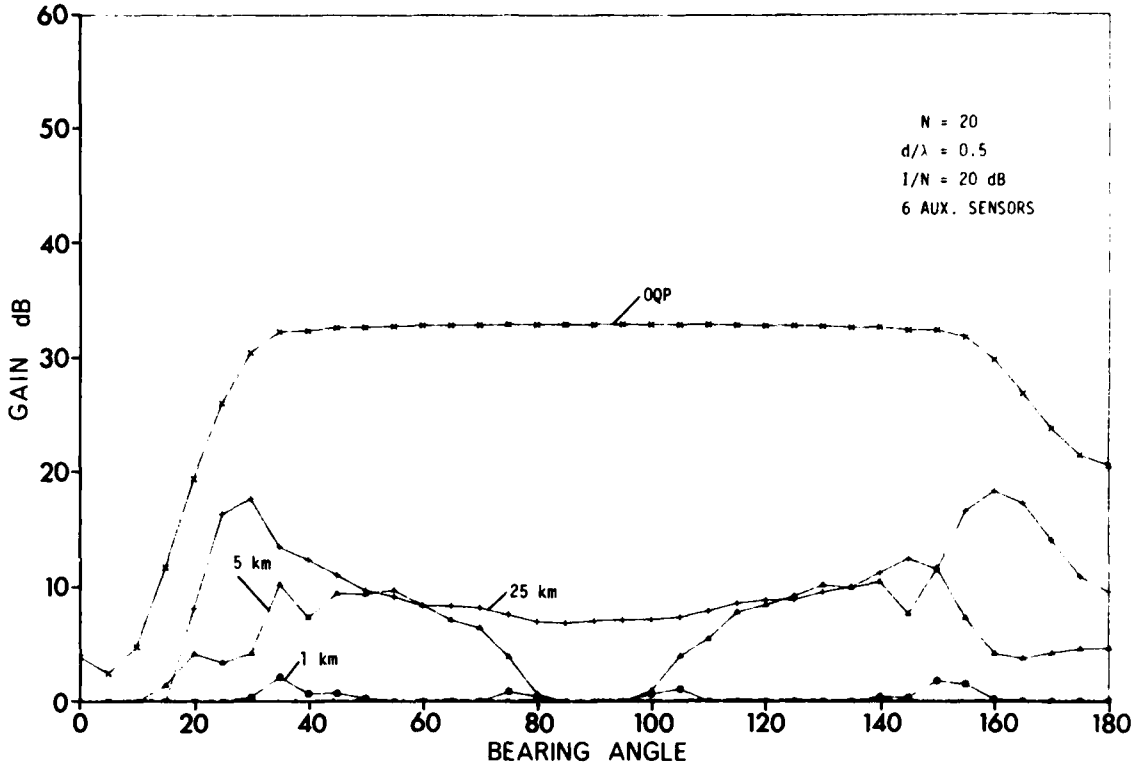

FIG. 81 AUXILIARY SENSORS: INCLUSION OF SIGNAL IN ADAPTATION

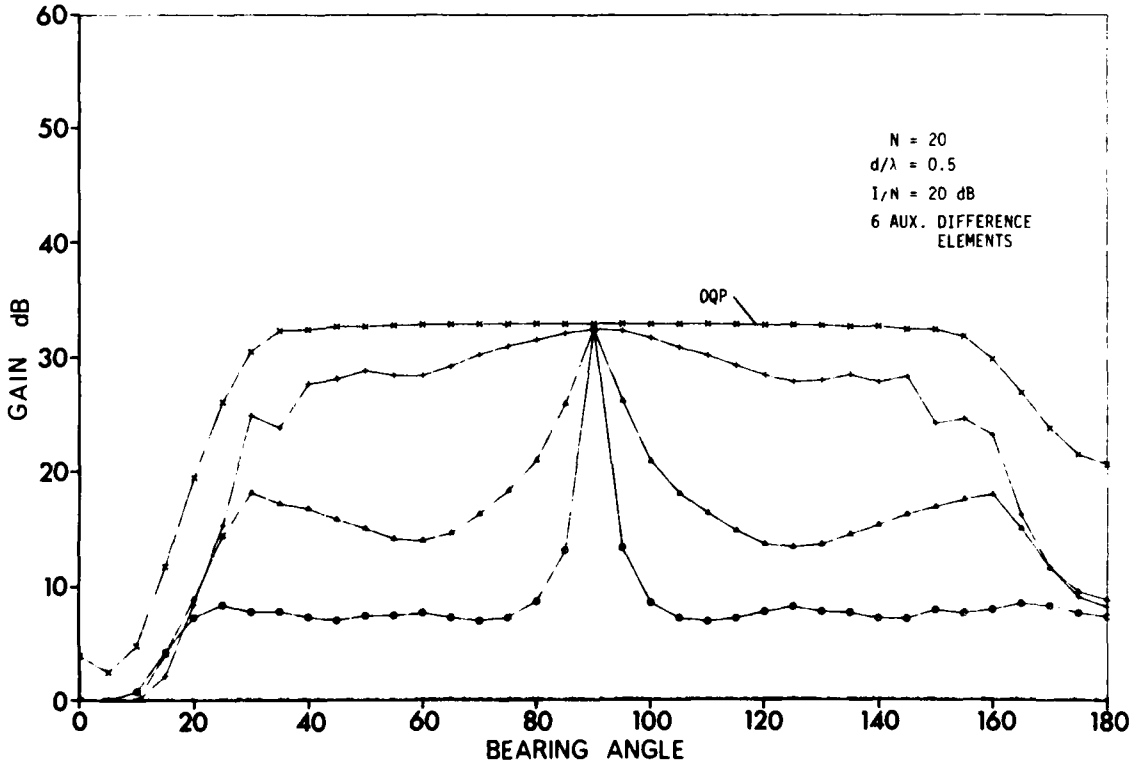

FIG. 82 AUXILIARY DIFFERENCE PATTERNS: INCLUSION OF SIGNAL IN ADAPTATION (I/N = 20 dB)

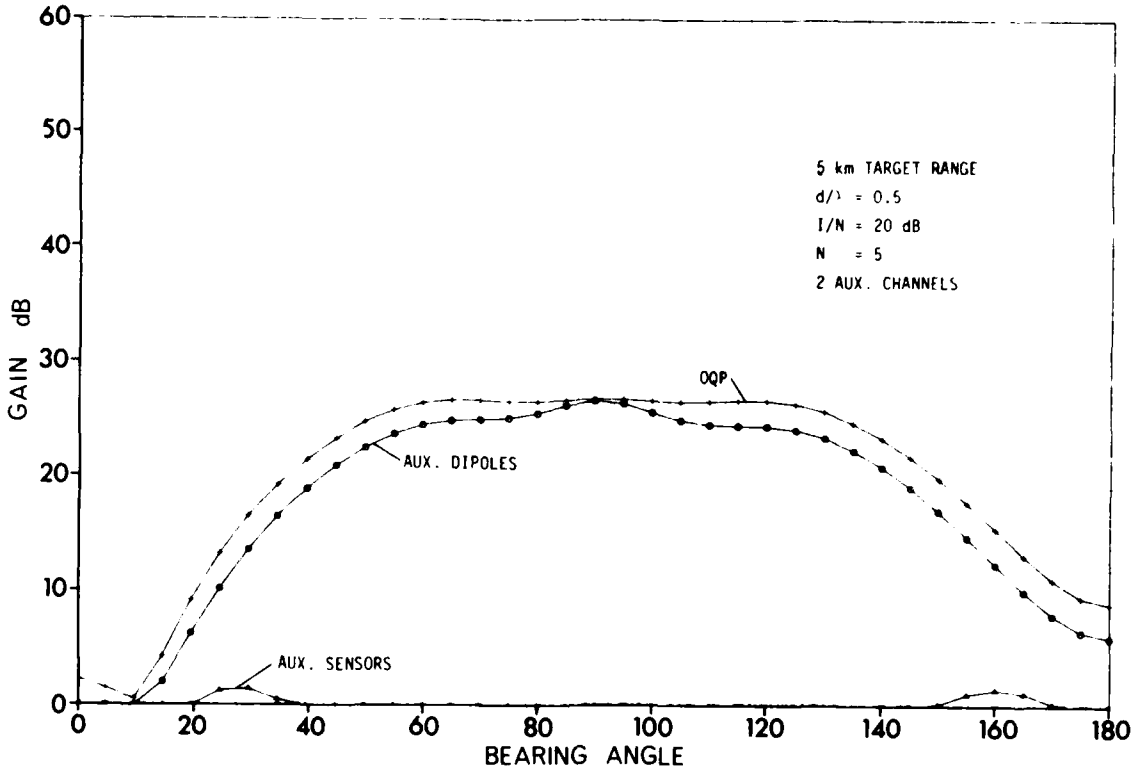

FIG. 83 INCLUSION OF SIGNAL IN ADAPTATION: SHORT ARRAY

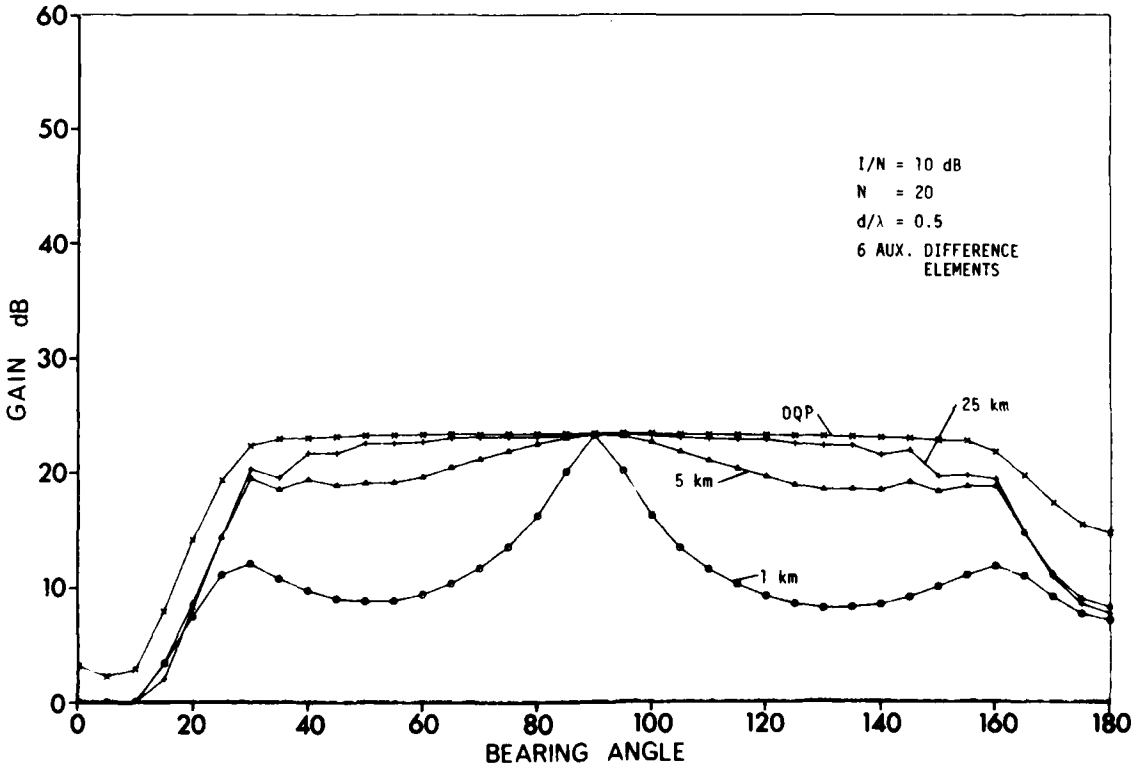

FIG. 84 AUXILIARY DIFFERENCE PATTERNS: INCLUSION OF SIGNAL IN ADAPTATION (I/N = 10 dB)

11 CARDIOID SENSOR PATTERNS

11.1 General Remarks

An obvious disadvantage of linear arrays is their rotational symmetry. On the one hand line arrays have a relatively poor performance if the noise is isotropic, which is more or less the case for surface noise and other kinds of ambient noise. Some additional gain can be achieved by using a two-dimensional array with a vertical beamwidth of about 40° in order to match the beamwidth properly to the vertical distribution of the signal energy (see Figs. 2 to 13). Even better performance can be achieved by covering an area of ±20° in the vertical by a bunch of beams narrower than 40° and integrating over the beams (multibeam processor). However, two-dimensional arrays are not so easy to handle, particularly in mobile systems.

Additional gain can also be obtained by using directive sensors, e.g. sensors with cardioid patterns. In the direction of the maximum of the cardioide 3 dB gain is achieved in uncorrelated noise. Furthermore, cardioide sensors offer the possibility of distinguishing between left and right. The gain calculation is straightforward. All the arrivals, as given by Eq. 9, have to be multiplied by the three-dimensional cardioide patterns, which is

$$d(\theta,\beta) = 1 + \sin\beta \cdot \cos\theta, \qquad \text{[Eq. 107]}$$

where θ and β denote elevation and azimuth in spherical coordinates, i.e. β = 0 to 360°, θ = -90° to 90°. θ = 0°, meaning the horizontal plane at the position of the array. For β = 90° and θ = 0° one gets the maximum $d(\theta,\beta) = 2$, for β = 270° and θ ° 0 it follows that $d(\theta,d) = 0$. A cross-section at β = 0° and 180° gives a vertical unit circle, i.e. at endfire and backfire direction of the array the sensors behave omni-directional. For arrivals due to different modes one gets the simple relation

$$\cos\theta_n = \frac{k_n}{k_o} \quad .$$

Therefore, Eq. 107 becomes

$$d_n(\beta,\theta) = 1 + \sin\beta \cdot \frac{k_n}{k_o} . \qquad \text{[Eq. 108]}$$

11.2 Gain Calculation

Now the array gain can be calculated as before. Figures 85 to 89 show gain curves for the OQP and the cosine processor (cardioid vs omnidirectional pattern). One noise source at 0° bearing is assumed. The point to be observed is that for 0.5λ spaced arrays it may happen that the gain is not unambiguous with bearing as it is with white noise (Fig. 85). For 0.5λ spacing the noise source at 0° causes a "grating minimum" at 180° such that there is another maximum beyond 180°, e.g. at 200° in Fig. 86. This effect is of course more serious with the cosine processor (Fig. 87). In the vicinity of the grating minimum strong targets may still be detected; however, no decision can be made as to whether the target is on the left or the right. This effect becomes less significant for larger arrays where the grating minimum becomes narrower and less deep. In any case it can be overcome by some smaller spacing, as seen in Figs. 88 and 89.

11.3 Conclusion on Cardioid Sensor Patterns

The use of cardioid patterns instead of omnidirectional sensors is an appropriate aid for distinguishing between left and right. The array spacing should be somewhat less than 0.5λ.

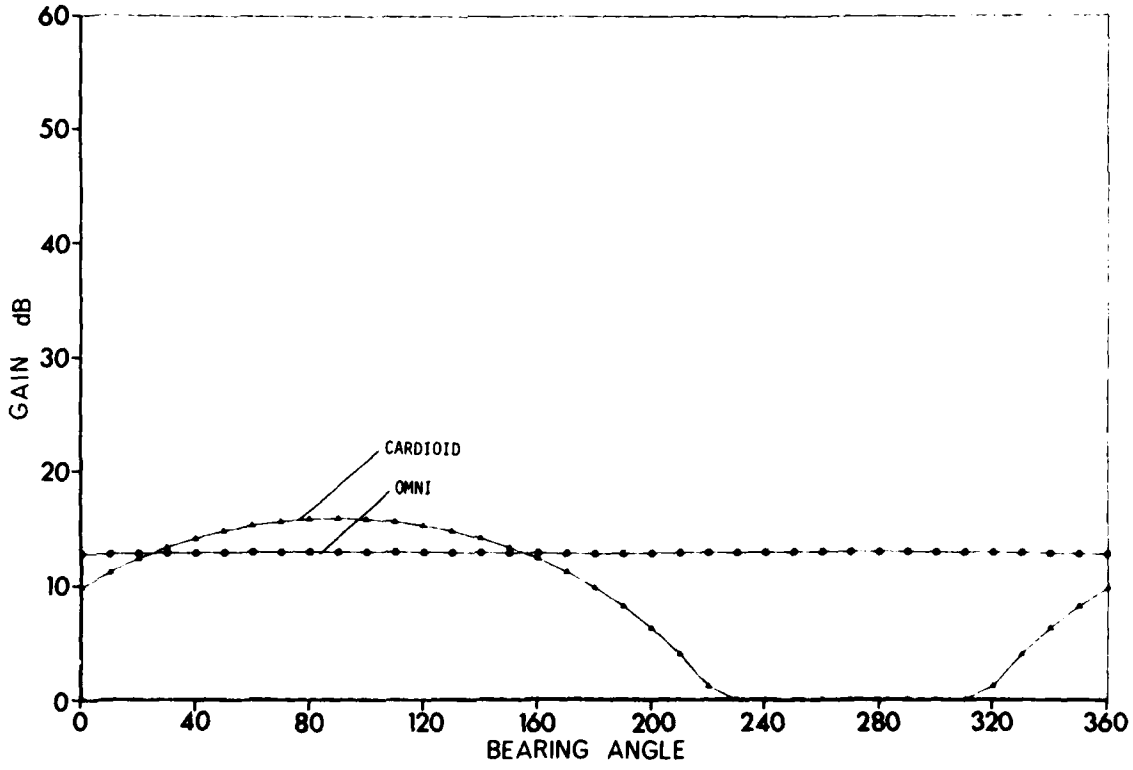

FIG. 85 WHITE NOISE GAIN - CARDIOID VERSUS OMNI

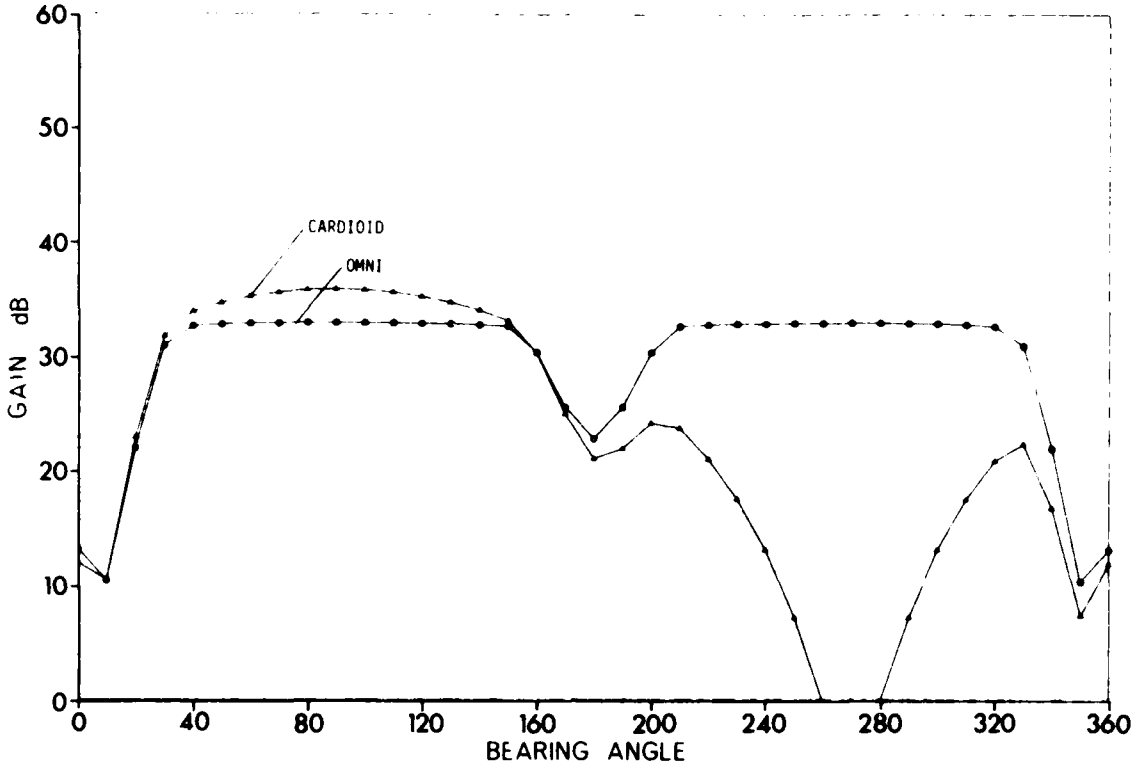

FIG. 86 OQP, 0.5λ SPACING - CARDIOID VERSUS OMNI

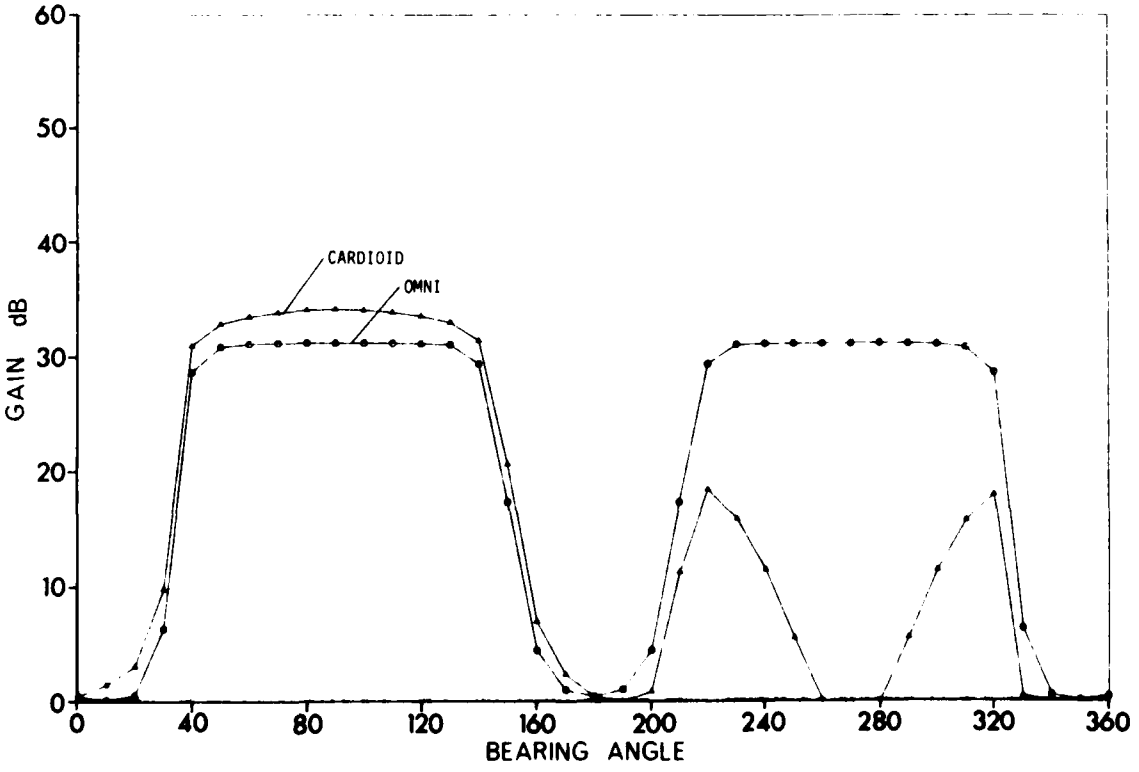

FIG. 87 COS-SHADING, 0.5λ SPACING - CARDIOID VERSUS OMNI

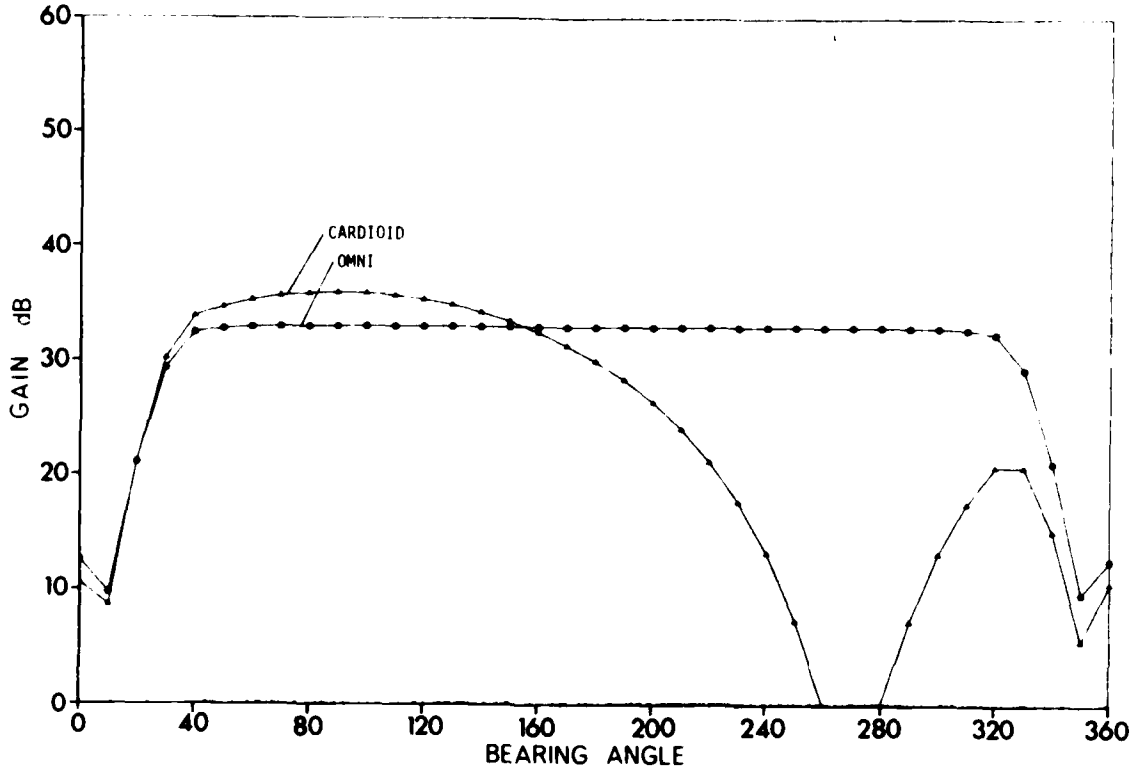

FIG. 88 OQP, 0.3λ SPACING - CARDIOID VERSUS OMNI

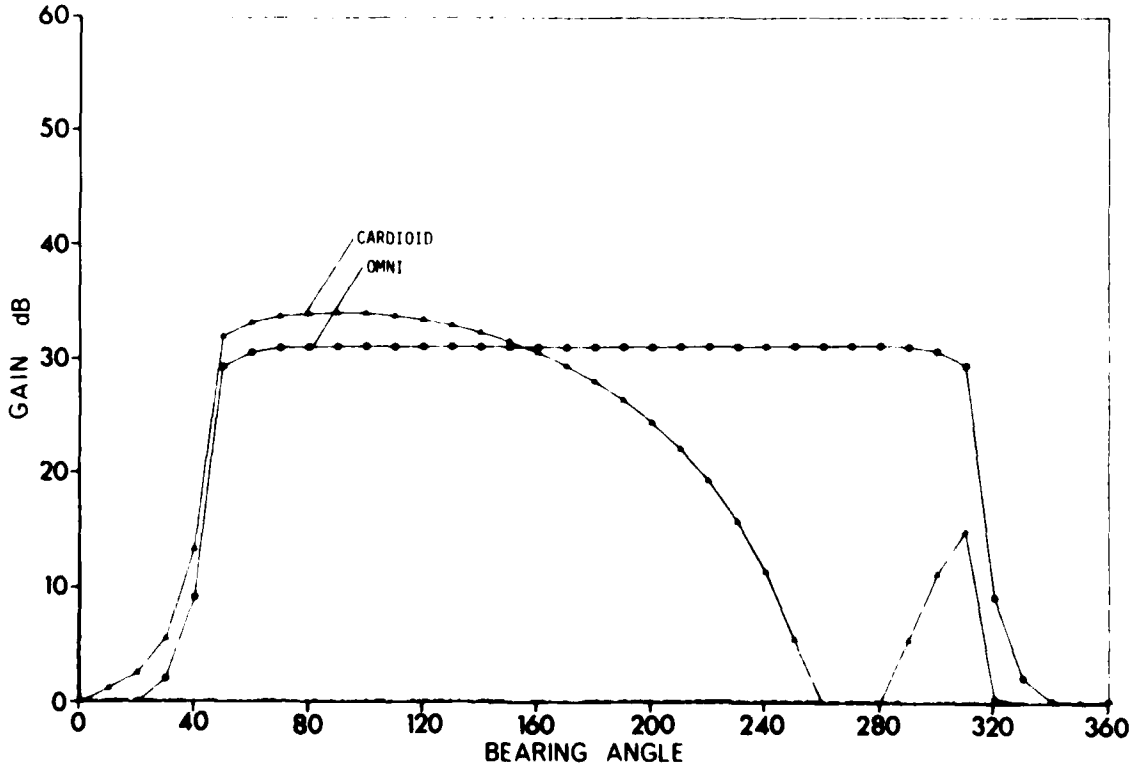

FIG. 89 COS-SHADING, 0.3λ SPACING - CARDIOID VERSUS OMNI

CONCLUSIONS

The detection performance (array gain) of horizontal linear hydrophone arrays operating in shallow water in the presence of directive interference has been investigated in some detail. The following summarizes those results that are important for applications. Further information is provided in the concluding Sections of Chs. 2 to 11.

a. In the shallow-water sound-propagation channel the sound energy of a point source may be spread over a vertical angle of about ±20°. The vertical energy spread appears to a horizontal line array as a horizontal spread. The horizontal spread is proportional to the cosine of the bearing, i.e. is zero for broadside and about ±20° at endfire.

b. Suppression of point sources is limited by the white noise rather than by the medium effect, i.e. the signal spread (Ch. 3).

c. For small apertures (less than 20λ) the linear adaptive processor (OLP) is almost optimum. For larger apertures quadratic beamforming has to be applied (Ch. 4).

d. Cosine shading is a useful approximation to optimum processing for about 50λ aperture. The loss compared with OQP is about 3 dB (Ch. 5).

e. One noise source with known direction (e.g. towing-ship noise) can be suppressed quite well by combining adjacent sensors to cardioid diagrams such that the null points into the noise direction (Ch. 6).

f. The adaptive multi beam processor is the best suboptimum array processor for arbitrary apertures. The loss compared with optimum processing is about 1 dB (depending on the number of beams, Ch. 7).

g. For apertures greater than 20λ, different slightly overlapping beams have to be formed in order to cover the whole area of signal spread. The beam outputs have to be summed incoherently (Ch. 7).

h. The sensor outputs should be followed by narrowband filters with rectangular frequency response (Ch. 8).

i. If the array is a flexible cable the deviation from a straight line should not exceed 0.1λ (Ch. 9).

j. The spatial spread of the signal makes adaptive processors very sensitive to inclusion of the signal in the adaptation process. Therefore adaptive processing is recommended only for very short passive arrays (Ch. 10).

k. The best array performance is achieved at broadside for several different reasons. Consequently mechanical steering (manoeuvring) should be taken into account (all chapters).

l. Cardioid sensor patterns are very useful for distinguishing between left and right (Ch. 11).

m. The signal spread causes adaptive systems to be very sensitive to inclusion of the signal in adaptation (passive systems). Even the performance of constrained processors is degraded seriously because, to be superimposed on adaptation, the constraint depends considerably on the actual parameters of the medium, i.e. on the actual signal energy distribution.

REFERENCES

1. COX, H. Interrelated problems in estimation and detection. In: Proceedings of a NATO Advanced Study Institute on Signal Processing with Emphasis on Underwater Acoustics held at Enschede, Netherlands 1968. Enschede, Netherlands, Technische Hogeschool Twente, 1969.

2. COX, H. Sensitivity in adaptive beamforming. In: GRIFFITHS, J.W.R. et al, eds. Proceedings of a NATO Advanced Study Institute on Signal Processing with Emphasis on Underwater Acoustics held at Loughborough, U.K., 1972. London, U.K., Academic Press, 1973: pp 619-645.

3. SCHULTHEISS, P.M. Some lessons from array processing theory. In: TACCONI, G. ed. Aspects of Signal Processing, Proceedings of a NATO Advanced Study Institute on aspects of Signal Processing with Emphasis on Underwater Acoustics held at Portovenere, Italy, 1976, NATO ASI Series C, No 33. Dordrecht, Netherlands, Reidel, 1977: p. 309.

4. COX, H. Resolving power and sensitivity to mismatch of optimum array processors. J. Acoustical Society America 54, 1973: 771-785.

5. ZIEGENBEIN, J. and WEBER, M. *Untersuchungen an einem adaptiven* Zweielement-Raumfilter (Investigations of an adaptive two-element spatial filter), FHP rpt 4-75. Werthoven, Germany, Forschungsinstitut für Hochfrequenzphysik, 1975.

6. OWSLEY, N. A recent trend in adaptive spatial processing for sensor arrays: constrained adaptation. In: GRIFFITHS, J.W.R. et al, eds. Proceedings of a NATO Advanced Study Institute on Signal Processing with emphasis on Underwater Acoustics held at Loughborough, U.K., 1972. London, U.K., Academic Press, 1973: pp 591-604.

7. FROST, O.L. An algorithm for linearly constrained adaptive array processing. Proceedings IEEE 60, 1972: 926-935.

8. GRIFFITHS, L.J. An adaptive beamformer which implements constraints using an auxiliary array processor. In: TACCONI, G. ed. Aspects of Signal Processing, Proceedings of a NATO Advanced Study Institute on aspects of Signal Processing with emphasis on Underwater Acoustics held at Portovenere, Italy, 1976, NATO ASI Series C, No 33. Dordrecht, Netherlands, Reidel, 1977: pp 517-524.

9. BUHRING, W. Adaptive antenna with rapid convergence. In: INSTITUTION OF ELECTRICAL ENGINEERS. Conference Publication No. 168 of the International Conference on Antennas and Propagation, November 1978, London. London, U.K. IEEE, 1979.

10. BUHRING, W. and KLEMM, R. Ein adaptives Filter zur Unterdrückung von Radarstörungen mit unbekanntem Spektrum (An adaptive filter for suppression of clutter with unknown spectrum). Frequenz 30, 9, 1976: 238-243.

11. WASILJEFF, A. Spatial horizontal coherence of acoustic signals in shallow water, SACLANTCEN SM-68. La Spezia, Italy, SACLANT ASW Research Centre, 1975. [AD A 011 560]

12. JENSEN, F.B. and FERLA, M.C. SWAP: the SACLANTCEN normal-mode acoustic propagation model, SACLANTCEN SM-121. La Spezia, Italy, SACLANT ASW Research Centre, 1979. [AD A 067 256]

13. URICK, R. Horizontal coherence of explosive reverberations. J. Acoustical Society America 47, 1970: 909-911.

14. URICK, R. Vertical coherence of explosive reverberations. J. Acoustical Society America 36, 1964: 2164-2170.

15. CLAY, C.S. Waveguides, arrays and filters. Geophysics 31, 3, 1966: 501-505.

16. KUPERMAN, W.K. SACLANT ASW Research Centre, La Spezia, Italy, Private communication.

17. BURG, J.P. A new analysis technique for time-series data. In: Proceedings of a NATO Advanced Study Institute on Signal Processing with emphasis on Underwater Acoustics held at Enschede, Netherlands 1968. Enschede, Netherlands, Technische Hogeschool Twente, 1969: pp 15-0.

18. WIDROW, B. Adaptive antenna systems. Proceedings IEEE 55, 1967: 2143-2159.

19. HARRIS, F.J. On the use of window for harmonic analysis with the discrete Fourier transform. Proceedings IEEE 66, 1, 1978: 51-83.

20. KLEMM, R. Suboptimale Verfahren zur räumlichen Störunter-drückung in Radargeräten mit phasengesteuerter Gruppenantenne (Suboptimum methods for spatial noise suppression in phased array radars). FFM rpt 240. Forschungsinstitut für Wertnoven, Germany, Forschungsinstitut für Funk und Mathematik, 1976.

21. ZURMUHL, R. Matrizen. Berlin, Germany, Springer-Verlag, 1964.

22. KLEMM, R. Adaptive clutter suppression step-scan radars. IEEE Transactions Aerospace and Electronic Systems 14, 1978: 658-688.

23. KLEMM, R. Ein digitales Filter zur adaptiven räumlichen Störunterdrückung (A digital filter for adaptive spatial noise suppression), FFM rpt 258. Forschungsinstitut für Werthoven, Germany, Forschungsinstitut für Funk und Mathematik, 1977.

BIBLIOGRAPHY

The following, which have not been cited in the text, are also relevant.

SKOLNIK, M. Radar Handbook. New York, N.Y., 1970: pp 11-12.

MIDDLETON, D. Introduction to Statistical Communication Theory. New York, N.Y., McGraw Hill, 1960: p. 742.

VAN TREES, H. Detection, Estimation and Modulation Theory, Pt. I. New York, N.Y., Wiley, 1968.

WIRTH, W.D. Suboptimal suppression of directional noise by a sensor array before beamforming. IEEE Transactions Antennas and Propagation 55, 12, 1967: 2143-2159.

GIROUDON, C. Results on active sonar optimum array processing. In: GRIFFITHS, J.W.R. et al, eds. Proceedings of a NATO Advanced Study Institute on Signal Processing with emphasis on Underwater Acoustics held at Loughborough, U.K., 1972. London, U.K., Academic Press, 1973: pp 591-604.

CRON, B.F. and SHERMAN, S.H. Spatial-correlation functions for various noise models. J. Acoustical Society America 34, 1962: 1732-1736.

GRIFFITHS, L.J. A simple adaptive algorithm for real-time processing in antenna arrays. Proceedings IEEE 57, 10: 1696-1704.

HINICH, M.J. Maximum likelihood signal processing for a vertical array. J. Acoustical Society America 54, 1973: 499-503.

CLAY, C.S., HINICH, M.J. and SHAMAN, P. Error analysis of velocity and direction measurements of plane waves using thick large-aperture arrays. J. Acoustical Society America 53, 1973: 1161-1166.

McCOOL, J.M. A constrained adaptive beamformer tolerant of array gain and phase errors. In: TACCONI, G. ed. Aspects of Signal Processing, Proceedings of a NATO Advanced Study Institute on aspects of Signal Processing with emphasis on Underwater Acoustics held at Portovenere, Italy, 1976, NATO ASI Series C, No 33. Dordrecht, Netherlands, Reidel, 1977.

BREKHOVSKY, L.M. Waves in a Layered Medium. New York, N.Y., Academic Press, 1960.

BARTRAM, J.F., RAMSEY, R.R. and HEINES, M.J. Fifth generation of digital sonar signal processing. IEEE J. Oceanic Engineering 2, 4, 1977: 337.

WILLE, P. and THIELE, R. Transverse horizontal coherence of explosive signals in shallow water. J. Acoustical Society America 50, 1971: 348-353.

INITIAL DISTRIBUTION

MINISTRIES OF DEFENCE	Copies
MOD Belgium	2
DND Canada	10
CHOD Denmark	8
MOD France	8
MOD Germany	15
MOD Greece	11
MOD Italy	10
MOD Netherlands	12
CHOD Norway	10
MOD Portugal	5
MOD Turkey	5
MOD U.K.	16
SECDEF U.S.	61

NATO AUTHORITIES	Copies
Defence Planning Committee	3
NAMILCOM	2
SACLANT	10
SACLANTREPEUR	1
CINCWESTLANT/COMOCEANLANT	1
COMIBERLANT	1
CINCEASTLANT	1
COMSUBACLANT	1
COMMAIREASTLANT	1
SACEUR	2
CINCNORTH	1
CINCSOUTH	1
COMNAVSOUTH	1
COMSTRIKFORSOUTH	1
COMEDCENT	1
COMMARAIRMED	1
CINCHAN	1

SCNR FOR SACLANTCEN	Copies
SCNR Belgium	1
SCNR Canada	1
SCNR Denmark	1
SCNR Germany	1
SCNR Greece	1
SCNR Italy	1
SCNR Netherlands	1
SCNR Norway	1
SCNR Portugal	1
SCNR Turkey	1
SCNR U.K.	1
SCNR U.S.	2
SECGEN Rep. SCNR	1
NAMILCOM Rep. SCNR	1

NATIONAL LIAISON OFFICERS	
NLO Canada	1
NLO Denmark	1
NLO Germany	1
NLO Italy	1
NLO U.K.	1
NLO U.S.	1

NLR TO SACLANT	
NLR Belgium	1
NLR Canada	1
NLR Denmark	1
NLR Germany	1
NLR Greece	1
NLR Italy	1
NLR Netherlands	1
NLR Norway	1
NLR Portugal	1
NLR Turkey	1
NLR UK	1
NLR US	1

Total initial distribution	236
SACLANTCEN Library	10
Stock	34
Total number of copies	280

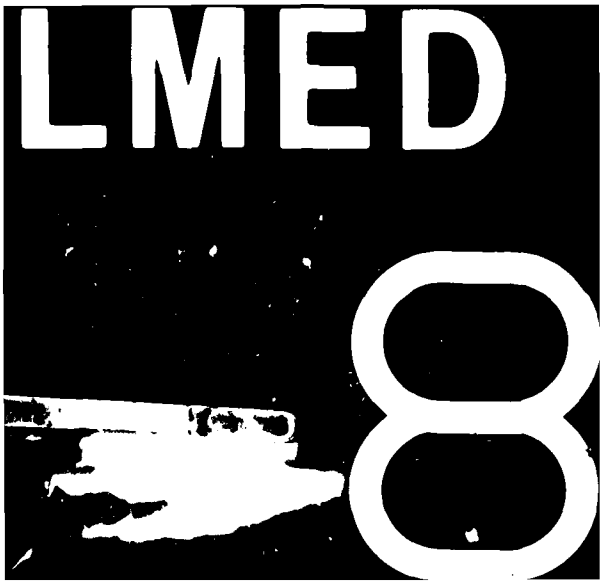
LMED
8